Available online at www.sciencedirect.com
ScienceDirect
Coordination Chemistry Reviews 251 (2007) 288–327
COORDINATION CHEMISTRY REVIEWS
www.elsevier.com/locate/ccr

Review

Advanced aspects of ab initio theoretical optical spectroscopy of transition metal complexes: Multiplets, spin-orbit coupling and resonance Raman intensities

Frank Neese *, Taras Petrenko, Dmitry Ganyushin, Gottfried Olbrich

Institut für Physikalische und Theoretische Chemie, Universität Bonn, Wegelerstr. 12, D-53115 Bonn, Germany

Received 31 January 2006; accepted 26 May 2006
Available online 3 June 2006

Dedicated to Prof. Volker Staemmler on occasion of his 65th birthday.

Contents

* Corresponding author. Tel.: +49 228732351; fax: +49 228739064.
E-mail address: theochem@thch.uni-bonn.de (F. Neese).

0010-8545/$ – see front matter
doi:10.1016/j.ccr.2006.05.019

Abstract

In this review some advanced aspects of the theoretical methods for the calculation of transition metal optical spectra with ab initio methods are discussed. Density functional theory (DFT) based methods are not covered. A brief introduction into the field of complete active space self-consistent field (CASSCF) calculations is provided. These methods allow the correct zeroth order description of arbitrary electron states including singly and doubly excited ligand field or atomic multiplet states. This is followed by a cursory discussion of the treatment of dynamic correlation by using multireference (MR) many body perturbation theory in form of a second order correction to the CASSCF energy (CASPT2). MR based configuration interaction (MRCI) methods are also briefly touched and the spectroscopy oriented CI (SORCI) variant developed in this laboratory is described in some detail. The operators to describe the leading relativistic effects (scalar relativity and spin-orbit coupling (SOC)) are described afterwards. The CASSCF and SORCI methods are first applied to the calculation of the multiplets of the free dipositive and tripositive first-row transition metal ions followed by a discussion of calculations of molecular d–d multiplet states in dipositive and tripositive hexaquo complexes of the first transition row. We then turn to the subject of the treatment of SOC in CASSCF and MRCI based approaches in some detail. The final part of the review provides an introduction into the theory of the resonance Raman effect, the possible quantum chemical calculation of resonance Raman intensities, the implementation of the method into the ORCA electronic structure program system followed by an application to the resonance Raman and absorption spectra of transition metal dithiolene complexes.

Keywords: Spin-orbit coupling; Multireference; Multiplets; Ab initio; Resonance Raman

1. Introduction

The absorption spectra of coordination complexes have formed a cornerstone of the theory of transition metal complexes since the early 1950s [1,2]. The beautiful colors exhibited by many coordination compounds are not only appealing from an aesthetic point of view but also carry a great deal of information about the electronic and geometric structures of the complexes [3–5]. Thus, a thorough analysis of the optical spectra of complexes yields information about the ligand field strengths, the coordination number and geometry and the covalencies of the metal-ligand bonds. Among the most successful experimental methods are absorption (ABS) spectra with or without linearly polarized light [6], circular dichroism (CD) spectra, and magnetic circular dichroism (MCD) spectra [7,8]. In addition, high-resolution information of the ground state-vibrational structure as well the excited state electronic and geometric structure may be obtained from a detailed consideration of resonance-Raman spectra [9–11]. The bonding descriptions that arise from such studies are highly useful in analyzing and interpreting the reactive properties of the complexes.

Since the early days of coordination chemistry mainly five types of electronic transitions have been found in (mononuclear) coordination compounds: (a) d–d transition that involve promotion of electrons within the partially filled d-orbitals of the metal ions. These transitions, which typically fall into the visible and near infrared region of the spectrum, are extremely sensitive indicators of the d^n configuration of the complexes, the total spin multiplicity of the ground state, the coordination number and the coordination geometry; (b) ligand-to-metal charge transfer (LMCT) transitions that involve transitions from filled ligand based orbitals to the partially occupied metal d shell. In most cases these transitions fall into the visible region of the spectrum if the oxidation state of the metal is high and the coordinating ligands are 'soft' in the chemical sense; (c) metal-to-ligand charge transfer (MLCT) transitions which involve promotion of electrons from mainly metal d-based orbitals to low lying empty ligand orbitals. Such transitions are typically observed in the visible region of the spectrum if the oxidation state of metal is low and the ligand contains low-lying empty π^*-orbitals; (d) intra-ligand transitions that involve promotion of electrons between mainly ligand based orbitals on the same ligand and (e) ligand-to-ligand charge transfer transitions in which an electron is moved from one ligand another one in the excited state [12]. Such transitions will be studied below [13] in some detail in a series of interesting metal-bridged diradicals [14].

The present study will be confined almost exclusively to the first type of electronic transitions. The interpretation of d–d spectra has been a domain of ligand-field theory (LFT; [15–19]) and its variants like the angular overlap model [20–22] for a

long time. While these approaches are semi-empirical in nature, they provide a tremendous amount of insight into the electronic structure, spectroscopy, thermochemistry, stereochemistry, photochemistry and kinetics of transition metal complexes and are thus a powerful guide to chemical thinking. The great achievement of ligand field theory has been that with a minimum amount of empirical parameters a great variety of properties could be explained and even reproduced with to good to excellent numerical accuracy. In the simplest form which is valid for cubic complexes only two parameters are necessary: the ligand field strength *10Dq* and the Racah *B* parameter which accounts for the interelectronic repulsion [1]. These relationships are most elegantly summarized in the Tanabe–Sugano diagrams which allow one to quickly and easily interpret the d–d spectra of metal ions in a cubic environment [23]. More refined treatments include parameters describing anisotropic covalency and spin-orbit coupling (SOC) which is a prerequisite for the interpretation of magnetic measurements [24]. However, while LFT provides a powerful and extremely useful language, it is not an accurate first-principles method that would allow one to compute the properties of transition metal complexes without recourse to experimental data. Yet, it provides a most convenient framework in which experiments and results from accurate first-principles calculations can be expressed and summarized.

Indeed, the application of rigorous first-principles approaches to transition metal electronic spectra has been found to be surprisingly difficult, at least compared to the success that ab initio quantum chemistry has enjoyed for a long time in organic and main group chemistry [25]. In order to provide a balanced treatment of several states of vastly different character (i.e. d–d versus CT states) it is inevitable to treat the correlation energy of the states involved. That is, uncorrelated calculations at the Hartree–Fock (HF) level and the CI with single excitations (CIS) from a HF reference are not adequate and typically show errors of several eV in the transition energies. In addition they have shortcomings in the qualitative ordering of the excited states or even to correctly predict the ground state. In this respect the success of the semi-empirical INDO/S method in this area is astonishing and has for a long time rivaled ab initio approaches in the area of transition metal spectroscopy [26–31] (for recent applications, see e.g. [32–44]).

For a long time, the application of more reliable first principle methods has been hindered by intricate problems that are so characteristic for the quantum chemistry of transition metal complexes. First, they are typically large, involving many atoms and electrons which causes the calculations to become very time consuming. Second, they typically involve significant near-degeneracy effects ('static correlation') which causes treatments that are based on a single reference (SR) configuration to be unreliable. This is a particularly pressing problem, since even in cases where there is only little static correlation, the HF methods frequently fails to provide a good starting point for more elaborate treatments. Thus, multireference (MR) approaches are often necessary to achieve quantitatively accurate results. Nevertheless, MR methods are complicated, time consuming, and in addition require much more insight from the user of a quantum chemical program than the SR approaches that can be done in an essentially black-box fashion using standard quantum chemical codes. Third, the dynamic correlation effects in transition metal complexes are also large and must be treated at some level of approximation in order to obtain reliable results. Fourth, since transition metal atoms are heavy, relativistic effects can be of substantial magnitude and should be dealt with in studies that aim at high accuracy.

During the past 10–15 years, however, significant progress has been made in the field of transition metal quantum chemical approaches. These are first of all due to the success of density functional theory (DFT) [45–51]. DFT can also be applied to the calculation of excitation spectra within the time-dependent linear response formalism [52–57]. However, the TD-DFT method has not met with the same success that ground state applications of DFT have enjoyed [58,59]. Secondly, extremely efficient MR approaches have been developed which, together with the enormous increase in available computer power, allow application to transition metal complexes of significant size on low-cost personal computers. Seminal contributions to this field have been made by Roos and co-workers who have developed the efficient CASPT2 method and have provided much insight into electron correlation effects in transition metal complexes. For reviews of these approaches and their application see [60–66]. However, the development of new methods that provide a good tradeoff between computational cost and obtainable accuracy is still an important goal of quantum chemical method development.

During the past few years we have been interested in the calculation and interpretation of transition metal optical spectra parallel to experimental investigations. To this end we have developed efficient computer codes to carry out such calculations [67]. In particular, a method called spectroscopy oriented configuration interaction (SORCI) was developed [68] and successfully tested in a number of applications [13,69–78]. SORCI is based on the important concepts of individual selection [79–83] and difference dedicated CI [84,85] and achieves efficiency through a combination of variation and perturbation theory [67]. In this review, we present a relatively elaborate discussion of some advanced subjects in transition metal optical spectroscopy with emphasis on the recent advances in the procedures implemented in the ORCA program package. In particular, methods for the calculation of multiplet energies, spin-orbit splitting and resonance-Raman intensities are discussed. The majority of this material has not previously been published but is included here in order to document the availability and accuracy of the available computational protocols.

2. Ab initio electronic structure methods

2.1. The Hartree–Fock method and the correlation energy

The Hartree–Fock method in its most elementary form considers a single-determinant *Ansatz* for the approximation of a N-electron state function $\Psi(\boldsymbol{x}_1, \ldots, \boldsymbol{x}_N) = \det|\psi_1 \ldots \psi_N|$, where $\boldsymbol{x}_i \equiv (\boldsymbol{r}_i, \sigma_i)$ is a compound index for the space- and spin-

variables of a single electron and the set of $\{\psi\}$s are orthonormal single-electron wavefunctions [86]. Owing to the variational principle, the expectation value $\langle\Psi|\hat{H}|\Psi\rangle/\langle\Psi|\Psi\rangle$ is always higher than the exact ground state energy. The Hamiltonian $\hat{H}$ is usually taken to be the clamped-nuclei Born-Oppenheimer Hamiltonian which only considers the leading electrostatic interactions (in atomic units):

$$\begin{aligned}\hat{H}_{\mathrm{BO}} &= -\frac{1}{2}\sum_i \vec{\nabla}_i^2 - \sum_{i,A}\frac{Z_\mathrm{A}}{|\mathbf{r}_i - \mathbf{R}_\mathrm{A}|} \\ &\quad + \frac{1}{2}\sum_{i\neq j}\frac{1}{|\mathbf{r}_i - \mathbf{r}_j|} + \frac{1}{2}\sum_{A\neq B}\frac{Z_\mathrm{A}Z_\mathrm{B}}{|\mathbf{R}_\mathrm{A} - \mathbf{R}_\mathrm{B}|} \\ &= \hat{T} + \hat{V}_{eN} + \hat{V}_{ee} + \hat{V}_{NN} = \hat{h} + \hat{V}_{ee} + \hat{V}_{NN} \end{aligned} \quad (1)$$

Here i, j sum over electrons at positions $\boldsymbol{r}_i$, A, B over nuclei with charge Z_A at positions $\boldsymbol{R}_\mathrm{A}$. Thus, from an energetic point of view the best single determinant is one which minimizes this expectation value. The entities to be varied in order to find an energy minimum (or more precisely a stationary point of the Ritz-functional) are the single-electron orbitals $\psi_i(\boldsymbol{x})$ themselves. Variation of the orbitals under the constraint of orthonormality leads to the HF equations in canonical form:

$$\hat{F}\psi_i = \left[\hat{h} + \sum_j \hat{J}_j - \hat{K}_j\right]\psi_i = \varepsilon_i\psi_i \quad (2)$$

where ε_i is the orbital energy and the Coulomb operator $\hat{J}_j$ and exchange operators $\hat{K}_j$ are defined by:

$$\hat{J}_j\psi_i(\boldsymbol{x}) = \psi_i(\boldsymbol{x})\int\frac{|\psi_j(\boldsymbol{x}')|^2}{|\boldsymbol{r}-\boldsymbol{r}'|}\mathrm{d}\boldsymbol{x}' \quad (3)$$

$$\hat{K}_j\psi_i(\boldsymbol{x}) = \psi_j(\boldsymbol{x})\int\frac{\psi_j^*(\boldsymbol{x}')\psi_i(\boldsymbol{x}')}{|\boldsymbol{r}-\boldsymbol{r}'|}\mathrm{d}\boldsymbol{x}' \quad (4)$$

Since the BO operator is spin-free it is customary to let the orbitals be eigenfunction of the single-electron spin-operator by choosing them to be either spin-up or spin-down orbitals. This leads to the spin-unrestricted (UHF) method ($\sigma = \alpha, \beta$):

$$\hat{F}^\sigma\psi_i^\sigma = \left[\hat{h} + \sum_{j\sigma'}\hat{J}_j^{\sigma'} - \delta_{\sigma\sigma'}\hat{K}_j^\sigma\right]\psi_i^\sigma = \varepsilon_i^\sigma\psi_i^\sigma \quad (5)$$

For a closed-shell system, the spin-up and spin-down operators are equal and the spin-orbitals are obtained in pairs of equal shape and energy. Instead of dividing the set of orbitals into spin-up and spin-down orbitals it is also possible to pursue a division into closed-shell and open-shell orbitals. This leads to the restricted open-shell HF (ROHF) method. The formalism for this method is a little more involved but the general ideas are identical to the UHF case. The ROHF wavefunction is an eigenfunction of the total spin squared ($\hat{S}^2$) operator while the UHF wavefunction does not have this feature. The energy of the UHF wavefunction, on the other hand, is lower than that of the ROHF wavefunction due to the increased variational freedom in the UHF case.

In practice, the HF-orbitals are approximated through a linear combination of fixed, atom-centered basis-functions $\{\varphi\}$:

$$\psi_i(\boldsymbol{x}) = \sum_\mu c_{\mu i}\varphi_\mu(\boldsymbol{x}) \quad (6)$$

The variational parameters are now the MO coefficients $\boldsymbol{c}$ instead of the orbitals themselves. The basis set is, of course, user-specified and many reasonable choices with differing degrees of accuracy have been proposed in the literature [87]. It turns out that the basis-set limit, e.g. the size at which the basis set approaches completeness, is relatively easily to approach at the HF level [88]. Already basis sets of double- or triple-ζ quality together with one-or more sets of polarization functions on each atom typically provide fairly good results.

The HF method essentially describes the movement of single electrons in the field of the nuclei and the average field of the other electrons. It typically recovers more than 99% of the exact, non-relativistic energy but the remaining error is, unfortunately, still large on the chemical energy scale and amounts to hundreds of kcal/mol. Energy differences may, however, be more accurate through error cancellation. Since the stabilizing exchange term only works for electrons of the same spin, the HF method strongly favors states with unpaired, parallel spins and therefore favors high-spin states over low-spin states. DFT methods tend to have the opposite bias [74,77].

The remaining difference between the exact energy and the HF energy is being defined as the correlation energy:

$$E_\mathrm{corr} = E_\mathrm{exact} - E_\mathrm{HF} \quad (7)$$

E_corr is always negative and is know to converge very slowly with the size of the basis set employed. Consequently, it turns out to be extremely difficult to calculate more than 80% of the exact correlation energy [89]. However, when it comes to calculations on excited states, the treatment of at least the differential correlation energy becomes very important and below we discuss some of the popular methods.

The correlation energy is usually calculated through an expansion of the wavefunction in a leading term (the HF determinant) and admixture of excited determinants in which one-, two-, three-, etc. occupied spin-orbitals of the HF determinant are replaced by virtual orbitals. Thus, the wavefunction is of the form:

$$\Psi(\boldsymbol{x}_1, \ldots, \mathbf{x}_N) = |\Phi_\mathrm{HF}\rangle + \sum_{ia} C_i^a|\Phi_i^a\rangle + \frac{1}{4}\sum_{ijab} C_{ij}^{ab}|\Phi_{ij}^{ab}\rangle + \ldots \quad (8)$$

the usual convention is that the labels i, j, k, l refer to occupied spin-orbitals in the HF reference and a, b, c, d to unoccupied ones. If the coefficients $\boldsymbol{C}$ are determined by the variational principle this is the configuration interaction (CI) method with single-, double-, triple-, etc. excitations. Alternatively, the coefficients may be estimated by many-body perturbation theory (MBPT) or coupled-cluster (CC) techniques. Importantly, if all 1-through N-fold excitations are included in the CI-procedure the exact solution of the BO-problem within the limitations imposed by the one-particle basis set is obtained (full-CI = FCI).

FCI is not a practical method since the computational effort scales factorially with the number of electrons. It is, however, very useful for benchmark purposes.

The excited determinants can be elegantly constructed through the action of the second quantized fermion creation and annihilation operators $a^+_{a\sigma}$ and $a_{i\sigma}$. Thus, the operator $a^+_{a\sigma}a_{i\sigma}$ replaces spin orbital ψ^σ_i by ψ^σ_a if ψ^σ_i is occupied and ψ^σ_a is unoccupied in the determinant that the operator acts on and yields zero otherwise. Powerful techniques have been developed to deal with the algebra of the creation and annihilation operators [90].

2.2. Multiconfigurational self-consistent field wavefunctions

The first step in the generalization of the HF method to arbitrary states is to allow a higher flexibility of the wavefunction. This is necessary to properly describe electronic situations like: (1) the construction of multiplet components which arise in transition metal complexes and which are often poorly described by a single Slater-determinant; (2) the description of weak or partially broken bonds such as they arise in the problem of magnetic coupling between several ions and which requires a delicate balance between neutral and ionic components and (3) the construction of reasonable approximations for excited states which may have to be represented as mixtures of single- and double-excitations. All of these problems require a multi-determinantal HF method as starting point. In this so-called multiconfigurational self-consistent field (MCSCF) method, the Ansatz for the N-electron wavefunction is [65]:

$$\Psi(\boldsymbol{x}_1, \ldots, \boldsymbol{x}_N) = \sum_I C_I |\Phi_I\rangle \tag{9}$$

The many-electron 'basis-functions' $\{\Phi\}$ are either single-Slater determinants built from a set of one-electron orbitals $\{\psi\}$ or linear-combinations of such determinations in order to produce wavefunctions of the desired spin- and space-symmetry (referred to as configuration-state functions, CSFs). The variational parameters in the MCSCF method are the CSF coefficients $\boldsymbol{C}$ and the MO coefficients $\boldsymbol{c}$ which are both varied in order to minimize the energy.

One of the most difficult steps in the MCSCF method is to find a good set of $\{\Phi\}$ which give a balanced description for the state(s) of interest. A systematic, although not very economic, way, is based on the subdivision of the orbital set into three spaces. First the set of inactive orbitals which are doubly occupied in each CSF (labels i, j, k, l), the set of active orbitals which have variable occupation numbers in the various CSFs (labels p, q, r, s) and finally the virtual (external) orbitals which are unoccupied in all CSFs (labels a, b, c, d). The labels t, u, v, w refer to orbitals from any subset.

A fixed number of active electrons is distributed in all possible ways over all active orbitals consistent with the desired overall spin- and space symmetry. The multiconfigurational character is then introduced by a full-CI within the active space. Therefore, the method has the acronym complete active space self-consistent field (CASSCF). A CASSCF wavefunction is (almost) unambiguously identified by its total spin multiplicity, the number of active electrons (n) and active orbitals (m) leading to the notation CASSCF (n, m). CASSCF calculations can also, and beneficially so, performed for the average of several states which leads to the 'state-averaged CASSCF formalism (SA-CASSCF)'. The optimization of such a CASSCF wavefunction is a highly nonlinear problem [91–95]. Some of the solutions are sensible approximations to accessible states of the system while others simply represent saddle points or other stationary points in the $(\boldsymbol{c}, \boldsymbol{C})$ variational space and may sometimes be hard to distinguish from sensible solutions. However, efficient programs exist for the calculation of massive CASSCF wavefunctions with more than one-million CSFs describing the state(s) of interest [67,96,97]. For technical reasons, the calculations become very difficult for more than ~14 active orbitals which sets some rather severe limitations on the applicability of the CASSCF method.

It is important to realize that CASSCF wavefunctions are not designed to recover large fractions of the correlation energy. Rather, the CASSCF method is designed to describe multiplet- and near-degeneracy situations in a reasonable and consistent way to 'zeroth-order' and therefore to provide a good starting point for the treatment of (dynamic) electron correlation. Detailed discussions of the application of the CASSCF method to transition metal chemistry can be found in the works of Roos and co-workers, where much useful information on theoretical, technical and practical details is assembled [60,61,63–66].

2.3. Single- and multireference perturbation theory

The most straightforward way to improve on the HF result is to include the effects of dynamic electron correlation through many-body perturbation theory (MBPT). Based on a single HF-determinant, a simple expression is obtained which is known as the second-order Møller-Plesset (MP2) approximation to the correlation energy [86]:

$$E_{\mathrm{MP2}} = E_{\mathrm{HF}} + \frac{1}{4}\sum_{ijab}\frac{|(ia|jb) - (ib|ja)|^2}{\varepsilon_i + \varepsilon_j - \varepsilon_a - \varepsilon_b} \tag{10}$$

with $(ia|jb) = \int\int \psi_i(\boldsymbol{x}_1)\psi_a(\boldsymbol{x}_1)\psi_j(\boldsymbol{x}_2)\psi_b(\boldsymbol{x}_2) r_{12}^{-1} \mathrm{d}\boldsymbol{x}_1 \mathrm{d}\boldsymbol{x}_2$ being a two-electron integral over MOs. By convention, i, j refer to occupied and a, b to unoccupied orbitals in the HF determinant. The MP2 energy-expression arises from dividing the total Hamiltonian into a zeroth' order part $\hat{H}_0 = \sum_i \hat{F}(\boldsymbol{x}_i)$ and a perturbation $\hat{V} = \hat{H}_{\mathrm{BO}} - \hat{H}_0$ which is called the 'fluctuation potential'. Since, the BO Hamiltonian does not contain more than two-body terms, Slater's rules show, that $\hat{V}$ can couple the HF determinant with at most double-excitations from the HF reference and this is how the MP2 energy expression arises. Singly-excited determinants do not contribute to the correlation energy in this approximations by virtue of Brillouin's theorem [86]. MP2 theory is very successful in organic chemistry and greatly improves upon the results of HF calculations [88]. Furthermore, highly sophisticated programs make it possible

to efficiently evaluate or approximate the $O(N^4)$ two-electron integrals $(ia|jb)$ such that the MP2 energy can also be calculated for large molecules [98–104]. In inorganic chemistry, in particular in the field of Werner type complexes, MP2 is not popular due to its frequent divergence because of near-degeneracy problems and also due to the poor quality of the HF reference wave function which makes perturbation theory a questionable approach for such systems (vide infra).

The generalization of MP2 theory from a single HF determinant to a multiconfigurational reference function (MRPT) turns out to be surprisingly difficult and many variants have been proposed in the literature [60,61,63,105–120]. The idea of a perturbative correction to a CASSCF energy is quite attractive since the CASSCF method takes care of all near-degeneracy effects ('static correlation') and the low-order perturbative correction is supposed to capture most of the remaining correlation ('dynamic correlation'). The most widely used method of this kind is the CASPT2 approach developed and extensively applied by Roos and co-workers [60,61,63–66]. The CASPT2 method is efficient, elegant and has shown considerable success in its application throughout chemistry and spectroscopy. In general, it is impossible to unambiguously partition the BO Hamiltonian into a zeroth order part and a perturbation and consequently many different versions exist. The most common procedure is to stay as closely as possible to closed-shell MP2 theory and to define a spin-averaged Fock-operator:

$$\hat{F} = \hat{h} + \sum_{tu} D_{tu} \left[\hat{J}_{tu} - \frac{1}{2} \hat{K}_{tu} \right] \tag{11}$$

with matrix elements:

$$F_{vw} = h_{vw} + \sum_{tu} D_{tu} \left[(tu|vw) - \frac{1}{2}(tv|uw) \right] \tag{12}$$

Here, the first-order density matrix of the multiconfigurational reference state $|0\rangle$ was introduced:

$$D_{ut} = \langle 0|E_t^u|0\rangle \tag{13}$$

The operator E_t^u is known as orbital replacement operator or 'generator of the unitary group' and is given by:

$$E_t^u = a_{u\alpha}^+ a_{t\alpha} + a_{u\beta}^+ a_{t\beta} \tag{14}$$

Using these operators, the BO Hamiltonian can be written in a second-quantized form as:

$$\hat{H}_{\mathrm{BO}} = \sum_{tu} h_{ut} E_t^u + \frac{1}{2} \sum_{tuvw} (tu|vw)[E_t^u E_v^w - \delta_{uv} E_t^w] + \hat{V}_{NN} \tag{15}$$

and the Fock operator becomes:

$$\hat{F} = \sum_{tu} T_{ut} E_t^u \tag{16}$$

The zeroth order Hamiltonian in MRPT is then defined as:

$$\hat{H}^{(0)} = \hat{P}\hat{F}\hat{P} + \hat{Q}\hat{F}\hat{Q} \tag{17}$$

where $\hat{P} = |0\rangle\langle 0|$ is the projector onto the reference wavefunction $|0\rangle$ and $\hat{Q} = \hat{1} - \hat{P}$ projects onto the orthogonal complement. It is readily verified that this definition leads back to MP partitioning in the case that $|0\rangle$ is a single closed-shell determinant. In the CASPT2 method a slight modification of $\hat{H}^{(0)}$ is used which has been discussed by Andersson and is supposed to give a more balanced treatment of closed- and open-shell states [62,121].

In second-order perturbation theory, the first order-wavefunction $|1\rangle$ is determined by:

$$(\hat{H}^{(0)} - E^{(0)})|1\rangle + (\hat{V} - E^{(1)})|0\rangle = 0 \tag{18}$$

$|1\rangle$ is expanded in terms of a set of excited CSFs $|\Psi_I\rangle$

$$|1\rangle = \sum_I C_I^{(1)} |\Psi_I\rangle \tag{19}$$

where $\boldsymbol{C}^{(1)}$ are the first-order wavefunction coefficients. They are determined by left-multiplying Eq. (18) with $\langle\Psi_K|$ resulting in a linear set of equations for the unknown $\boldsymbol{C}^{(1)}$:

$$\sum_I \langle\Psi_K|\hat{H}^{(0)} - E^{(0)}|\Psi_I\rangle C_I^{(1)} = -\langle\Psi_K|\hat{V}|0\rangle \tag{20}$$

$(E^{(0)} = \langle 0|\hat{H}^{(0)}|0\rangle)$. Finally, the second-order perturbation energy is:

$$E_{\mathrm{MRPT2}} = E_{\mathrm{CASSCF}} + \langle 0|\hat{V}|1\rangle \tag{21}$$

To second-order in perturbation theory, the first order wavefunction contains contributions from CSFs which are singly- and doubly- excited with respect to any of the reference CSFs. Thus, potentially the so-called first-order interacting space (FOIS) for a multiconfigurational zeroth order wavefunction is larger by a factor number-of-reference-*CSFs* than the FOIS for a single reference determinant. Since the number of CSFs in $|0\rangle$ may reach 10^6 the FOIS would very quickly become unmanageable even for moderately sized molecules. Fortunately, there is a way around this problem by making use of the principle of 'internal contraction' first introduced independently by Meyer and Siegbahn [122]. In this method, one spans the FOIS of a multiconfigurational reference wavefunction by acting with the excitation operators onto the entire multiconfigurational reference wavefunction together. For example:

$$|\Phi_{ij}^{ab}\rangle = E_i^a E_j^b |0\rangle = \sum_I C_I E_i^a E_j^b |\Phi_I\rangle \tag{22}$$

where the coefficients C_I are fixed by the preceding CASSCF calculation. The matrix elements of the BO Hamiltonian over internally contracted wavefunctions becomes very difficult. Secondly, the set of excited CSFs constructed by acting with all unique single- and double- replacement operators on $|0\rangle$ is not linearly independent and not orthogonal which creates additional technical challenges. Finally, the considerable sparsity of the Hamiltonian which is characteristic of an uncontracted FOIS is lost. Nevertheless, the savings offered by internal contraction and the efficiency gained in high-quality implementations are impressive and justify the considerable effort for their derivation and implementation. The CASPT2 method has been efficiently

incorporated in slightly different forms into the MOLCAS [97] and MOLPRO [96] programs where they are widely used. To the best of our knowledge, the only place where the necessary formula apparatus is fully documented is the Ph.D. thesis of Andersson [123].

A CASPT2 study of the excited states of a given system usually involves the successive determination of CASSCF wavefunctions $|0\rangle$ for each state of interest followed by a calculation of the second-order estimate of the correlation energy as described above. Thus, for each state there is a separate set of orbitals and self-consistent field process. For significant numbers of states this may become time consuming. It may also be problematic to obtain converged CASSCF wavefunctions for higher excited states of a given symmetry. These problems may at least be partially overcome by determining a common set of orbitals through the SA-CASSCF procedure. The second, more severe, problem is the possibility of intruder states which lead to ill-conditioned linear equation systems (20) and invalidate the second-order perturbation theory approach. A number of methods have been suggested to overcome the intruder state problem [66,110,120]. However, it remains the most severe obstacle in the application of MRPT procedures and ultimately requires much insight and care from the user.

2.4. Multireference configuration interaction

There are many variants of multireference CI (MRCI). All of them share the feature of starting from a multiconfigurational zeroth order wavefunction. The MRCI wavefunction is written as a linear combination of the zeroth order wavefunction and excited CSFs. For simplicity, all CSFs in the reference space and the excited CSFs are combined into a single set of CSFs $|\Phi_I\rangle$. The coefficients with which these CSFs enter into the MRCI wavefunction are variationally determined through solution of the MRCI eigenvalue problem.

$$\boldsymbol{HC} = E\boldsymbol{C} \tag{23}$$

with $H_{IJ} = \langle\Phi_I|\hat{H}_{\mathrm{BO}}|\Phi_J\rangle$ and $|\Psi_{\mathrm{MRCI}}\rangle = \sum_I C_I|\Phi_I\rangle$. Since the vast majority of MRCI calculations does not consider excited CSFs beyond double excitations, the MRCI wavefunction can be conveniently rewritten as:

$$|\Psi_{\mathrm{MRCI}}\rangle = \sum_{Iv} C_{Iv}|\Phi_{Iv}\rangle + \sum_{Iva} C^a_{Iv}|\Phi^a_{Iv}\rangle + \sum_{Ivab} C^{ab}_{Iv}|\Phi^{ab}_{Iv}\rangle \tag{24}$$

The three parts consist of configurations I with spin-coupling pattern v which have zero, one- and two-particles located in external orbitals (a, b). By far the largest group are commonly the doubly external CSFs $|\Phi^{ab}_{Iv}\rangle$. Writing the MRCI wavefunction in form of Eq. (24) allows the formulation and implementation of very efficient MRCI algorithms [91,124–127].

Again, the excited configurations can either be determined by performing single- and double- excitations relative to each CSF in the reference space or in an internally contracted way by applying excitation operators to the entire zeroth order wavefunction. However, the determination of the matrix elements H_{IJ} is even more involved than in the case of MRPT since $\hat{H}_{\mathrm{BO}}$ contains one- and two-body terms while $\hat{H}^{(0)}$ is an effective one-body operator. The internally contracted MRCI method, attractive as its properties are, has turned out to be so complicated to realize that there is a single major program (MOLPRO) which can perform such calculations and even in this program a number of difficult CSFs is left uncontracted. One is thus faced with the problem of the explosive growth of the list of $|\Phi_I\rangle$'s if the excitations are performed relative to each individual reference CSF. The most efficient programs for this task are either based on the graphical unitary group approach (GUGA, as realized in the COLUMBUS program) or simply use single-determinants to span the $|\Phi_I\rangle$ space. In either case, calculations with 10^{10} CSFs can be performed with present day hard- and software. However, even this impressive number is rather quickly reached even for moderately large molecules and the calculations remain very time consuming. It is therefore tempting to truncate the list of $|\Phi_I\rangle$'s by only including those functions with interact appreciably with $|0\rangle$. This is the essence of the individually selecting approach pioneered by Buenker and Peyerimhoff [81,82] and Malrieu and co-workers [79,80]. There are many possible selection criteria [109]. For example, in the individually selecting MRCI program of the ORCA package, a CSF is included in the variational space if:

$$\frac{|\langle\Phi_K|\hat{H}_{\mathrm{BO}}|0\rangle|^2}{|\langle\Phi_K|\hat{H}^{(0)}|\Phi_K\rangle| - \langle 0|\hat{H}^{(0)}|0\rangle} \geq T_{\mathrm{sel}} \tag{25}$$

where T_{sel} is a user defined threshold. Experience indicates that it should not be larger than $10^{-5}\ E_{\mathrm{h}}$ in order to obtain reliable results. $T_{\mathrm{sel}} = 10^{-6}\ E_{\mathrm{h}}$ appears to yield results sufficiently close to the desired limit $T_{\mathrm{sel}} = 0$ at several orders of magnitude reduced computational effort. However, an estimate for the effect of the rejected configurations is necessary in order to obtain reliable results. The ingenious idea in the MRD-CI program of Buenker and Peyerimhoff was to obtain an estimate of E_{MRCI} ($T_{\mathrm{sel}} = 0$) by performing several calculations at finite T_{sel} and then to use extrapolation to $T_{\mathrm{sel}} = 0$ [82]. In the ORCA program, we have, nevertheless, chosen a different approach and obtain the missing correlation energy through second-order perturbation theory based on the MP partitioning described above:

$$\Delta E_{\mathrm{PT}} = \sum_{K\notin S} \frac{|\langle\Phi_K|\hat{H}_{\mathrm{BO}}|0\rangle|^2}{\langle\Phi_K|\hat{H}^{(0)}|\Phi_K\rangle - \langle 0|\hat{H}^{(0)}|0\rangle} \tag{26}$$

The sum is over the unselected CSFs (the selected CSFs constitute the 'S-space'). This equation would be fully correct, if the $|\Phi_K\rangle$ space would diagonalize $\hat{H}^{(0)}$ which is certainly not the case. However, one can still hope that Eq. (26) is a reasonable approximation since $\hat{H}^{(0)}$ is diagonally dominant and the nominators are guaranteed to be individually small due to the selection process. In practice, the selected space is typically not much larger than a few hundred thousand CSFs while the number of terms in the sum in Eq. (26) may reach 10^{11} or even 10^{12}.

The disadvantage of MRCI compared to MRPT procedures is the higher computational effort for the former due to the more complicated structure of $\hat{H}_{\mathrm{BO}}$ compared to $\hat{H}^{(0)}$. Seemingly, this extra effort is invested in higher accuracy since in MRCI one

obtains 'infinite order' results for the coefficients of the excited CSFs instead of a first-order perturbation estimate. However, there is a distinct disadvantage of MRCI procedures. This is the fact that MRCI (like all other forms of truncated CI) is not size consistent. Size consistency refers to the property that for two noninteracting fragments A and B the energy of the supersystem E(AB) = E(A) + E(B). This is the case for MRPT procedures with the MP partitioning if the reference space is chosen to have this property. For MRCI procedures this is unfortunately not the case which means that MRCI procedures deteriorate in quality for larger molecules and this is, in addition to the high computational effort, the main obstacle for the application of MRCI procedures to larger molecules. Since size consistency is brought about by disconnected higher excitations many procedures exist to correct for the lack of these excitations in MRCI. The simplest and most widely used is the multireference Davidson correction which reads [128]:

$$\Delta E_{\mathrm{D}} = (1 - W_0)(E_{\mathrm{MRCI}} - E_{\mathrm{CASSCF}}) \tag{27}$$

where W_0 is the weight of the reference space and $E_{\mathrm{MRCI}} - E_{\mathrm{CASSCF}}$ is the correlation energy calculated by the MRCI variational procedure. In summary, for individually selecting MRCI procedures, the final energy of a given state is:

$$E_{\mathrm{IS-MRCI}} = E_{\mathrm{MRCI}} + \Delta E_{\mathrm{PT}} + \Delta E_{\mathrm{D}} \tag{28}$$

It would clearly be much more satisfactory to build size-consistency directly and rigorously into the procedure. In the multireference case this is surprisingly difficult to achieve and multireference coupled-cluster procedures are still not commonplace. The best one is presently able to do are the ACPF [129] and AQCC [130] procedures which treat the unlinked terms in a crude and average way. Perhaps the most rigorous size-consistent method is the MCCEPA variant by Fink and Staemmler [131] which also uses an internally contracted FOIS and explores the elegant concept of pair-natural orbitals [122] to achieve substantial efficiency.

2.5. The spectroscopy oriented configuration interaction method

We have recently developed a simplified multireference method for the calculation of excitation energies and optical as well as magnetic spectra. The approach has been termed 'spectroscopy oriented configuration interaction' (SORCI) and combines elements of MRPT and MRCI. The main goal of the method is to achieve a *balanced* description of a predefined set of many electron states. In order to meet the objectives of efficiency, balance, accuracy and stability a combination of truncation techniques motivated and discussed in detail in ref. [68] is used. Briefly, the most important features of the method are (compare Fig. 1):

(a) The method is an uncontracted multireference treatment based on spin- (and potentially also space) symmetry adapted CSFs. It starts with the diagonalization of an initial reference space of the CAS or restricted active space (RAS) type using any type of input molecular orbitals. From this limited CI the most important configurations are selected if their contribution to any state is larger than a threshold T_{pre}. The selected space is rediagonalized to give the zeroth order wavefunctions for all states of interest. This reduction of the number of reference CSFs is necessary in order to keep the computational effort manageable. For $T_{\mathrm{pre}} = 10^{-2}$ the final reference space contains only the essential CSFs required for a physically sensible zeroth order description of the states of interest. For $T_{\mathrm{pre}} \leq 10^{-4}$ the errors due to the reference space selection become very small and are hardly visible in the final results.

(b) Single and double excitations relative to all selected references are performed and included in the "strongly interacting subspace" R' if their second order energy (at the MR-MP level) exceeds a second threshold T_{sel} as described above.

(c) Only configurations giving nonzero contributions to *energy differences* in second order perturbation theory are included in (the important concept of difference dedicated CI (DDCI); [84,85]). In the first iteration (vide infra) only configurations with up to two degrees of freedom are considered, in the second iteration up to three degrees of freedom are included (a degree of freedom is defined as a hole in the inactive orbitals or a particle in the external orbitals).

(d) The Hamiltonian in the basis of the reference CSFs and strongly interacting CSFs from the FOIS is diagonalized to give CI energies and wavefunctions. This step relaxes the reference space coefficients from their initial CASCI values and formally treats the dynamic correlation contributions from the most strongly interacting CSFs in the first-order interacting space (FOIS) to infinite order. This step also removes any potentially present intruder states which plagues methods relying entirely on perturbation theory.

(e) The effect of higher excitations is estimated by a multireference Davidson correction as described above.

(f) The effect of CSFs from the FOIS which are only weakly interacting with the reference space and therefore not included in the diagonalization step is estimated at the second-order MR-MP level using the relaxed and renormalized reference part of the CI wavefunctions as described above.

(g) The average density matrix of all states is computed and diagonalized in order to obtain approximate average natural orbitals (AANOs). AANOs with occupation numbers less than a third threshold T_{nat} are excluded from the treatment and those with an occupation number closer than T_{nat} to 2.0 are frozen for the subsequent calculation. This set of AANOs is designed to remove any bias that the initial set of MOs might have had. In addition it often drastically reduces the one-particle space. Since the computational effort grows with a high power ($\geq$4) of the size of the one-particle basis this may lead to computational savings of a several orders of magnitude.

(h) The whole calculation is repeated with the AANOs in place of the input MOs.

(i) If necessary, the effect of the neglected inactive double excitations is computed using second order MP perturbation theory using an internally contracted basis.

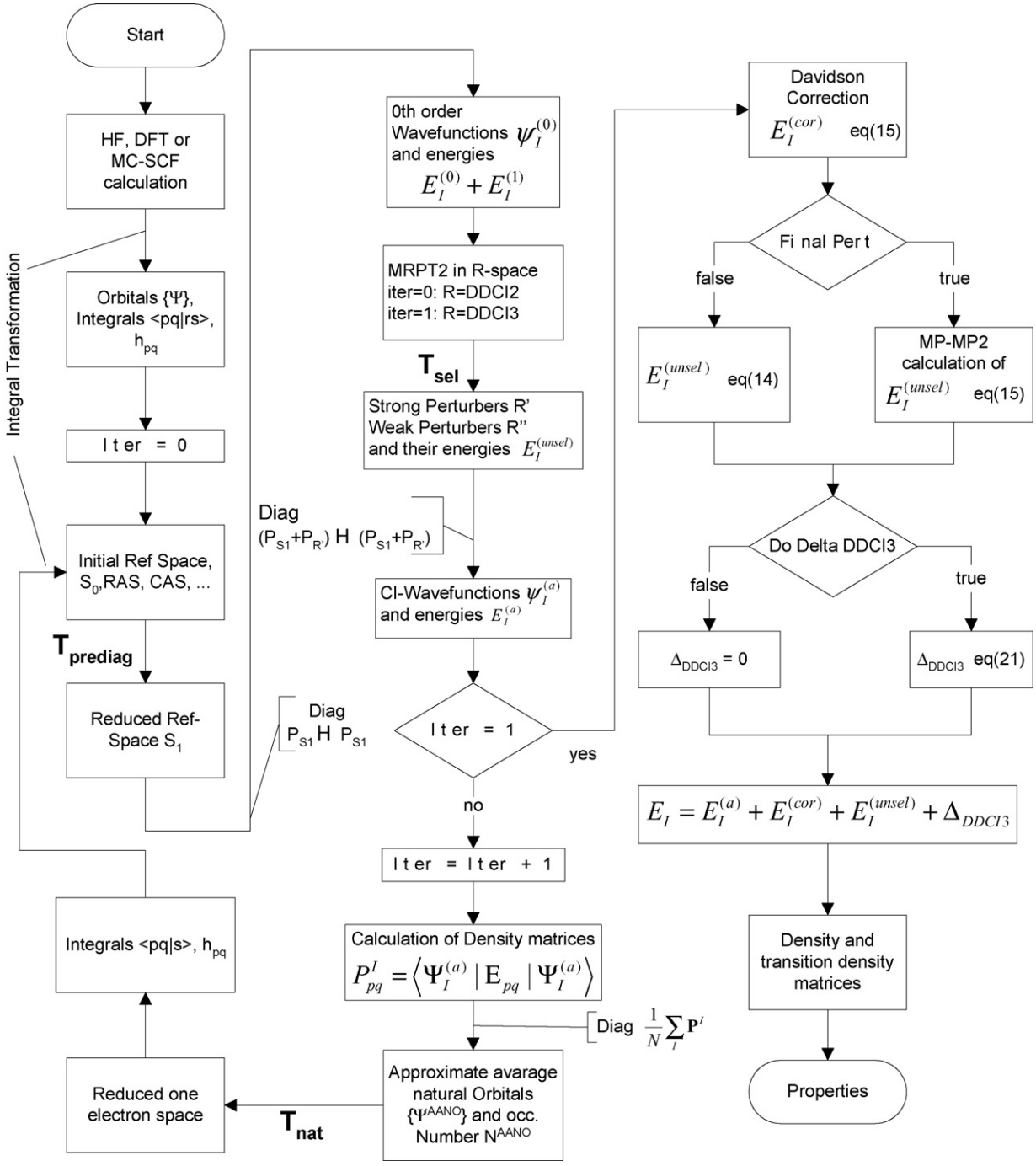

Fig. 1. Flowchart of the SORCI procedure. For details see ref. [68].

In the first iteration of this procedure the diagonalization of the CI matrix is feasible since the DDCI2 list only grows as $O(N_{Refs} \times N^2)$ compared to the prohibitive $O(N_{Refs} \times N^4)$ growth of the configuration list for the parent MRCI scheme. In the second iteration the diagonalization of the selected DDCI3 matrix remains feasible since the size of the significant AANO basis is often much smaller than the complete MO space. Since only the active space electrons are effectively correlated, the size consistency errors of the method are moderate. The SORCI wavefunctions still explicitly contain the leading dynamic and all static correlation effects which gives rise to the hope that the state and transition densities required for the computation of first- and second-order properties are reasonably accurate. This can, however, only be verified or disproved by test calculations or by comparison to highly accurate computational benchmark results.

The SORCI method has seen several successful applications [13,69–78] and is available in the ORCA package [67]. Below, we will present a benchmark study for the multiplets of transition metal ions and hexaquo complexes using the SORCI method.

2.6. Relativistic effects

Beyond the BO approximation a number of terms arise in the molecular Hamilton operator which describe relativistic effects and interactions of the electrons with external magnetic and electric fields. For molecules with not too heavy atoms (∼up to Krypton) these effects are of limited importance for the structure and bonding of molecules. They are nevertheless essential for correctly calculating spectral properties. Here we only deal with the two most important relativistic effects which are commonly (but not uniquely, see ref. [132]) subdivided into so-called scalar-relativistic and spin-orbit coupling (SOC) effects which are characterized by being spin-independent and spin-dependent, respectively [133].

2.6.1. Scalar relativistic effects

Close to the nucleus, electrons are moving close to the speed of light. This has severe influences on the shape of the effective potentials that the core electrons see. The 'relativistic potential' looks like an attractive interaction and therefore, core orbitals become much steeper and the core-orbital energies much lower. This mainly concerns the deep lying s- and p-levels but also propagates into the valence region where stabilization of s- and p-levels is also observed. The opposite effect is true for d- and f-electrons. These electrons effectively 'see' less of the nuclear charge since due to the contraction of the core-orbitals, the nuclear charge is more effectively shielded. Consequently, a destabilization of d- and f-levels is observed.

There are many different ways to deduce the correct form of the scalar relativistic equations. All of them start from the four-component Dirac equation and its generalization to *N*-electrons which is commonly at the simplest possible level, where the non-relativistic electron–electron repulsion is added to the one-electron Dirac terms and results in the *N*-electron Dirac-Coulomb operator. Full four component calculations can nowadays be done to high precision for small molecules and yield very accurate results when appropriate allowance is made for electron correlation effects (Dirac program [134]). However, for larger molecules further approximations are commonplace and yield computational formalisms with essentially the same computational cost as a standard nonrelativistic calculation.

The first step is to decouple the large- and small components through some approximate expansion procedure. The second step is to separate spin-dependent and spin-independent terms in the expansion which are then identified as spin-orbit and scalar-relativistic effects, respectively. If the SOC is included in the self-consistent field calculation, one ends up with so-called two-component schemes in which the SOC effects are treated on an equal footing with the remaining interactions. Two-component schemes may be thought of as generalizations of the *j–j* coupling scheme which is sometimes used in atomic theory.

The complete reduction of the four-component Dirac equation into one-component form requires either the neglect of SOC or its a posteriori treatment by perturbation theory or some other procedure. The resulting equations have the distinct advantage that most of the computational machinery developed for the non-relativistic case can be used with minor modifications. Except for cases with complete or near orbital degeneracy, perturbation theory for the SOC is a good approximation for the first 3–4 rows of the periodic table. The majority of scalar-relativistic one-component all-electron calculations are done in a way which only requires a modification of the one-electron matrix.

The oldest decoupling method is the Pauli-expansion of the Dirac equation in powers of $1/c^2$. This method has fallen into disuse due to the fact that the resulting scalar-relativistic operators (the Darwin- and mass–velocity terms) are not bounded from below and can therefore not be used in variational treatments. Presently, the two most widely used quasi-relativistic methods are the zeroth order regular approximation (ZORA [135]) and the Douglas–Kroll–Hess (DKH [136–138]) approach up to second-order in the external potential. Both methods are variationally stable but differ in many other aspects. The ZORA method has the disadvantage that it is not gauge invariant which causes certain problems in the calculation of electric properties and molecular gradients but is readily implemented otherwise [139,140]. (However, see [141]). Furthermore, the ZORA method has the defect that the core-orbital energies are much too low in energy. Procedures to correct for this shortcoming are known [142]. The formalism of the DKH approach is fairly involved, but at least to second order, it is also readily implemented, at least if the transformation of the electron–electron interaction terms are disregarded as is common practice [143,144].

In the ORCA program used in this work, both the ZORA and the second-order DKH method are implemented and usually yield similar relativistic corrections to molecular structures, energies and properties. In addition, an interface to the higher-order DKH module of Wolf, Reiher, and Hess [143] is available. ORCA features two ZORA implementations which closely follow the ideas by van Wüllen [139] and Filatov [140], respectively and yield identical results in the limit of infinite basis set and exact numerical integration. Furthermore, the extension of the ZORA approach to infinite order (IORA [145]) is available.

2.6.2. Spin-orbit coupling

The importance of SOC for the properties of transition metal ions has been recognized since the initial days of LFT. Indeed, LFT ideas with consideration of SOC effects have given a large amount of insight into the spectroscopic properties of transition metals ions. Most commonly, the SOC operator which has been employed was taken from the theory of atomic spectra [146] and is:

$$\hat{H}_{\mathrm{SOC-LFT}} = \lambda \boldsymbol{L}\boldsymbol{S} \tag{29}$$

where λ is some effective many-electron SOC constant, $\boldsymbol{L}$ the total orbital angular momentum operator and $\boldsymbol{S}$ is the total spin operator. Such an approach has several conceptual shortcomings. First, the many-electron SOC constant λ is ill defined for molecules since the molecular terms usually do not derive cleanly from atomic terms and ligand-SOC is neglected. Secondly, the operator in Eq. (29) will not mix states of different multiplicities, which, however, is one of the most important

effects of SOC. A slightly more satisfying approach is to use:

$$\hat{H}'_{\mathrm{SOC-LFT}} = \sum_i \xi(\boldsymbol{r}_i)\boldsymbol{l}_i\boldsymbol{s}_i \tag{30}$$

in which the orbital- and spin-operators for each electron i enter and $\xi(\boldsymbol{r}_i)$ is an operator which only depends on the distance of the electron from the nucleus. Owing to the presence of the individual rather than the total electron spin, this operator does mix states of different multiplicity and there is no ambiguity as to the origin and sign of $\xi(\boldsymbol{r}_i)$. In polyatomic molecules this SOC operator is readily generalized to [147]:

$$\hat{H}''_{\mathrm{SOC-LFT}} = \sum_A \sum_i \xi(\boldsymbol{r}_{iA})\boldsymbol{l}_i^A\boldsymbol{s}_i \tag{31}$$

Here, 'A' sums over all nuclei and $\boldsymbol{l}_i^A$ is the angular momentum of the ith electron relative to the Ath nucleus. This operator can be used in a ligand field as well as in an ab initio framework, if a suitable choice is made for $\xi(\boldsymbol{r}_i)$. The most popular form is:

$$\xi(\boldsymbol{r}_{iA}) = \frac{\alpha^2}{2}\frac{Z_A^{\mathrm{eff}}}{|\boldsymbol{R}_A - \boldsymbol{r}_i|^3} \tag{32}$$

where Z_A^{eff} is a semi-empirically chosen charge for nucleus A at position $\boldsymbol{R}_A$ and $\alpha \sim 1/137$ in atomic units is the fine structure constant. Semi-empirical values for Z_A^{eff} have been given by Koseki et al. [148–150] for most of the periodic table. Their disadvantage is that they are somewhat basis set dependent. Nevertheless, the effective nuclear charge approach performs reasonably well for the 2p- and 3d-elements but deteriorates in quality for the higher main group and heavier transition metals.

In order to arrive at a more satisfying ab initio SOC operator, one has to go back to the microscopic form of the SOC operator, most commonly in the Breit–Pauli (BP) approach [151–155]. The ZORA and DKH forms of the microscopic SOC operator are somewhat more complicated. However, a reasonable discussion is already possible on the basis of the BP operator. It includes one- and two-electron contributions:

$$\hat{H}_{\mathrm{BP}} = \hat{H}_{\mathrm{BP}}^{(1)} + \hat{H}_{\mathrm{BP}}^{(2)} \tag{33}$$

$$\hat{H}_{\mathrm{BP}}^{(1)} = \frac{\alpha^2}{2}\sum_i \sum_A Z_A r_{iA}^{-3}\hat{\mathbf{l}}_{iA}\hat{\mathbf{s}}_i \tag{34}$$

$$\begin{aligned}\hat{H}_{\mathrm{BP}}^{(2)} &= \hat{H}_{\mathrm{SSO}}^{(2)} + \hat{H}_{\mathrm{SOO}}^{(2)} \\ &= -\frac{\alpha^2}{2}\sum_i \sum_{j\neq i} r_{ij}^{-3}\hat{\mathbf{l}}_{ij}\hat{\mathbf{s}}_i - \sum_i \sum_{j\neq i} \alpha^2 r_{ij}^{-3}\hat{\mathbf{l}}_{ij}\hat{\mathbf{s}}_j\end{aligned} \tag{35}$$

Here $\hat{H}_{\mathrm{SSO}}^{(2)}$ and $\hat{H}_{\mathrm{SOO}}^{(2)}$ denote the spin-same orbit (SSO) and spin-other-orbit (SOO) contributions. $\hat{\boldsymbol{p}}_i$, $\hat{\mathbf{s}}_i$ stand for the momentum and the spin operator of the ith electron, and $r_{iA} = |\boldsymbol{r}_i - \boldsymbol{R}_A|$ is the distance between the electron i and the nucleus A. The angular momentum operator of the electron i calculated with respect to the nucleus A at the position $\boldsymbol{R}_A$ is defined as $\hat{\boldsymbol{l}}_{iA} = (\boldsymbol{r}_i - \boldsymbol{R}_A) \times \hat{\boldsymbol{p}}_i$. Similarly, $\boldsymbol{r}_{ij} = |\boldsymbol{r}_i - \boldsymbol{r}_j|$ represent the distance between the electrons i and j; $\hat{\boldsymbol{l}}_{ij} = (\boldsymbol{r}_i - \boldsymbol{r}_j) \times \hat{\boldsymbol{p}}_i$ symbolizes the orbital momentum operator of the electron i with respect to the position of the electron j. Boldface printed operators conventionally have three cartesian components x, y, z.

Usually the one-electron term of the BP Hamiltonian is the dominant contribution to the SOC matrix elements because of extensive cancellation between the two-center one- and two-electron terms. The one-electron term describes the interaction of the spin of electron i with the magnetic moment induced by the orbiting of the same electron in the nuclear electrostatic field. Although it is 'near-sighted' owing to the r^{-3} dependence, two- and three-center contributions cannot be neglected altogether if high accuracy is requested. Accordingly, the two-electron SSO term arises from the interaction of electron i with the magnetic moment induced by the movement of electron i in the field of electron j. The SOO term describes the coupling of the spin magnetic moment of electron i with the orbital magnetic moment of electron j and vice versa. These two terms provide screening of the one-electron term similarly to the contributions of the nuclear-electron attraction and electron–electron repulsion interactions in the BO Hamiltonian. The one-electron contribution to SOC grows rapidly with the nuclear charge, whereas the two-electron part increases more slowly as one moves down the periodic table.

Although the approximation free computational treatment of the BP Hamiltonian is certainly feasible (this was demonstrated by the works of several groups [156–162]), the direct utilization of the SOC operator in the form of Eqs. (33)–(35) is very demanding in terms of memory and computer time due to the large number of two-electron four-center integrals arising from Eq. (35). Therefore, suitable approximations could considerably increase the size of the systems which are feasible to treat and the speed of the calculations. One way to simplify Eq. (33) is to completely ignore the two-electron term. However, this approximation drastically overestimates SOC splitting [148] because the two-electron screening contribution is ignored. This would seem to immediately lead back to the effective nuclear charge SOC operator. In order to go beyond the accuracy of this method, an alternative approach suggested by Hess et al. is used [163]. It deals with the two-electron SOC contribution to the BP Hamiltonian by a mean-field approximation in a way which is analogous to the treatment of the electron–electron repulsion in the HF method (spin-orbit mean-field (SOMF) operator). Because the HF approach itself recovers 99.7–99.9% of the total non-relativistic energy, the SOMF scheme seems to be very attractive for the estimation of spectroscopic parameters since almost all SOC energy will be recovered and SOC effects are roughly four orders of magnitude smaller than electrostatic effects due to the α^2 dependence of the operator.

We have recently slightly reformulated and implemented the SOMF operator into the ORCA package [160,163,164] and will briefly sketch the working equations below. The goal of the SOMF treatment is to convert the BP-SOC Hamiltonian into effective one-electron form:

$$\hat{H}_{\mathrm{SOMF}} = \sum_i \hat{z}_i\hat{\mathbf{s}}_i \tag{36}$$

Given the first-order density matrix $\boldsymbol{P}$ for the state of interest (no matter whether it comes from a SCF, a correlated ab initio

or a DFT calculation), the density is:

$$\rho(\boldsymbol{r}) = \sum_{\mu,\nu} P_{\mu\nu}\phi_\mu(\boldsymbol{r})\phi_\nu(\boldsymbol{r}) \tag{37}$$

Employing the following notations:

$$\hat{\boldsymbol{h}}_i^{1\mathrm{el}-\mathrm{SOC}} = \frac{\alpha^2}{2}\sum_A Z_A r_{iA}^{-3}\hat{\boldsymbol{l}}_{iA} \tag{38}$$

$$\hat{\boldsymbol{g}}^{\mathrm{SOC}} = -\frac{\alpha^2}{2}\hat{\boldsymbol{l}}_{ij} r_{ij}^{-3} \tag{39}$$

and, omitting the full derivation [160,163,164], the final working equation for our SOMF implementation can be written as:

$$\begin{aligned}\langle\varphi_\mu|\hat{z}|\varphi_\nu\rangle = {} & \langle\varphi_\mu|\hat{\boldsymbol{h}}^{1\mathrm{el}-\mathrm{SOC}}|\varphi_\nu\rangle + (\varphi_\mu\varphi_\nu|\hat{\boldsymbol{g}}^{\mathrm{SOC}}|\rho) \\ & - \frac{3}{2}\sum_{\kappa\tau} P_{\kappa\tau}[(\varphi_\mu\varphi_\kappa|\hat{\boldsymbol{g}}^{\mathrm{SOC}}|\varphi_\tau\varphi_\nu) \\ & + (\varphi_\tau\varphi_\nu|\hat{\boldsymbol{g}}^{\mathrm{SOC}}|\varphi_\mu\varphi_\kappa)]\end{aligned} \tag{40}$$

From Eq. (40) it is apparent that the SOMF operator contains a one-electron, a Coulomb and an exchange part, very much like the spin-averaged HF operator in Eq. (12). However, the two-electron SOC integrals $(\varphi_\mu\varphi_\nu|\hat{\boldsymbol{g}}^{\mathrm{SOC}}|\varphi_\kappa\varphi_\tau)$ have less permutation symmetry than the corresponding electron–electron repulsion integrals in HF theory and therefore some care is required in the derivation and implementation. Computationally, the most expensive term is the Coulomb contribution $(\varphi_\mu\varphi_\nu|\hat{\boldsymbol{g}}^{\mathrm{SOC}}|\rho)$ for which efficient and accurate approximations were recently discussed [164]. There have been many successful applications of the SOMF concept [165–172] in the framework of the AMFI program developed by Schimmelpfennig [173]. The results suggest that the SOMF approach gives results roughly within a few wavenumbers of the full BP-SOC treatment which is considered to be fairly satisfactory given the strongly reduced computational effort. In the AMFI program two-additional approximations were introduced in that only one-center integrals are kept and the density entering the Coulomb and exchange contributions is taken from HF calculations on neutral atoms. Both approximations are largely avoided in the ORCA implementation and have recently been discussed in the framework of g-tensor calculations [164].

It is instructive to compare the SOMF operator with the 'effective potential' SOC operator commonly used in DFT programs. In this case, the spatial part of the effective one-electron operator is:

$$\langle\varphi_\mu|\hat{\boldsymbol{V}}^{\mathrm{eff}}|\varphi_\nu\rangle = \frac{\alpha^2}{2}\langle\varphi_\mu|\nabla V\times\hat{\boldsymbol{p}}|\varphi_\nu\rangle \tag{41}$$

Where the molecular potential V is interpreted to be the local Kohn–Sham potential used in the Kohn–Sham self-consistent field process which is given by

$$\begin{aligned}V_{\mathrm{KS}}(\boldsymbol{r}) = {} & -\sum_A \frac{Z_A}{|\boldsymbol{r}-\boldsymbol{R}_A|} + \int\frac{\rho(\boldsymbol{r}')}{|\boldsymbol{r}-\boldsymbol{r}'|}\mathrm{d}\boldsymbol{r}' \\ & + \frac{\delta E_{\mathrm{X}}[\rho]}{\delta\rho(\boldsymbol{r})} + \frac{\delta E_{\mathrm{C}}[\rho]}{\delta\rho(\boldsymbol{r})}\end{aligned} \tag{42}$$

The terms represent the electron-nuclear attraction, Coulomb potential, exchange potential and correlation potential, respectively. This operator is computationally attractive but has been criticized since it does not contain the SOO interaction and tends to overestimate SOC effects [171,174]. Schreckenbach and Ziegler have argued that the SOO interaction is small because a model system in which one unpaired electron interacts with a closed shell system leads to vanishing SOO contributions and that if there is more than one unpaired electron the effect is probably small [175]. However, the SOO contribution to the exchange has apparently not been considered by Schreckenbach and Ziegler and here the SOO contribution is large in the SOMF treatment, i.e. twice that of the SSO term. The one-electron term of the V^{eff} treatment is identical to the SOMF operator and the Coulomb potential leads to precisely the same SSO term as in the SOMF treatment. Since the SOO part to the Coulomb contribution is zero, these parts also agree. The contribution from the correlation potential has been shown to be negligible [164,175]. Thus, the only difference between the SOMF and V^{eff} SOC operators comes from the exchange part, where the V^{eff} treatment only models the SSO contribution to the SOMF treatment. However, since the SSO part is precisely equal to twice the SSO contribution to the exchange part in the SOMF derivation, a very simple and effective way of improving the V^{eff} SOC operator would be to scale its exchange part by +3. However, as has been shown in ref. [164], the DFT V^{eff} exchange contribution *is of the wrong sign* and from numerical experience, the best scaling is obtained by multiplying the V^{eff} exchange term by −2 (this has been referred to as $V^{\mathrm{eff}}(-2X)-\mathrm{SOC}$). It has been shown that this operator is indeed a good approximation to the SOMF operator and leads to significantly improved molecular SOC results at no extra cost compared to the conventional $V^{\mathrm{eff}}-\mathrm{SOC}$ operator. However, since the SOMF operator is also readily implemented and evaluated there is no need for further approximations. It should be stressed that the V^{eff} operator yields results which are in error by as much as 30% compared to the more accurate SOMF treatment. These errors sometimes partially cancel with other errors made in DFT procedures.

3. Calculation of multiplets

3.1. Introduction

In this section, the CASSCF and SORCI methods are applied to the calculation of the atomic and molecular multiplets of di- and tri-valent transition metal ions and hexaquo-complexes. While it would be feasible to obtain more accurate results with larger basis sets, the purpose of this section is to document the performance of the models if basis sets of moderate size are used that can also be used for calculations on larger molecules. The basis sets are, nevertheless, of polarized triple-ζ quality and are consequently large enough to meaningfully assess the quality of the methods themselves.

The calculation of multiplets is not a simple undertaking as the majority of atomic and molecular multiplet components are inherently multideterminantal (though not necessarily multiconfigurational) in character. This poses problems for all methods

that are based on a single reference determinant such as DFT and standard single-reference correlation models such as many-body perturbation or coupled cluster theory. Hybrids between ligand-field theory and DFT have been put forward for the calculation of multiplet structures [176–179] and have also shown some success. They do, however, not follow naturally from rigorous DFT theory and will therefore not be reviewed here.

Multiplets can be described in a natural and straightforward way if the restrictions imposed by a single reference determinant are lifted and a multiconfigurational treatment is used for the underlying self-consistent field calculation. In this section, the calculations are based on SA-CASSCF wavefunctions. Since the CASSCF calculations do not include any dynamic correlation, some remaining errors are expected. These errors can be large enough to require the use of a multiconfigurational method which recovers at least the differential dynamic correlation effects. In this section, the SORCI method is used for this purpose which should allow a fair assessment of its strengths and weaknesses for such multiplet calculations.

The di- and trivalent transition metal hexaquo-species provide a 'classic' series for the prediction of d–d spectra. However, with the exception of the INDO/S work of Andersson et al. [29], we are not aware of a systematic theoretical study of their d–d spectra.

3.2. Computational details

3.2.1. Basis sets

After some preliminary calculations we decided to employ the following combination of basis sets for the actual computations, henceforth denoted as the standard basis: On the metal centers the basis set of Wachters [180] was used, together with the polarization set of Bauschlicher et al. [181] (altogether (14s11p6d3f) → [8s6p4d2f]). On the oxygens we used the TZV basis [182] with a (2d) polarization set [183] such that a (11s6p2d1f) → [5s3p2d] basis set arose; for the hydrogen atoms the TZVP (5s1p) → [3s1p] set was used. Since the SORCI method makes use of the resolution of the identity (RI) approximation [184–188] to approximate the numerous four-index electron–electron repulsion integrals over molecular orbitals, an auxiliary basis set is necessary. In this work, the auxiliary basis optimized for RI-MP2 calculations with the TZVP basis set optimized by Weigend et al. [102,103] were used. They are of the following size: metals: 9s8p7d6f4g, oxygen: 8s6p4d3f1g, hydrogen: 4s3p2d1f. All calculations were done with the ORCA program package [67].

3.2.2. CASSCF calculations

The reference wavefunctions were of the SA-CASSCF type. Depending on the context, the active space consistent of the five metal d-orbitals or the five metal-d-orbitals together with the 4s orbital (i.e. CAS (n, 5) and CAS (n, 6), respectively). The average was taken over all target states and multiplicities.

3.2.3. SORCI method

The SORCI method introduces three thresholds, which control the size of the reference space (T_{pre}), the size of the strongly interacting and variationally treated subspace (T_{sel}) and the size of AANO basis (T_{nat}). Based on a previous calibration study [71] we have modified the original default parameters [68] to $T_{pre} = 10^{-4}$, $T_{Sel} = 10^{-6}$ Eh and $T_{nat} = 10^{-5}$ which should provide results within 0.1 eV of the methods limit when all parameters are set to zero. Since any individual selection procedure leads to slight breakings of the degeneracy of orbitally degenerate states we report the arithmetic mean of the individual components in such cases. The symmetry breaking effects were typically $\leq 20\,cm^{-1}$. Core electrons were frozen in the calculations but the 3sp electrons were included which essential for obtaining accurate results. No virtual orbitals were rejected.

Table 1
The metal-ligand bond distances (in Ångström) used in the present study

	Divalent [189]	Trivalent [190]
Ti	–	2.028
V [191]	2.128	1.992
Cr [191]	2.052	1.959
Mn	2.192	1.991
Fe	2.114	1.995
Co	2.106	1.873
Ni	2.061	–
Cu [191]	1.964	–

3.2.4. Geometries

Since the present study represents a survey study we have decided to base our computations on idealized geometries of T_h symmetry with metal ligand distances taken from experimental studies (Table 1). Such an approach neglects low-symmetry distortions by the environment as well as Jahn–Teller distortions which occur in orbitally degenerate ground states. However, for Cr(II), Cu(II) and Mn(III) the Jahn–Teller distortions are too large to be ignored and in these cases only limited agreement with measured spectra can be expected. For the water molecules an standard arrangement of r(O–H) = 0.9817 Å and of a HOH angle of 107.7° was assumed.

3.2.5. Multiplets in octahedral symmetry

Within the metal d-shell the following terms summarized in Table 2 arise and are commonly classified under O_h symmetry. Some higher lying terms which exist have not been considered due to the lack of experimental data.

3.3. Results for 'naked' transition metal ions

In the first step of the calibration procedure, we have studied the performance of the SORCI method for the well-known spectra of the 'naked' dipositive and tripositive transition metal ions. These spectra are known to be notoriously difficult to describe with ab initio methods. The results are compared in Table 3 to the experimental multiplet energies that were taken from the NIST tables [192]. Since we do not include spin-orbit coupling in the calculations, the "experimental" values refer to degeneracy-weighted multiplet averages, according to [77]:

$$\bar{E}(L, S) = \frac{\sum_J (2J+1) E(J, L, S)}{\sum_J 2J+1} \quad (43)$$

Table 2
Terms in the d^N series which arise from d–d excitations considered in this work

d^N	Ground term		Spin-allowed transitions	Spin-forbidden transitions
	O_h	Configuration		
d^9	^2E_g	$t_{2g}^6e_g^3$	$^2T_{2g}(t_{2g}^5e_g^4)$	None
d^8	$^3A_{2g}$	$t_{2g}^6e_g^2$	$^3T_{2g}(t_{2g}^5e_g^3)$ $^3T_{1g}(t_{2g}^5e_g^3)$ $^3T_{1g}(t_{2g}^4e_g^4)$	$^1E_g(t_{2g}^6e_g^2)$ $^1T_{2g}(t_{2g}^5e_g^3)$
d^7	$^4T_{1g}$	$t_{2g}^5e_g^2$	$^4T_{2g}(t_{2g}^4e_g^3)$ $^4T_{1g}(t_{2g}^4e_g^3)$ $^4A_{2g}(t_{2g}^3e_g^4)$	$^2E_g(t_{2g}^6e_g^1)$ $^2A_{2g}(t_{2g}^5e_g^2)$ $^2T_{2g}(t_{2g}^5e_g^2)$
d^6	$^5T_{2g}$	$t_{2g}^4e_g^2$	$^5E_g(t_{2g}^3e_g^3)$	$^3T_{2g}(t_{2g}^5e_g^1)$
d^5	$^6A_{1g}$	$t_{2g}^3e_g^2$	None	$^4T_{1g}$, $^4T_{2g}$ $(t_{2g}^4e_g^1)$ $^4A_{1g}$, ^4E_g, $^4T_{2g}(t_{2g}^3e_g^2)$
d^4	^5E_g	$t_{2g}^3e_g^1$	$^5T_{2g}(t_{2g}^2e_g^2)$	$^3T_{1g}(t_{2g}^2e_g^2)$
d^3	$^4A_{2g}$	$t_{2g}^3e_g^0$	$^4T_{2g}(t_{2g}^2e_g^1)$ $^4T_{1g}(t_{2g}^2e_g^1)$ $^4T_{1g}(t_{2g}^1e_g^2)$	$^2E_g(t_{2g}^3)$ $^2T_{1g}(t_{2g}^3)$
d^2	$^3T_{1g}$	$t_{2g}^2e_g^0$	$^3T_{2g}(t_{2g}^1e_g^1)$ $^3T_{1g}(t_{2g}^1e_g^1)$	$^1E_g(t_{2g}^2)$ $^1T_{2g}(t_{2g}^2)$ $^1A_{1g}(t_{2g}^2)$
d^1	$^2T_{2g}$	$t_{2g}^1e_g^0$	$^2E_g(t_{2g}^0e_g^1)$	None

where $\bar{E}(L, S)$ is the averaged energy of a given L, S term and $E(J, L, S)$ is the energy of each individual total angular momentum ($J = L + S$) component for each multiplet. The averaging gives corrections of at most a few hundred wavenumbers compared to the transition energy between the two lowest J-components of the ground- and excited states under investigation.

Upon inspection of Tables 3 and 4, which summarize the results for the multiplets in d^n configurations, it is evident that the SA-CASSCF method already captures the majority of the mul-

Table 3
Comparison of calculated and experimental transition energies between multiplets of dipositive transition metal ions

Configuration	Term	SA-CASSCF	SORCI	Exp.
d^2 (^{3}F)	^{1}D	11014	8452	8470
	^{3}P	13321	10205	10620
	^{1}G	17231	15187	14400
	^{1}S	42546	31476	32480
d^3 (^{4}F)	^{4}P	14637	11308	11710
	^{2}G	14746	12750	12090
	^{2}P	19625	16042	15560
	^{2}D	19625	16110	16360
	^{2}H	19625	18250	16910
d^4 (^{5}D)	^{3}P	22154	18260	17680
	^{3}H	19861	18481	17430
	^{3}F	22835	19761	18540
	^{3}G	25139	22495	20890
d^5 (^{6}S)	^{4}G	32289 (32348)	29540 (29475)	26860
	^{4}P	37279 (37347)	31824 (31356)	29210
	^{4}D	40215 (40289)	35703 (35590)	32380
d^6 (^{5}D)	^{3}P	24999	21590	19730
	^{3}H	22416	22758	20230
	^{3}F	25774	23600	21600
	^{3}G	28383	27400	24800
d^7 (^{4}F)	^{4}P	18854	15840	15300
	^{2}G	18950	18358	17280
	^{2}P	25235	22500	20320
	^{2}H	25235	24843	23010
	^{2}D	27420	24042	23410
d^8 (^{3}F)	^{1}D	16366	14955	14030
	^{3}P	19833	17039	16830
	^{1}G	25622	24530	23110
$\Delta_{mean-unsigned}$		3929	1295	
$\Delta_{mean-signed}$		3929	1146	
Δ_{max}		10071	3328	

Table 4
Comparison of calculated and experimental transition energies between multiplets of tripositive transition metal ions

Configuration	Term	SA-CASSCF	SORCI	Exp.
d^2 (^{3}F)	^{1}D	13598	10905	10960
	^{3}P	16323	12689	13400
	^{1}G	21215	19230	18390
	^{1}S	52488	41709	42260
d^3 (^{4}F)	^{4}P	17506	13716	14370
	^{2}G	17781	15832	15270
	^{2}P	23616	19911	19450
	^{2}D	25700	20233	20660
	^{2}H	23616	22533	20660
d^4 (^{5}D)	^{3}P	26289	21768	22960
	^{3}H	23539	23125	21530
	^{3}F	27065	23520	22900
	^{3}G	29743	26775	25730
d^5 (^{6}S)	^{4}G	37679 (37739)	35764 (34844)	32280
	^{4}P	43559	36232	35310
	^{4}D	46872	41861	38870
d^6 (^{5}D)	^{3}P	28976	22787	23350
	^{3}H	25954	26303	23920
	^{3}F	29843	26221	25590
	^{3}G	32813	31396	28810
d^7 (^{4}F)	^{4}P	21503	18449	18240
	^{2}G	21752	20627	20260
	^{2}P	28920	23127	23820
	^{2}H	28920	28705	26910
	^{2}D	31453	26627	27600
d^8 (^{3}F)	^{1}D	18651	15833	16250
	^{3}P	22486	19664	19800
	^{1}G	29145	28141	26910
$\Delta_{mean-unsigned}$		4143	615	
$\Delta_{mean-signed}$		4143	1069	
Δ_{max}		10226	3484	

tiplet effects albeit with rather limited accuracy (average error $\sim$4000 cm^{-1} and maximum error $\sim$10,000 cm^{-1}). The errors are reduced by a factor of 3–4 by the SORCI method. The SORCI errors for the di- and tripositive ions average to $\sim$1100 cm^{-1} which is in the desired accuracy range of 0.1–0.2 eV relative to experiment. In both cases, the major errors come from the ions with five and six d-electrons.

In general, it was found that the errors of the method increase with increasing numbers of unpaired electrons and also for higher orbital angular momentum multiplets. We speculate that the main defects come from a disturbingly slow convergence of the differential dynamic correlation with basis set size. However, for Mn^{2+} (d^5) calculations with the much larger QZVP basis set (24s18p10d3f1g contracted to 11s6p5d3f1g) yield transition energies which are only very slightly improved at the SORCI level. We have therefore also considered the possibility that not enough dynamic correlation was recovered and have carried out additional calculations using the MR-MP2 method on top of the CASSCF wavefunction. These calculations should yield results very close to those obtained by the CASPT2 method, the main difference being that the internally contracted FOIS of the CASPT2 method is replaced by an individually selected uncontracted FOIS ($T_{sel} = 10^{-8}$ Eh was used in these calculations). The MR-MP2 calculations together with the QZVP basis set yielded transition energies of 29,570; 31,880 and 35,530 cm^{-1} to the ^{4}G, ^{4}P and ^{4}D states, respectively. These numbers are virtually identical to the SORCI results with the same basis. In order to recover even more dynamic correlation, the perturbation treatment was extended to fourth order (MR-MP4 [193]). These calculations yielded transition energies of 28,440; 31,160 and 34,440 cm^{-1}, a small but consistent improvement over the SORCI and MR-MP2 results. Finally, if all electrons are correlated in MR-MP2 calculations with the QZVP basis set, the transition energies become 27,620; 29,370 and 32,750 cm^{-1} which are now in excellent agreement with the experimental values. Thus, core-correlation beyond the contribution of the 3sp is another important factor for a truly quantitative prediction of transition metal multiplets. The SORCI method also profits from the inclusion of the core orbitals. With the Wachters basis, the calculated transition energies are 28,970; 29,740 and 33,890 cm^{-1} to the ^{4}G, ^{4}P and ^{4}D which are in distinctly better agreement with experiment than the values in Table 3.

It is interesting to compare these results to numbers reported in the literature for the ^{6}S–^{4}G splitting in Fe^{3+} (d^5). It has been calculated to be 35,640 cm^{-1} by CCSD(T) [194] and 33,640 cm^{-1} by CASPT2 [194] and 33,370 cm^{-1} by ACPF [194] compared to 32,280 cm^{-1} observed experimentally and 35,760 cm^{-1} from SORCI. However, the SORCI result was obtained with a much smaller basis set. Using the extensive QZVP basis set, the SORCI prediction for the position of the ^{4}G state becomes 34,840 cm^{-1}. Inclusion of scalar relativistic effects through the DKH2 procedure further lowers the transition energy to 34,680 cm^{-1}. Finally, the simultaneous inclusion of core-correlation, scalar relativistic effects and the QZVP basis yields the best SORCI value of 33,480 cm^{-1}. While this value is as good as the best CASPT2 and ACPF results, the QZVP basis set is too large for standard applications in molecules. Likewise, the MR-MP4 method is computationally too expensive for standard applications and also suffers from the intruder state problem to at least the same extent as CASPT2 and MR-MP2. Nevertheless, these results once more document that extensive dynamic correlation treatments are necessary in order to predict the states of transition metal ions to high accuracy.

Table 5
Comparison of calculated and experimental 3d → 4s excitation energies energies for dipositive ions

Configuration	Excitation	SA-CASSCF	SORCI	Exp.
d^1	$^2D(d^1s^0) \rightarrow {}^2S(d^0s^1)$	28245	23503	25420
d^2	$^3F(d^2s^0) \rightarrow {}^3D(d^1s^1)$	43232	38140	38040
d^3	$^4F(d^3s^0) \rightarrow {}^4F(d^2s^1)$	47417	45420	44010
d^4	$^5D(d^4s^0) \rightarrow {}^5F(d^3s^1)$	48680	51530	49670
d^5	$^6S(d^5s^0) \rightarrow {}^6D(d^4s^1)$	55658	66425	63050
d^6	$^5D(d^6s^0) \rightarrow {}^7S(d^5s^1)$	22844	30026	29670
d^7	$^4F(d^7s^0) \rightarrow {}^6D(d^6s^1)$	41031	48850	46160
d^8	$^3F(d^8s^0) \rightarrow {}^5F(d^7s^1)$	47665	57710	53840
d^9	$^2D(d^9s^0) \rightarrow {}^4F(d^8s^1)$	56953	68900	61280

Calculated 3d → 4s excitation energies are collected in Table 5. Their quality is comparable to the results obtained for the d^n multiplets. The occasionally large errors of the SA-CASSCF method are nearly quantitatively corrected by the SORCI procedure with the exception of the d^9 configuration where the CASSCF result is largely overcorrected and the predicted transition energy is in error by the unusually large amount of 7000 cm^{-1}. However, this is a fairly high-energy transition and one may face again the limitations of the basis set in this case.

From the results of this section it is concluded that the SORCI method based on SA-CASSCF wavefunctions give a fairly accurate description of the various d^n and d → s multiplets in di- and tripositive transition metal ions. The typical accuracy is $\sim$0.1–0.2 eV in the transition energies. Some larger errors occur for increasing numbers of unpaired electrons and higher angular momentum states. Both deficiencies are mainly related to the one-particle basis set and in these cases the convergence of the differential dynamic correlation energy is very slow. In addition, core-correlation even beyond the contributions from the 3sp shell may make contributions as large as $\sim$2000 cm^{-1} to the transition energies.

3.4. Results for hexaquo complexes

3.4.1. Multiplets and configurations

3.4.1.1. Convergence of the results. Before discussing the results obtained for the series of transition metal ions it is important to test the influence of the various approximations made on the results. As a prototypical test case we have chosen the hexaquo–Ni(II) complex. Similar results are obtained for other ions. For historical reasons, the results of this subsection were obtained based on spin-averaged Hartree–Fock (SAHF) orbitals [195,196] which yield very similar results compared to the more elaborate CASSCF treatment used in the remainder of the study.

3.4.1.1.1. The spectrum of $[Ni(H_2O)_6]^{2+}$. The absorption spectrum of $[Ni(H_2O)_6]^{2+}$ consists of three dominant bands of

Table 6
Comparison of the transition energies (in cm^{-1}) of the Ni(II) complex using different approximations

Approximation	$^3T_{2g}$	$^3T_{1g}$	$^3T_{1g}$	^1E_g	$^1T_{2g}$	Deviation[a]
Standard geometry	7820	13299	25841	16025	22986	607
Optimized geometry	7405	12580	24900	16111	22742	774
Scalar-relativistic effect[b]	7947	13476	25943	15948	23061	566
Solvent effect[c]	7724	13109	25737	16389	22922	703
RAS reference space[d]	8355	13926	26311	16331	23773	857
Higher thresholds	7214	12272	25348	16356	22889	881
Lower thresholds	8079	13725	25545	15237	23080	427
TD-DFT (B3LYP)	11937	19241				
Exp.[e]	8500 ± 1200	13500 ± 1100	25300 ± 1500	15400 ± 1200	22000 ± 1200	

[a] Average absolute deviation from the experimental values.
[b] Computed with the second-order Douglas–Kroll–Hess method.
[c] Computed with the COSMO solvent model and $\varepsilon = 80$ to simulate an aqueous solution.
[d] Larger reference space which includes the metal 3s, and 3p orbitals.
[e] Data from ref. [215].

typical intensity for spin-allowed d–d excitations. They were assigned to the three spin-allowed transitions from the $^3A_{2g}$ ground term to $1-{}^3T_{2g}$, $1-{}^3T_{1g}$ and $2-{}^3T_{1g}$, respectively. While $1-{}^3T_{2g}$ arises from a $t_{2g} \rightarrow e_g$ single-excitations, the two $^3T_{1g}$ states are heavy mixtures of $t_{2g} \rightarrow e_g$ single- and double-excitations. The assignment of the spin-forbidden transitions is more subtle in this system. From a very detailed analysis of the fine structure of the $1-{}^3T_{1g}$ transition and its temperature dependence, Solomon and Ballhausen [197] assigned the spin-forbidden $^3A_{2g} \rightarrow 1-{}^1E_g$ transition to the high-energy shoulder of the split $1-{}^3T_{1g}$ band. The unusually high intensity of this spin-forbidden excitation is attributed to efficient spin-orbit coupling with the $^3T_{1g}$ state. A similar conclusion was reached in a MCD study by Thomson and co-workers [198,199]. On the low-energy side of the $^3A_{2g} \rightarrow 2-{}^3T_{1g}$ transition an additional shoulder is observed in the experimental spectrum at $\sim$22,000 cm^{-1} which was assigned to the $^3A_{2g} \rightarrow {}^1T_{1g}$ spin-forbidden excitation by Thomson and co-workers [198,199]. Thus, the d–d excited states of $[Ni(H_2O)_6]^{2+}$ appear to be well understood. Since spin-allowed and spin-forbidden excitations as well as single- and double-excitations are observed and in addition since the ground state is orbitally non-degenerate the system is particularly well suited for calibrating the theoretical methodology below.

3.4.1.1.2. Geometry dependence. To check for the precision of the standard geometries, the geometry of the $[Ni(H_2O)_6]^{2+}$ was optimized at the BP86/TZVPP level and the transition energies were recalculated. Ni–O distances of 2.078 Å, O–H distances of 0.975 Å, and an HOH angle of 108.11° were obtained which are in acceptable agreement with the standard geometry. The transition energies computed with the standard and optimized geometries are quite close to each other and show average deviations of 607 cm^{-1} and 774 cm^{-1} from the experimental values, respectively. Thus, the standard geometries are acceptable a good choice for this study.

3.4.1.1.3. Scalar relativistic effects. A possible source of error in the study of transition metal complexes could be the neglect of relativistic effects. Thus, we performed a SORCI calculation with inclusion of the scalar-relativistic second-order Douglas–Kroll–Hess (DKH2) approximation [136–138,143,144,200]. In this approach, only the one-electron part of the Hamiltonian is decoupled to the second order in external potential which has been found to be satisfactory for the description of valence states in a number of studies [144,201–203]. As seen in Table 6, the scalar relativistic effects calculated with this method are fairly limited. They amount to $\sim$100 cm^{-1} on the transition energies and perhaps slightly improve the agreement with experiment (the mean absolute deviation drops from 607 to 566 cm^{-1}).

3.4.1.1.4. Solvent effects. Since the calculations always refer to isolated molecules while the experimental data are obtained in condensed phases, it is important to have at least a rough estimate of the effects of the environment. This is expected to be especially important for anions, which have very diffuse charge densities but less critical for the cations studied in this work. A straightforward way to crudely describe such effects is the use of continuum solvation models [204]. We have recently implemented and tested the conductor like screening (COSMO [205]) model into our MR-CI program and have obtained fairly accurate predictions of solvent shifts in aprotic media [206]. In cases where specific hydrogen bonding effects are important it is, however, necessary to include a few solvent molecules explicitly in the quantum chemical calculation. However, in the present case, the transitions under investigation are well localized on the metal center and consequently, the introduction of a polar, unstructured environment appears to be sufficient [207]. The results in Table 6 indicate that the computed shifts are only of the order of $\sim$100 cm^{-1} and do not improve the agreement with the experimental values.

3.4.1.1.5. Reference space. In all CI calculations presented until now we used the 'minimal' CAS (*N*,5) reference space which correlates primarily the 3d-electrons involved in the transitions under investigation. In order to extend the treatment to the correlation of the 3s3p electrons a more extensive RAS reference space was constructed in which double excitations out of the 3s and 3p-orbitals into were allowed in the reference space. Again, the effect on the transition energies is remarkably small and amounts to less than 100 cm^{-1} with a mean absolute deviation of 857 cm^{-1} to experiment.

3.4.1.1.6. Thresholds. Perhaps the most important parameter is the convergence of the results with respect to the three thresholds introduced into the SORCI procedure. Previous test calculations [71] suggested standard values of 10^{-4}, 10^{-6} Eh and 10^{-5} for these parameters. To further check for the influence of the thresholds two additional sets of calculations were performed, one with all three parameters one order of magnitude larger, the other with all parameters one order of magnitude smaller than the default values. The results in Table 6 show the expected pattern: the calculations with looser thresholds lead to slightly larger deviations from the experimental values than the standard parameters while the tighter thresholds give somewhat better agreement. The achieved average absolute deviation of only 427 cm^{-1} shows the intrinsically high accuracy of the SORCI methods. However, since the results with the standard thresholds are already quite good and obtained at much lower computational cost, they were kept for the remainder of the study.

3.4.1.1.7. Comparison to TD-DFT. The last issue we want to discuss shortly pertains to why we used such a complicated CI procedure instead of the popular TD-DFT. Thus, we performed a TD-DFT calculation within the Tamm–Dancoff approximation (TDA) for the $[Ni(H_2O)_6]^{2+}$ complex using the B3LYP functional [208–210] and the same basis sets as in the SORCI calculations. The results in Table 6 demonstrate several shortcomings of the TD-DFT approach. First, the calculated transition energies are much worse than those of the SORCI calculations and the errors exceed 5000 cm^{-1}. Second, the TD-DFT method is even incapable of predicting the correct number of d–d transitions in this complex. The second $^3T_{1g}$ state is not obtained. The reason for this is clear from the basic ligand field discussion above: The two $^3T_{1g}$ states contain substantial $t_{2g} \rightarrow e_g$ single- as well as double-excitation character. Such double excitations cannot be described with the TD-DFT method within the constraints of the adiabatic approximation [52]. Procedures to overcome these difficulties have been suggested (for a review see [59]). Third, the description of the spin-forbidden excitations based on TD-DFT methods is not evident (however, see recent results by Ziegler and co-worker [211] and the combined DFT/LFT procedures such as proposed by Atanasov et al. [176,177]). In addition to these results, we have found in many TD-DFT calculations on transition metal hexaquo species that in particular non-hybrid functionals which lack the HF exchange tend to give water-to-metal LMCT transition at unphysically low energies. This is a well known defect of TD-DFT (among others [212–214]) which has been reported in a number of studies (for a review see [59]). From these admittedly rather superficial discussion, we may conclude that TD-DFT should only be applied with great care to the calculation of the absorption spectra of transition metal complexes and we will not pursue it further in this work.

3.4.1.1.8. Summary. From the data collected in Table 6 we conclude that the SORCI method with the standard basis set, standard geometries based on experimental values, a minimal CAS (*N*, 5) reference space and the standard threshold values leads to rather good transition energies. The inclusion of relativistic corrections, continuum dielectric corrections to simulate the condensed phase, larger basis sets and tighter thresholds all do not change this agreement by more than 100–200 cm^{-1}.

3.4.2. Results for complexes

In this section the calculated transition energies of the hexaquo complexes of di- and trivalent transition metal complexes are presented and compared with experimental values [1,216]. Wherever possible, we did take into account spin-forbidden transitions.

Our results are summarized in Table 7, where comparison to experimentally estimated transition energies is made. It should be noted that the experimental transition energies have been inferred from band maxima and do not strictly correspond to the vertical transition energies calculated here (vide infra). In addition, any low-symmetry and environmental effects have been neglected in the present study. We nevertheless believe, that the results are still indicative of the typical accuracy with which transition metal d–d spectra can be predicted by the employed methodology.

As seen from Table 7 the results for hexaquo-complexes follow closely the trends observed for the same methodology for the free ions. The CASSCF results are qualitatively reasonable but show some large errors all of which are consistent with an overestimation of electronic repulsion and an underestimation of the ligand field splitting. These errors are almost quantitatively reduced by the SORCI method which gives, with a few exceptions discussed below, accurate results for the hexaquo-complexes studied. In particular, in the cases where the CASSCF results are already good, the SORCI method usually yields very accurate results. In the cases where the CASSCF method has large errors, the SORCI values always represent a large improvement but does not fully correct the CASSCF deficiencies.

3.4.2.1. d^1 Configuration. $[Ti(H_2O)_6]^{3+}$ is a classic example for ligand field transitions. Despite the experimentally observed Jahn–Teller Splitting of ~2500 cm^{-1} in the excited ^2E_g state, the complex was calculated in T_h symmetry (Table 7). The error in the calculated transition energy is only ~700 cm^{-1} compared to the average transition energy of 18,800 cm^{-1}. The complexes containing d^1 and d^2 ions generally exhibit static trigonal Jahn–Teller distortions in crystals which lead to symmetry lowering to D_{3d} symmetry [220,221]. Despite this fact, we used models with T_h symmetry since the distortions are not exceedingly large and the small additional splitting is not the focus of the present investigation.

3.4.2.2. d^2 Configuration. The $^3T_{1g}(t_{2g}{}^2e_g^0)$ ground term in the d^2 configuration is also Jahn–Teller active, but the t_{2g} Jahn–Teller splitting is not exceedingly large such that $[V(H_2O)_6]^{3+}$ was also studied in T_h symmetry. Two spin-allowed transitions to orbitally triply degenerate multiplets with $(t_{2g}^1)(e_g^1)$ configuration are expected and calculated in excellent in agreement with experiment. Using large ANO basis sets, Daniel and co-workers [222] calculated the $^3T_{2g}$ and $^3T_{1g}$ states at 9660 and 23,680 cm^{-1} with the CASSCF method and 9830 and 19,930 cm^{-1} with CASPT2; the errors are much larger than those obtained with the SORCI method.

Table 7
Comparison of calculated (CASSCF and SORCI levels) and experimental transition energies (in cm^{-1}) for di- and trivalent first row transition metal hexaquo complexes in T_h symmetry (symmetry labels correspond to O_h; solution data taken from Griffith [1] (Table A.40) and Holmes and McClure [216] unless otherwise noted)[a]

		$[M(H_2O)_6]^{2+}$			$[M(H_2O)_6]^{3+}$		
		CASSCF	SORCI	Exp.	CASSCF	SORCI	Exp.
$d^1(^2T_{2g})$	$^2E_g(t_{2g}^0e_g^1)$	–	–	–	16685	17880	~20300[b] Ti^{3+}
$d^2(^3T_{1g})$	$^3T_{2g}(t_{2g}^1e_g^1)$	–	–	–	14761	16830	17100 V^{3+}
	$^3T_{1g}(t_{2g}^1e_g^1)$	–	–	–	27966	25120	25200
	$^1E_g(t_{2g}^2e_g^0)$	–	–	–	14242	11730	–
	$^1T_{2g}(t_{2g}^2e_g^0)$	–	–	–	13868	11850	–
	$^1A_{1g}(t_{2g}^2e_g^1)$	–	–	–	28858	23920	–
$d^3(^4A_{2g})$	$^4T_{2g}(t_{2g}^2e_g^1)$	11328	12350	12400 V^{2+}	15718	17580	17400 Cr^{3+}
	$^4T_{1g}(t_{2g}^2e_g^2)$	18339	18470	18500	24450	24740	24700
	$^4T_{1g}(t_{2g}^1e_g^2)$	29960	28550	28000	38511	38540	37800
	$^2E_g(t_{2g}^3e_g^0)$	16421	14320	–	19485	17630	15000
	$^2T_{1g}(t_{2g}^3e_g^0)$	17317	15400	–	20535	18840	–
$d^4(^5E_g)$	$^5T_{1g}(t_{2g}^2e_g^2)$	9073	10195	~12300[c] Cr^{2+}	12903	15770	~15940[d] Mn^{3+}
	$^3T_{1g}(t_2^2e_g^2)$	12936	10070		13374	9040	
$d^5(^6A_{1g})$	$^4T_{1g}(t_{2g}^4e_g^1)$	27543	22560	18800 Mn^{2+}	26729	16690	12600
	$^4T_{2g}(t_{2g}^4e_g^1)$	30677	27830	23100	32425	22730	18500
	$^4T_{1g}(t_{2g}^3e_g^2)$	31808	29780	25000	34907	28910	24300
	$^4E_g(t_{2g}^3e_g^2)$	31691	29820	25250	35159	29580	24600
	$^4T_{2g}(t_{2g}^3e_g^2)$	37940	32490	28100	41268	32710	–
$d^6(^5T_{2g})$	$^5E_g(t_{2g}^3e_g^3)$	7783	9020	10400 Fe^{2+}	–	–	–
	$^3T_{2g}(t_{2g}^3e_g^3)$	17348	14250	–	–	–	–
$d^6(^1A_{1g})$	$^3T_{2g}(t_{2g}^5e_g^1)$	–	–	–	2499	5257	–
	$^3T_{1g}(t_{2g}^5e_g^1)$	–	–	–	8096	10779	–
	$^1T_{1g}(t_{2g}^5e_g^1)$	–	–	–	12714	15670	16600 Co^{3+}
	$^1T_{2g}(t_{2g}^5e_g^1)$	–	–	–	23078	23600	24900
$d^7(^4T_{1g})$	$^4T_{2g}(t_{2g}^4e_g^3)$	5551	6630	8100 Co^{2+}	–	–	–
	$^4T_{1g}(t_{2g}^4e_g^3)$	23015	19970	19400	–	–	–
	$^4A_{2g}(t_{2g}^4e_g^3)$	12152	14313	16000	–	–	–
	$^2E_g(t_{2g}^6e_g^1)$	15889	13130	11300	–	–	–
	$^2T_{2g}(t_{2g}^5e_g^2)$	20247	19110	21550	–	–	–
	$^2A_{2g}(t_{2g}^5e_g^2)$	23965	19150	–	–	–	–
$d^8(^3A_{2g})$	$^3T_{2g}(t_{2g}^5e_g^3)$	6397	7760	8500 Ni^{2+}	–	–	–
	$^3T_{1g}(t_{2g}^5e_g^3)$	11128	13160	13500	–	–	–
	$^3T_{1g}(t_{2g}^4e_g^4)$	27435	25320	25300	–	–	–
	$^1E_g(t_{2g}^6e_g^2)$	18662	15740	15400	–	–	–
	$^1T_{2g}(t_{2g}^5e_g^3)$	24148	22710	22000	–	–	–
$d^9(^2E_g)$	$^2T_{2g}(t_{2g}^5e_g^4)$	7548	9190	~8500[e] Cu^{2+}	–	–	–

[a] Note that column 2 only gives the leading configuration for each term. In the actual calculations there sometimes is rather strong configurational mixing which renders the assignment to a particular configuration ambiguous (e.g. $^3T_{1g}$ states in d^8).

[b] Estimated as an average over the two components of the absorption band, ref. [217], p. 205.

[c] Estimated from the reported band maxima at 8000, 14,550 and 18,050 cm^{-1} and their assignment (D_{4h} symmetry notation) as due to the $^5A_{1g} \rightarrow {}^5B_{1g}$ (transition between the components of the $^5E_g(O_h)$ Jahn–Teller spit ground state) $^5A_{1g} \rightarrow {}^5B_{2g}$, $^5A_{1g} \rightarrow {}^5E_g$(components of $^5T_{2g}(O_h)$) according to (14,450 + 18,050)/2 − 8000/2, ref. [218].

[d] Estimated from the reported band maxima at 10,400; 21,140 cm^{-1} and their assignment as due to the $^5A_{1g}(D_{4h}) \rightarrow {}^5B_{1g}(D_{4h})$ (transition between the components of the $^5E_g(O_h)$ Jahn–Teller spit ground state) and $^5A_{1g}(D_{4h}) \rightarrow {}^5T_{2g}(O_h)$, according to (21,140–10,400/2, ref. [219]).

[e] Estimated from the reported absorption band position at ~7000 and ~12,000 cm^{-1} due to the $^2B_{1g} \rightarrow {}^2A_{1g}$ and $^2B_{1g} \rightarrow {}^2B_{2g}, {}^2E_g$($D_{4h}$ notations) according to (12,000–7000/2), ref. [217] p. 210).

3.4.2.3. d^3 Configuration. The ground term in the d^3 configuration is $^4A_2(t_{2g}^3)$ which is orbitally nondegenerate and therefore not Jahn–Teller active. Consequently, T_h symmetry is an excellent approximation for $[V(H_2O)_6]^{2+}$ and $[Cr(H_2O)_6]^{3+}$. The singly excited d–d states give rise to two orbitally triply excited states with $(t_{2g}^2)(e_g^1)$ configuration ($^4T_{1g}$ and $^4T_{2g}$). The third excited quartet state corresponds to a doubly excited configuration $^4T_{1g}(t_{2g}^1e_g^2)$. The agreement between the SORCI predictions and the experimental values is excellent for both complexes with errors well below 1000 cm^{-1}. It is particularly noteworthy that

the double excitations are predicted with the same accuracy as the single excitations by the SORCI method. This would not be the case for the majority of single-reference methods and shows that the SORCI method is well balanced. Anderson et al. [29] obtained very similar transition energies in their detailed INDO/S study of first-row transition metal hexaquo species. The close agreement between the semi-empirical INDO/S and ab initio SORCI results attests to the quality of the semi-empirical approach for such systems.

3.4.2.4. d^4 Configuration. The $[Cr(H_2O)_6]^{2+}$ and $[Mn(H_2O)_6]^{3+}$ complexes feature a $^5E_g(t_{2g}{}^3e_g^1)$ orbitally degenerate ground configuration and are subject to a rather strong e_g-type Jahn–Teller effect. Experimentally only one broad absorption band is found around 14,000 cm^{-1} for $[Cr(H_2O)_6]^{2+}$ which corresponds to the unresolved components of the Jahn–Teller split $^5T_{2g}(t_{2g}{}^2e_g^2)$ multiplet. For both ions, the SORCI results appear to give somewhat too low transition energies. However, due to the crude geometries used in the calculations, we do not attach too much significance to this result.

3.4.2.5. d^5 Configuration. The high-spin d^5 configuration leads to a $^6A_{1g}(t_{2g}{}^3e_g^2)$ ground term which is orbitally nondegenerate. However, there are no spin-allowed transitions within the d-shell for this configuration. Consequently, the observed transitions are all very weak and correspond to sextet–quartet transitions. Apparently, the sextet–quartet spectrum is not well predicted by the SORCI method for both $[Mn(H_2O)_6]^{2+}$ and $[Fe(H_2O)_6]^{3+}$. All transition energies are systematically too high by 3000–4000 cm^{-1}. This result might have been anticipated on the basis of a similar discrepancy obtained for the corresponding sextet–quartet transitions in the d^5 ions. The result indicates a slight bias of the SORCI method for high spin states or likewise, a tendency to underestimate the ligand field splitting since the quartet excited states all correspond to $e_g \rightarrow t_{2g}$ de-excitations.

Using the more extensively correlated CCSD(T) and CASPT2 methods, Ghosh and Taylor predicted positions of the first $^4T_1$ term in $[Fe(H_2O)_6]^{3+}$ that are even worse than SORCI (21,254 cm^{-1} for CASPT2, 19,941 cm^{-1} for CCSD(T), 16,690 for SORCI compared to 12,600 cm^{-1} observed experimentally). Thus, for the high-spin d^5 configuration the SORCI method appears to have a bias of about 4000 cm^{-1} in favor of the high-spin state. To remove this bias very extensive correlation treatments with very large basis sets are necessary which will be very costly computationally. In their CASPT2 and CCSD(T) study on $[Fe(H_2O)_6]^{3+}$ the authors speculated that the experimental assignment may be in error in this case [194]. However, based on our results this appears to be unlikely and a more reasonable assumption is that the sextet–quartet spectra are simply difficult to predict by ab initio methods.

3.4.2.6. d^6 Configuration. The $^5T_{2g}(t_{2g}{}^4e_g^2)$ ground configuration of $[Fe(H_2O)_6]^{2+}$ is again subject to a limited Jahn–Teller distortion which typically leads to splitting on the order of ~2000 cm^{-1} which is a diagnostic feature for six-fold coordination in the MCD spectra of ferrous complexes [223]. In T_h symmetry we calculate the ^5E_g state at 9020 cm^{-1} which is ~1400 cm^{-1} lower than the observed band maximum of the ferrous ion in aqueous solution. The position of the first triplet excited state at ~14,200 cm^{-1} is also in good agreement with the experimental observation.

The $[Co(H_2O)_6]^{3+}$ complex is unusual in the series, since it is the only member which features a closed-shell low-spin d^6 configuration $^1A_{1g}(t_{2g}{}^6e_g^0)$. The spin-allowed single excitation of the $t_{2g} \rightarrow e_g$ type lead to two orbitally triply degenerate multiplets of $^1T_{1g}$ and $^1T_{2g}$ symmetry which are excellently predicted by the SORCI method.

3.4.2.7. d^7 Configuration. The $^4T_{1g}(t_{2g}{}^5e_g^2)$ configuration of the $[Co(H_2O)_6]^{2+}$ complex is orbitally degenerate and exhibits a weak Jahn–Teller distortion, which was neglected in our calculations. Consequently, there are a number of spin-allowed tranisitons arising from $t_{2g} \rightarrow e_g$ excitations. The agreement between the SORCI predictions and the experimentally observed transition energies is reasonable with errors not exceeding ~1500 cm^{-1}. This also holds for the $^4A_{2g}$ state which corresponds to a double excitation.

3.4.2.8. d^8 Configuration. The spectrum of the $[Ni(H_2O)_6]^{2+}$ complex was discussed above. The SORCI predictions are in excellent agreement with the experimental observations. This holds for triplet–triplet transitions as well as for triplet–singlet transitions and for single-excitations as well as for double excitations. Using an ANO basis, Daniel and co-workers [222] report the vertical transition energies for the three triplet-to-triplet transitions of 5678, 8398, and 24,830 cm^{-1} from CASSCF and 7039, 9724, and 23,703 cm^{-1} from CASPT2 calculations. Again, these results are significantly inferior to the SORCI results obtained in this work. Iuchi et al. [224] recently reported a multiconfiguration quasi-degenerate perturbation theory (MC-QDPT) study of the same ion based on SA-CASSCF results and arrived at vertical transition energies of 8436 cm^{-1} ($^3A_{2g} \rightarrow {}^3T_{2g}$), 13,904 cm^{-1} ($^3A_{2g} \rightarrow {}^3T_{1g}$) and 27,456 cm^{-1} ($^3A_{2g} \rightarrow {}^3T_{1g}$) at a Ni–O distanceof 2.055 Å. These numbers compare very well with both experiment and the SORCI results and shows that the different multireference treatments converge to essentially the same answers.

3.4.2.9. d^9 Configuration. The $[Cu(H_2O)_6]^{2+}$ complex with ground configuration $^2E_g(t_{2g}{}^6e_g^3)$ exhibits a large static Jahn–Teller distortion which has been the subject of many investigations [225]. Our calculations in T_h symmetry are therefore definitely oversimplified. The calculated transition energy is close to 10,000 cm^{-1}, which is a 'generic' transition energy for hexaquo–copper complexes, but may be on the low-end of what is reasonable for such systems. Tanaka and Johansen [226] found transition energies of 9437, 9840, and 10,969 cm^{-1} from SDCI calculations using the MIDI4 basis which are similar to our values. However, this basis is too small for conclusive results at the correlated ab initio level.

In summary, the SORCI method tends to give accurate results for the d^n multiplets of the first row transition metal complexes. The method greatly improves on CASSCF results and in many cases gives near quantitative agreement with experimental results. Problems mainly occur for the spin-forbidden transitions of the d^5 configuration, where the dynamic correlation effects are very large due to the presence of five unpaired electrons which introduces a high degree of (dynamic) Coulomb-correlation which is difficult to model with ab initio methods since very large basis sets in conjunction with a treatment of core-correlation are needed to obtain sufficient convergence in the correlation treatment. The errors are in favor of the high-spin state (as in the parent HF method) and amount to 3000–4000 cm^{-1} which must be kept in mind when applying this methodology to systems with large numbers of unpaired electrons.

4. Calculation of spin-orbit coupling effects

The next important step in modeling the optical properties of transition metal ions is a realistic treatment of SOC. The intricacies of the SOC operator as being a complicated multicenter two-electron operator where already alluded to in Section 2.6.2. Yet, a treatment of SOC is indispensable for the correct prediction of many spectroscopic phenomena such as intersystem crossing rates, intensities in forbidden transitions, fine-structure (=zero-field) splitting, g-tensors, metal-hyperfine couplings and MCD intensities to name only a few. The effect of SOC is that it mixes states of different multiplicities (with $\Delta S = 0, \pm 1$) and splits the different M_S members of a given total S multiplet. The effect may occur to first order in perturbation theory, if the state under investigation is orbitally degenerate and to second order for all states. As such, the SOC reintroduces some angular momentum into the wavefunction, even if the first-order SOC is 'quenched' by low-symmetry. This gives rise to the rich phenomena studied in magnetic resonance spectroscopy on paramagnetic transition metal ions. However, this is a large subject by itself, which is covered elsewhere [24,76] and will not be touched upon in this review. Here, we discuss the calculation of SOC induced splitting in total S multiplets through quasi-degenerate perturbation theory at the SA-CASSCF and SORCI levels.

4.1. Spin-orbit matrix elements

The starting point for the introduction of SOC is that several multiconfigurational states $|\Psi_I^{SS}\rangle = \sum_\mu C_{\mu I}|\Phi_\mu^{SS}\rangle$ where calculated by a multiconfigurational method which is either taken to be the SA-CASSCF or SORCI method in the present work (the superscript 'SS' indicates that the wavefunction is of total spin S with spin-projection quantum number $M_S = S$). These functions are approximations to the eigenfunctions of the BO-operator $\hat{H}_{BO}$ and we whish to calculate the effects of turning on the SOC with operator $\hat{H}_{SOC}$. Since $\hat{H}_{BO}$ is spin-independent, the functions $|\Psi_I^{SS}\rangle$ are calculated in blocks of different multiplicity (and spatial symmetry if applicable). Furthermore, it is sufficient to restrict the attention to a single member of each total S multiplet since the eigenfunctions of $\hat{H}_{BO}$ with total spin S are $2S+1$ fold degenerate. These restrictions must be lifted once SOC is introduced. Thus, the basis of the treatment are the states $|\Psi_I^{SM}\rangle$ where I covers all roots calculated in the first step of the procedure and $M = -S...S$ enumerates all members of a given multiplet. The $|\Psi_I^{SM}\rangle$ are easily generated from $|\Psi_I^{SS}\rangle$ through the successive application of shift operators, since all $2S+1$ members of the multiplet share the same spatial part of the wavefunction.

4.1.1. Quasi-degenerate perturbation theory

In the basis of these functions, SOC effects are conveniently treated through quasi-degenerate perturbation theory which amounts to the diagonalization of the (complex valued) matrix representation of $\hat{H}_{BO} + \hat{H}_{SOC}$ in the basis of the states $\{\Psi_I^{SM}\}$. Since the basic states $\{\Psi_I^{SM}\}$ can always be chosen to be real valued, the matrix elements are simply:

$$\langle \Psi_I^{SM}|\hat{H}_{BO} + \hat{H}_{SOC}|\Psi_J^{S'M'}\rangle = \delta_{IJ}\delta_{SS'}\delta_{MM'}E_I^{(S)} + \langle \Psi_I^{SM}|\hat{H}_{SOC}|\Psi_J^{S'M'}\rangle \quad (44)$$

Thus, the main task to be accomplished is the calculation of the SOC matrix elements over pairs multiconfigurational wavefunctions which may correspond to long expansions with potentially may involve several million CSFs each.

4.1.2. Reduction of the SOC matrix elements

It was argued in Section 2.6.2, that the full two-electron BP-SOC operator is well approximated through the effective one-electron SOMF operator $\hat{H}_{SOMF} = \sum_i \hat{z}(i)\hat{s}(i)$, where $\hat{z}_i$ is the spatial vector operator which involves a given input density $\boldsymbol{P}$ which we take to be the first order density of the lowest state $|\Psi_0^{SS}\rangle$, possibly averaged over spatially degenerate components. Employing the standard tensor angular momentum operators notations for an arbitrary angular momentum operator $\hat{J}$ [227]:

$$\hat{J}_0 = \hat{J}_z,\ \hat{J}_{+1} = -\frac{1}{\sqrt{2}}(\hat{J}_x + i\hat{J}_y),\ \hat{J}_{-1} = \frac{1}{\sqrt{2}}(\hat{J}_x - i\hat{J}_y) \quad (45)$$

the SOC Hamiltonian can be rewritten as

$$\hat{H}_{SOMF} = \sum_{m=0,\pm1}(-1)^m \sum_i \hat{z}_{-m}(i)\hat{s}_m(i) \quad (46)$$

It is highly useful to employ symmetry relations and selection rules for SOC matrix elements with angular momentum operators [228–230]. Using the Wigner–Eckart theorem (WET) it is sufficient to calculate only a few matrix elements and then generate the others by a few simple relations [228–230]. Because the CI wavefunctions employed in our spin-free calculations are linear combinations of CSFs and, therefore, eigenfunctions of S_z, so that $M_S = S$, it is logically to evaluate the matrix elements between functions $|\Psi_\mu^{SS}\rangle$ only. The WET states that the M, M', m dependence of the matrix

element $\left\langle \Psi_I^{SM} \left| \sum_i \hat{s}_m(i) \right| \Psi_J^{S'M'} \right\rangle$ is entirely included in the Clebsch–Gordan coefficients $\begin{pmatrix} S' & 1 & S \\ M' & m & M \end{pmatrix}$ (CGCs) [231]. Thus, the matrix element can be written as [227]:

$$\left\langle \Psi_I^{SM} \left| \sum_i \hat{s}_m(i) \right| \Psi_J^{S'M'} \right\rangle = \begin{pmatrix} S' & 1 & S \\ M' & m & M \end{pmatrix} \langle \Psi_I^S || \hat{S} || \Psi_J^{S'} \rangle \tag{47}$$

The quantity $\langle \Psi_I^S || \hat{S} || \Psi_J^S \rangle$ denotes a 'reduced matrix element' of the set of the operators $\hat{S}_m$. Application of the WET to the case of the SOMF-operator yields:

$$\left\langle \Psi_I^{SM} \left| \sum_{m=0,\pm1} (-1)^m \sum_i \hat{z}_{-m}(i) \hat{s}_m(i) \right| \Psi_J^{S'M'} \right\rangle = \begin{pmatrix} S' & 1 & S \\ M' & m & M \end{pmatrix} \underbrace{\left\langle \Psi_I^S \left\| \sum_i \hat{z}_{-m}(i) \hat{s}(i) \right\| \Psi_J^{S'} \right\rangle}_{Y_{IJ}^{SS'}(-m)} \tag{48}$$

The remaining task is now to calculate the reduced matrix elements. As explained elsewhere in detail [24,232], one obtains for the three possible cases $S - S' = 0, \pm 1$ the following matrix elements:

$$Y_{IJ}^{SS}(m) = \frac{\sqrt{S(S+1)}}{S} \left\langle \Psi_I^{SS} \left| \sum_i \hat{z}_m(i) \hat{s}_0(i) \right| \Psi_J^{SS} \right\rangle \tag{49}$$

$$Y_{IJ}^{SS-1}(m) = \left\langle \Psi_I^{SS} \left| \sum_i \hat{z}_m(i) \hat{s}_{+1}(i) \right| \Psi_J^{S-1S-1} \right\rangle \tag{50}$$

$$Y_{IJ}^{SS+1}(m) = \sqrt{\frac{2S+3}{2S+1}} \left\langle \Psi_I^{SS} \left| \sum_i \hat{z}_m(i) \hat{s}_{-1}(i) \right| \Psi_J^{S+1S+1} \right\rangle \tag{51}$$

4.1.3. Second quantized form of the SOC operator

In order to arrive at manageable expressions for the reduced matrix elements, it is common and useful to employ the second quantization formalism [233] for the calculations of the SOC matrix elements. The one-electron SOC operator in the second quantization approach can be written in the form of:

$$\hat{H}_{\mathrm{SOMF}} = \sum_{m=0,\pm1} (-1)^m \sum_{p\sigma;q\sigma'} \underbrace{\langle \psi_p | \hat{z}_{-m} | \psi_q \rangle}_{z_{pq}^{-m}} \langle \sigma | \hat{s}_m | \sigma' \rangle a_{p\sigma}^+ a_{q\sigma'} \tag{52}$$

Here $\{\psi\}$ is the set of one-electron orbitals used to construct the CSFs $\{\Phi\}$, σ, $\sigma' = \alpha$, β loops over spin-components and $a_{p\sigma}^+$ and $a_{p\sigma}$ are the operators for the creation and destruction of an electron with spin σ in orbital ψ_p, respectively. Using the short-hand notation $a_{p\alpha}^+ = \hat{a}_p^+$ and $a_{p\beta}^+ = \hat{b}_p^+$ and likewise for the destruction operators, the summations over spins can be rewritten as:

$$\sum_{\sigma\sigma'} \langle \sigma | \hat{s}_0 | \sigma' \rangle a_{p\sigma}^+ a_{q\sigma'} = \frac{1}{2} [\hat{a}_p^+ \hat{a}_q - \hat{b}_p^+ \hat{b}_q] \tag{53}$$

$$\sum_{\sigma\sigma'} \langle \sigma | \hat{s}_{+1} | \sigma' \rangle a_{p\sigma}^+ a_{q\sigma'} = -\frac{1}{\sqrt{2}} \hat{a}_p^+ \hat{b}_q \tag{54}$$

$$\sum_{\sigma\sigma'} \langle \sigma | \hat{s}_{-1} | \sigma' \rangle a_{p\sigma}^+ a_{q\sigma'} = +\frac{1}{\sqrt{2}} \hat{b}_p^+ \hat{a}_q \tag{55}$$

Combining the last two equations with Eq. (50) and using $z_{pq}^{\pm} = z_{pq}^x \pm i z_{pq}^y$, the SOC operator in the framework of the second quantization formalism is finally written as [159,234,235]:

$$\hat{H}_{\mathrm{SOMF}} = \frac{1}{2} \sum_{pq} z_{pq}^- \hat{a}_p^+ \hat{b}_q + z_{pq}^+ \hat{b}_p^+ \hat{a}_q + z_{pq}^0 [\hat{a}_p^+ \hat{a}_q - \hat{b}_p^+ \hat{b}_q] \tag{56}$$

In this form, the operator is most conveniently handled and all aspects having to do with the subtlety of the electron spin are transferred to the second-quantized spin-operators. Note that the operator $\frac{1}{2}[\hat{a}_p^+ \hat{a}_q - \hat{b}_p^+ \hat{b}_q]$ corresponds here to the spin density operator, and the terms $-2^{-1/2} \hat{a}_p^+ \hat{b}_q$ and $2^{-1/2} \hat{b}_p^+ \hat{a}_q$ are spin-rising and -lowering operators. The latter three operators can also be considered as the $M = 0$ and ± 1 components of a triplet vector operator while the operator $E_q^p = \hat{a}_p^+ \hat{a}_q + \hat{b}_p^+ \hat{b}_q$ which occurs exclusively in spin-independent operators is the $M = 0$ component of a singlet operator [236].

4.1.4. Calculation of reduced matrix elements

At this point the problem of calculating the SOC matrix elements has been simplified as much as possible and what remains to be done is the evaluation of the reduced matrix elements of the form:

$$\begin{aligned} &\langle \Psi_I^{SM} | \hat{H}_{\mathrm{SOC}} | \Psi_J^{S'M'} \rangle \\ &= \sum_{\mu\nu} C_{\mu I} C_{\nu J} \langle \Phi_\mu^{SM} | \hat{H}_{\mathrm{SOC}} | \Phi_\nu^{S'M'} \rangle \\ &= \frac{1}{2} \sum_{\mu\nu} C_{\mu I} C_{\nu J} \sum_{pq} \langle \Phi_\mu^{SM} | z_{pq}^- \hat{a}_p^+ \hat{b}_q + z_{pq}^+ \hat{b}_p^+ \hat{a}_q \\ &\quad + z_{pq}^0 [\hat{a}_p^+ \hat{a}_q - \hat{b}_p^+ \hat{b}_q] | \Phi_\nu^{S'M'} \rangle \end{aligned} \tag{57}$$

The two-problems that arise in the evaluation of this equation are: (1) the matrix elements of the spin-dependent operators over general CSFs are complicated and (2) there are very many of them since the expansions can reach several million CSFs. In the ORCA code, Eq. (57) is not evaluated as it stands. It is much more convenient to proceed via the reduced transition density matrices which are defined as follows:

$$D_{pq}^{IJ} = \sum_{\mu\nu} C_{\mu I} C_{\nu J} \langle \Phi_\mu^{SM} | \hat{a}_p^+ \hat{a}_q + \hat{b}_p^+ \hat{b}_q | \Phi_\nu^{S'M'} \rangle \tag{58}$$

$$D_{pq}^{IJ}(0) = \sum_{\mu\nu} C_{\mu I} C_{\nu J} \langle \Phi_\mu^{SM} | \hat{a}_p^+ \hat{a}_q - \hat{b}_p^+ \hat{b}_q | \Phi_\nu^{S'M'} \rangle \tag{59}$$

$$D^{IJ}_{pq}(+) = \sum_{\mu\nu} C_{\mu I} C_{\nu J} \langle \Phi^{SM}_{\mu} | \hat{a}^{+}_{p} \hat{b}_{q} | \Phi^{S'M'}_{\nu} \rangle \tag{60}$$

$$D^{IJ}_{pq}(-) = \sum_{\mu\nu} C_{\mu I} C_{\nu J} \langle \Phi^{SM}_{\mu} | \hat{b}^{+}_{p} \hat{a}_{q} | \Phi^{S'M'}_{\nu} \rangle \tag{61}$$

Here, D^{IJ}_{pq} corresponds to the standard reduced transition one-particle density matrix and $D^{IJ}_{pq}(0)$ to the standard reduced transition one-particle spin-density. The two other density matrices are 'coupling' or 'transition' spin-coupling density matrices. Once these density matrices are available, it is straightforward to evaluate the reduced matrix elements in Eqs. (49)–(51) which are subsequently contracted with the appropriate CGCs in order to set up the entire SOC matrix. Diagonalization of this complex matrix then yields the desired spin-orbit resolved energy levels.

Since the vast majority of the matrix elements in Eqs. (58)–(61) are zero for two wavefunctions of the form of Eq. (24), it is important to identify and calculate the remaining matrix elements with high-efficiency in order for the SOC calculation not to become a bottleneck of the treatment. Unfortunately, the calculation of SOC matrix elements requires a detailed description of the employed CSF basis. There are many ways to construct suitable CSFs. The principle step which is always involved is that the singly occupied orbitals of a given configuration are coupled in some consistent way into the complete set of linearly independent spin-eigenfunctions which are consistent with the number of unpaired electrons and the requested multiplicity. Details of popular techniques like the 'symmetric group approach' (SGA) and the 'graphical unitary group approach' (GUGA) are beyond the scope of this review and can be found in the specialist literature [237–240].

In the ORCA program, we adopted a simple but efficient and very flexible way: the bonded functions method [241–243]. However, the originally used graphical techniques for matrix element evaluations [244,245] are not efficient enough for large-scale use. Instead, the matrix elements are calculated using ideas based on the work of Golebiewski and Broclawik [246] which employs second quantization in a straightforward manner. A bonded function can be written as [246]:

$$|\Phi^{SS}_{I}\rangle = \hat{A}(i_1 i_2)(i_3 i_4)\dots(i_{k-1} i_k)(i_{k+1})\dots(i_N) \tag{62}$$

$$(ij) = 2^{-1/2}\psi_i(\boldsymbol{r}_1)\psi_j(\boldsymbol{r}_2)[\alpha(1)\beta(2) - \beta(1)\alpha(2)] \quad \text{for } i \neq j \tag{63}$$

$$(ii) = \psi_i(\boldsymbol{r}_1)\psi_i(\boldsymbol{r}_2)\alpha(1)\beta(2) \tag{64}$$

$$(i) = \psi_i(\boldsymbol{r}_1)\alpha(1) \tag{65}$$

Thus, a bonded function is antisymmetrized product of fragments of doubly occupied MOs, singly occupied singlet-coupled MOs and singly occupied uncoupled MOs that are occupied by spin-up electrons. $\hat{A}$ is the antisymmetrization operator which includes the usual normalization factor $(N!)^{-1/2}$. The bonded functions possess the following useful properties [246]:

1. Substitution of the pair (ij) by (ji) does not change the bonded function.
2. Interchange of the two pairs (ij) and (rs) does not change the bonded function.
3. Interchanging of (ij) and an unpaired term (r) does not influence the bonded function.
4. Shift of an unpaired term (r) from the position p to the position q leads to the multiplication of the bonded function by $(-1)^{p+q}$.

Therefore, the positions of bonded terms are not vital and only the order of the unpaired terms type of (r) is important [246]. In order to treat the terms $\hat{a}^{+}_{i}\hat{a}_{j} - \hat{b}^{+}_{i}\hat{b}_{j}$ and $\hat{b}^{+}_{i}\hat{a}_{j}$ of Eqs. (53)–(55), we followed the suggestion of Böckmann et al. [234] and extended the standard set of bonded functions with the additional building units of the following types

$$(ij)_{+} = 2^{-1/2}\psi_i(\boldsymbol{r}_1)\psi_j(\boldsymbol{r}_2)[\alpha(1)\beta(2) + \beta(1)\alpha(2)] \tag{66}$$

$$(\bar{i}) = \psi_i(\boldsymbol{r}_1)\beta(1) \tag{67}$$

which represent triplet coupled electron pairs and singly-occupied orbitals with spin-down, respectively. Such extended bonded functions can, in principle, describe the states with $M_S \neq S$ [234]. This property, however, will not be used explicitly since we will always employ the matrix elements between standard states with $M_S = S$. The extended bonded functions only occur after the action of the operator $\hat{a}^{+}_{i}\hat{a}_{j} - \hat{b}^{+}_{i}\hat{b}_{j}$ on a standard bonded function and then immediately vanish in the procedure of contraction with the other bonded function in order to calculate the matrix element.

The evaluation of the matrix elements of the SOC Hamiltonian of Eqs. (53)–(55) is performed in two steps. Firstly, the action of the operators $\hat{a}^{+}_{i}\hat{a}_{j} - \hat{b}^{+}_{i}\hat{b}_{j}$ and $\hat{a}^{+}_{i}\hat{b}_{j}$ (one can avoid the calculation of the operator $\hat{b}^{+}_{j}\hat{a}_{i}$ because it corresponds to the operator $\hat{a}^{+}_{i}\hat{b}_{j}$ due to the relation$(\hat{S}_{+1})^{+} = -(\hat{S}_{-1})$) on a bonded function is considered. The action of these operators on all possible cases is listed in Table 8. Consider, for instance, the action of the operator $\{\hat{a}^{+}_{i}\hat{a}_{j} - \hat{b}^{+}_{i}\hat{b}_{j}\}$ on the bonded function $|\Phi^{SS}_{I}\rangle = \hat{A}(ik)(j)$. Employing Eqs. (62)–(65) and expanding $|\Phi^{SS}_{I}\rangle$ into its constituent Slater determinants, one obtains:

$$|\Phi^{SS}_{I}\rangle = \frac{1}{\sqrt{2}}(|i\bar{k}j| - |\bar{i}kj|) \tag{68}$$

Then,

$$\{\hat{a}^{+}_{i}\hat{a}_{j} - \hat{b}^{+}_{i}\hat{b}_{j}\}|\Phi^{SS}_{I}\rangle = \{\hat{a}^{+}_{i}\hat{a}_{j} - \hat{b}^{+}_{i}\hat{b}_{j}\}\frac{1}{\sqrt{2}}(|i\bar{k}j| - |\bar{i}kj|) = \frac{1}{\sqrt{2}}(ii)(k) \tag{69}$$

which corresponds to rule no. 11 of Table 8. The remaining rules of Table 8 can be derived in the similar way.

Secondly, the overlap between the bonded function on the left hand side and the bonded function after the action of the operators of Eqs. (53)–(55) is calculated. This process is called '*contraction*'. The overlap integral is zero if the bonded functions differ by any orbital. All possible combinations of bonded

Table 8
List of operator rules[a]

	Category	$\|J\rangle$	$\{a_i^+ a_j - b_i^+ b_j\}\|J\rangle$	$a_i^+ b_j \|J\rangle$	$b_i^+ a_j \|J\rangle$
1	a. no j	Arbitrary	0	0	0
2	b. $2x$ j	Arbitrary	0	0	0
3	c. $i=j$	(ii)	0	0	0
4		(i)	(i)	0	$(\bar{i})$
5		(ik)	$(ik)_+$	$-\frac{1}{\sqrt{2}}(i)(k)$	$\frac{1}{\sqrt{2}}(\bar{i})(\bar{k})$
6	d. $i \neq j$	(jj)	$\sqrt{2}(ij)_+$	$(j)(i)$	$(\bar{i})(\bar{j})$
7		(j)	(i)	0	$(\bar{i})$
8		(ik)	$(ik)_+$	$-\frac{1}{\sqrt{2}}(i)(k)$	$\frac{1}{\sqrt{2}}(\bar{i})(\bar{k})$
9		(ij)	0	0	0
10		$(ik)(j)$	$-\frac{1}{\sqrt{2}}(ii)(k)$	0	$-\frac{1}{\sqrt{2}}(ii)(\bar{k})$
11		$(jk)(i)$	$\frac{1}{\sqrt{2}}(ii)(k)$	0	$\frac{1}{\sqrt{2}}(ii)(\bar{k})$
12		$(ik)(jl)$	$-\frac{1}{\sqrt{2}}(ii)(kl)_+$	$\frac{1}{2}(ii)(k)(l)$	$\frac{1}{2}(ii)(\bar{k})(\bar{l})$
13		$(i)(j)$	0	0	(ii)
14		$(jj)(i)$	$(ii)(j)$	0	$(ii)(j)$
15		$(jj)(ik)$	$(ii)(jk)_+$	$-\frac{1}{\sqrt{2}}(ii)(j)(k)$	$-\frac{1}{\sqrt{2}}(ii)(\bar{j})(\bar{k})$

[a] Rules were originally derived in refs. [234,246].

functions contraction rules are listed in Table 9. Using the two sets of rules for the application of a general second quantized operator on a bonded function and the contraction between two sets of bonded functions with identical orbitals but different spin coupling the matrix elements of any second quantized spin-dependent and spin-independent operator can be calculated. The only remaining problem is that of an efficient implementation. However, this subject would lead to far astray in the present context.

4.2. Illustrative calculations

In order to illustrate the calculation of SOC in transition metal complexes, we start with SA-CASSCF calculation of the di- and tripositive free ions. Comparison is made to experimental data using the LS coupling rules. In this method, the energy of a given J-term is:

$$E(J, L, S) = \tfrac{1}{2}\lambda(J(J+1) - L(L+1) - S(S+1)) \qquad (70)$$

where λ is the 'many-electron SOC constant'. Its value is determined from experiment by averaging the splitting $E(J, L, S) - E(J_{max}, L, S)$ of the lowest LS term and theoretical from a single energy difference $E(J, L, S) - E(J-1, L, S)$ after the quasi-degenerate perturbation procedure. The results in Table 10 show that the ionic fine structure can be quite accurately predicted by the combination of the SOMF operator with CASSCF wavefunctions even if rather moderate basis sets are used. The remaining deviations only amount to a few wavenumbers. Deviations of this magnitude would even be expected in an exact treatment of electron correlation and SOC since the direct dipolar spin–spin coupling was not taken into account but certainly also contributes to the splitting. However, the level of agreement between theory and experiment is quite pleasing given that there is no empiri-

Table 9
List of contraction rules[a]

	in $\|I\rangle$	in $\|J\rangle$	in $\|I\rangle$	in $\|J\rangle$
1	(rs)	(rs)	1	1
2	(rs)	$(ri)(s)$	1	$-\frac{1}{2}(i)$
3	(rs)	$(ri)(sj)$	1	$-\frac{1}{2}(ij)$
4	(rs)	$(r)(s)$	1	0
5	(rs)	$(rs)_+$	1	0
6	(rs)	$(ri)_+$ (s)	1	$\frac{1}{2}(i)$
7	(rs)	$(ri)_+$ (sj)	1	$\frac{1}{2}(ij)_+$
8	$(r)(si)$	$(rs)_+$	$-\frac{1}{2}(i)$	1
9	$(rs)(si)$	(rs)	$-\frac{1}{2}(i)$	1
10	(r)	(r)	1	$(-1)^p$
11	(r)	$(\bar{r})$	1	0
12	$(\bar{r})$	(r)	1	0
13	$(\bar{r})$	$(\bar{r})$	1	$(-1)^p$

[a] Rules were originally derived in refs. [234,246].

Table 10
SA-CASSCF-SOC results for the spin-orbit splitting of the lowest states of the naked divalent transition metal ions

Configuration	M^{2+}		M^{3+}	
	λ_{calc} (cm^{-1})	λ_{exp} (cm^{-1})	λ_{calc} (cm^{-1})	λ_{exp} (cm^{-1})
$d^1(^2D)$	83	79	153	153
$d^2(^3F)$	62	62	106	109
$d^3(^4F)$	59	58	95	95
$d^4(^5D)$	61	62	93	94
$d^6(^5D)$	105	107	149	153
$d^7(^4F)$	177	182	245	256
$d^8(^3F)$	331	332	448	456
$d^9(^2D)$	816	829	1102	1104

Wachters basis set, tight CASSCF convergence, SOMF operator with semianalytic integration and Grid5.

Table 11
Electron correlation effects on SOC constant λ (cm^{-1}) for the neutral Mn and Cu atoms

	Mn(^{6}D)	Cu(^{2}D)
Method		
CASSCF	−59.76	−804.28
Correlation of:		
3d4s-	−51.47	−821.08
3p-	−53.44	−840.64
3s-	−54.23	−842.85
2p-	−52.47	−822.87
2s-	−52.43	−822.89
1s-	−52.50	−822.90
Exp.	−51.05	−817.14

MRCI calculations with full valence CASSCF reference function and different active spaces, TZVPP basis set. Experimental data are taken from ref. [192].

cism involved whatsoever. Beyond the basis set only natural constants such as the speed of light enter these calculations.

While, the CASSCF values are already surprisingly accurate one may wonder how the calculated SOC constants are affected by dynamic correlation. Dynamic electron correlation contributes to the calculated SOCs mainly in two ways. Firstly, it affects the spin-free state energies and, therefore, defines the order of the states (terms in atoms). Secondly, it alters the spacing between energy levels with different J inside one term by modifying the matrix elements of the SOC matrix. Table 11 demonstrates the effect of the dynamic correlation for the neutral Mn and Cu atoms. Already the valence-shell correlation decreases the deviation of the calculated SOC constants from the fully-correlated all-electron calculation. At the same time the further inclusion of 3s- and 3p-orbitals into the active space somewhat deteriorates the results by decreasing the value of SOC matrix elements. This deviation can be compensated by the inclusion of the 2p orbitals into the correlation treatment. Further expansion of the active space does not influence significantly the calculated SOC constants. At the time that all electrons are correlated, the results are in excellent agreement with the experimental measurements.

The method outlined above is by no means restricted to small molecules. It can be applied for any molecule for which the SS-CASSCF or MRCI or SORCI method can be carried out. Presently, the MR-CI method is restricted to small molecules (<10 atoms), the SORCI method to medium sized molecules (<30–50 atoms) while the SA-CASSCF method in our implementation can be applied to fairly large molecules with ∼100 atoms or 700–1000 basis functions, respectively.

In our opinion, the prospects of treating all kinds of SOC effects in transition metal complexes by this method are fairly promising. In particular, since the method involves an explicit construction of all M_S components of each multiplet it is much more readily and naturally applied to the problem of SOC than single-determinant methods such as DFT where sometimes rather artificial procedures are employed. We are currently investigating a number of molecular spectroscopic phenomena (in particular zero-field splitting) with this method and will report results in due course.

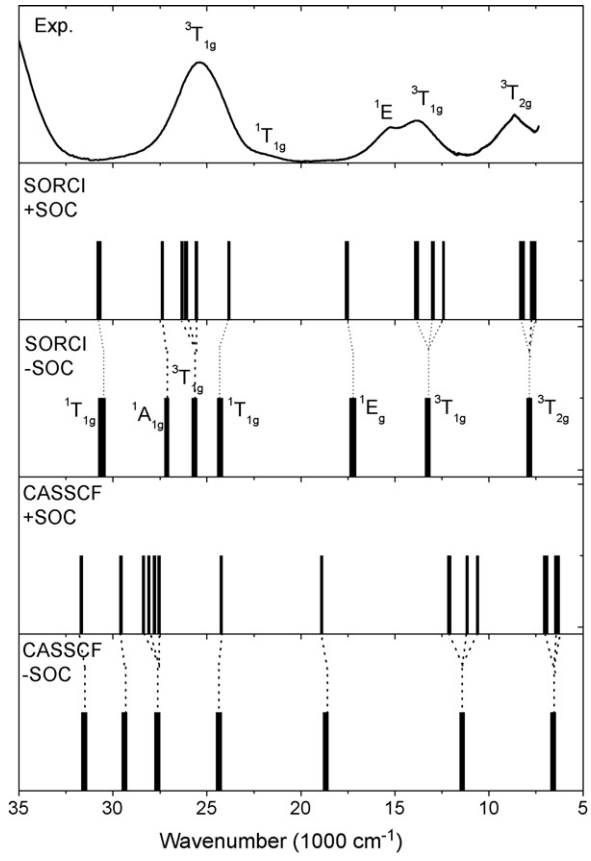

Fig. 2. Comparison of measure (top) and calculated (bottom four panels) d–d spectra of $[Ni(H_2O)_6]^{2+}$. The calculations where done at the SORCI and CASSCF levels with and without the treatment of SOC effects.

As an initial example in the field of optical spectroscopy, consider the absorption spectrum of the hexquo–Ni^{2+} ion (Fig. 2). Calculations were carried out at the SA-CASSCF and SORCI levels with and without inclusion of SOC. One can see that the SOC introduces splitting of the order of a few hundred wavenumbers in the T_{2g} and T_{1g} terms which split in first order by SOC. Since the three components of the SOC operator transform under the T_{1g} representation in O_h symmetry, the $^3T_{1g}$-states split into $A_{1g} + E_g + T_{1g} + T_{2g}$ by the effect of SOC while $^3T_2$ states split into $A_{2g} + E_g + T_{1g} + T_{2g}$ components. The splitting of the $^3T_{1g}$ and $^3T_{2g}$ states amounts to $2\zeta_{Ni}$ and ζ_{Ni}, respectively, where ζ_{Ni} is the covalently reduced one-electron SOC constant of Ni^{2+} (∼600–700 cm^{-1}). The calculated transition energies at the SORCI + SOC level are in excellent agreement with the experimental spectrum shown on top of Fig. 2. A detailed treatment of these effects in the framework of ligand field theory in this complex has been given in the classic paper by Solomon and Ballhausen [197]. However, a more thorough treatment is outside the scope of this review.

5. Calculation of resonance Raman spectra and excitation profiles

The final subject covered in this review is the calculation of resonance-Raman intensities. While rR spectroscopy has been intensely used in inorganic and bioinorganic chem-

istry [10,247–252] the quantum chemistry of this important method has not been well developed. There are several works describing the calculation of rR spectra of organic compounds [251,253–255] but truly first-principles calculations of the spectra of inorganic complexes are extremely sparse if existent at all. Below we give an introduction into this area with emphasis on a recent study performed in our laboratory.

5.1. General theory of electronic absorption and resonance Raman scattering

After averaging over different molecular orientations and polarizations of the incident light beam the absorption cross section $\sigma_A(E_L)$ can be written in SGS units as:

$$\sigma_A(E_L) = \frac{4\pi}{3\hbar c} E_L \sum_V \sum_{\rho=1}^{3} \frac{|\langle V|m_p|I\rangle|^2 \Gamma}{(E_V - E_I - E_L)^2 + \Gamma^2} \tag{71}$$

In Eq. (71) E_L is the incident photon energy; $|I\rangle$ and $|V\rangle$ the initial and excited vibronic states; E_I and E_V are their energies; Γ the homogeneous linewidth; and m_ρ is the vector component of the transition dipole moment operator. The formal theory of Raman scattering is well-known [256]. Quantum mechanically, Raman scattering is described by second order time-dependent perturbation theory. The central result is the polarizability tensor given in the energy frame, which for vibrational Raman scattering is of the form:

$$(\alpha_{\rho\lambda})_{I\to F} = \sum_V \frac{\langle F|m_p|V\rangle\langle V|m_\lambda|I\rangle}{E_V - E_I - E_L - i\Gamma} + \sum_V \frac{\langle F|m_p|V\rangle\langle V|m_\lambda|I\rangle}{E_V - E_I + E_S - i\Gamma} \tag{72}$$

Here $|F\rangle$ denotes the final vibronic state; E_S the scattered photon energy. The polarizability tensor $(\alpha_{\rho\lambda})_{I\to F}$ was first given by Kramers and Heisenberg [257] in analogy to classical dispersion theory. Later, Dirac [258] derived it by considering an atom interacting with a quantized radiation field. All the developments in the study of Raman scattering since have been based on the Kramers–Heisenberg–Dirac (KHD) expression, Eq. (72). The corresponding expression for the resonance Raman (rR) cross section $\sigma_{I\to F}(E_L)$, averaged over all orientations of the molecule and integrated over all directions and polarizations of scattered radiation (4π solid angle) is:

$$\sigma_{I\to F}(E_L) = \frac{8\pi E_s^3 E_L}{9\hbar^4 c^4} \sum_{\rho,\lambda} |(\alpha_{\rho\lambda})_{I\to F}|^2 \tag{73}$$

The intensity of the scattered light at a given direction is determined by the differential cross-section $\sigma' = \mathrm{d}\sigma/\mathrm{d}\Omega$) where $\mathrm{d}\Omega$ is an element of solid angle. σ' is some function of squares of polarizability tensor invariants and the illumination-observation geometry [256]. The first "resonant" term in Eq. (72) describes a Raman scattering which is a two-photon process involving virtual absorption to the entire manifold of excited vibronic states, followed by the virtual emission to the final state. The "non-resonant" second term in Eq. (72) corresponds to the case where emission precedes absorption. According to Eqs. (71)–(73) contributions from all intermediate states are summed at the amplitude level before squaring. The magnitude of the contribution from each state depends on both the transition length and the energy denominator. Thus, as the energy of the incident radiation approaches resonance with a particular electronic state, vibronic levels of that state begin to dominate the sum. A number of further simplifications and specializations of the expressions (71)–(73) are usually assumed under conditions of electronic resonance. The Born–Oppenheimer approximation is employed to separate the vibronic states into products of electronic and vibrational states:

$$I = g(\boldsymbol{r}, \boldsymbol{Q})i(\boldsymbol{Q}) \qquad F = g(\boldsymbol{r}, \boldsymbol{Q})f(\boldsymbol{Q})$$
$$V = e(\boldsymbol{r}, \boldsymbol{Q}')\nu(\boldsymbol{Q}') \tag{74}$$

where $\boldsymbol{r}$ denote the electron coordinates; $\boldsymbol{Q}$ and $\boldsymbol{Q}'$ are the normal modes corresponding to the ground and excited states; $g(\boldsymbol{r}, \boldsymbol{Q})$ and $e(\boldsymbol{r}, \boldsymbol{Q}')$ are the ground and excited electronic wavefunctions, respectively; $i(\boldsymbol{Q})$, $f(\boldsymbol{Q})$ and $\nu(\boldsymbol{Q}')$ are the corresponding vibrational eigenfunctions of these electronic states. Under these approximations, the transition dipole length matrix elements in Eqs. (71)–(73) become:

$$\langle F|m_\rho|V\rangle = \langle f|\langle g|m_\rho|e\rangle|V\rangle = \langle f|M_{\mathrm{ge},\rho}(\boldsymbol{Q})|V\rangle \tag{75}$$

where $M_{\mathrm{ge},\rho}(\boldsymbol{Q}) = \langle g|m_\rho|e\rangle$ is the electronic transition length matrix element between the ground and excited electronic wavefunctions $g(r, (\boldsymbol{Q})$ and $e(r, (\boldsymbol{Q}')$. $M_{\mathrm{ge},\rho}(\boldsymbol{Q})$ is the function of nuclear coordinates because Born–Oppenheimer electronic states depend parametrically on the nuclear coordinates.

The next level of approximation used to simplify the expressions for absorption cross section and Raman polarizability consists in the neglect of the nuclear coordinate dependence of the electronic transition length when on resonance with a strongly allowed electronic transition, that is, $M_{\mathrm{ge},\rho}(\boldsymbol{Q})$ is replaced by $M_{\mathrm{ge},\rho}(\boldsymbol{Q}_0)$, where $\boldsymbol{Q}_0$ is the ground state equilibrium geometry. This is the famous Franck–Condon (FC) approximation [259–261]. It amounts to assuming that $M_{\mathrm{ge}}(\boldsymbol{Q}_0)$ is much larger than the variation of M_{ge} over the range of $\boldsymbol{Q}$ in which the initial and final vibrational wavefunctions are localized. Under the BO and FC approximations the expressions for the absorption cross section (71) and the rR polarizability (72) become:

$$\sigma_A(E_L) = \frac{4\pi}{3\hbar c} E_L \sum_n (M_{0n})^2 \times \sum_{\nu_p} \frac{\Gamma_n |\langle \nu_n|i\rangle|^2}{(\varepsilon_{\nu n} - \varepsilon_{i0} + E_{0n} - E_L)^2 + \Gamma_n^2} \tag{76}$$

$$(\alpha_{\rho\lambda})_{I\to F} = \sum_n M_{0n,\rho} M_{0n,\lambda} \times \sum_{\nu_n} \frac{\langle f|\nu_n\rangle\langle \nu_n|i\rangle}{(\varepsilon_{\nu n} - \varepsilon_{i0} + E_{0n} - E_L) - i\Gamma_n} \tag{77}$$

where n labels electronic states (index 0 corresponds to the ground electronic state); E_{0n} is the adiabatic minima separation energy between the ground and the nth excited state; Γ_n and

$\boldsymbol{M}_{0n}$ are the corresponding homogeneous linewidth and transition dipole moment; $\varepsilon_{\nu n}$ and ε_{i0} are the energies of the vibrational states $|\nu_n\rangle$and $|i\rangle$. The FC approximation has been shown to be sufficiently accurate for the description of strongly dipole allowed electronic transitions [262–267].

The calculation of dipole-forbidden transitions ($\boldsymbol{M}_{\mathrm{ge}}(\boldsymbol{Q}_0) = 0$) or weakly dipole-allowed transitions ($\boldsymbol{M}_{\mathrm{ge}}(\boldsymbol{Q}_0) \approx 0$) is not possible in terms of the FC approximation, because vibronically induced transition moments are neglected. The simplest approach to account for the variations of the electronic transition dipole moments with the nuclear coordinates is to expand $\boldsymbol{M}_{\mathrm{ge}}(\boldsymbol{Q})$ as a Taylor series around the ground-state equilibrium geometry (Herzberg–Teller approach [268]):

$$M_{\mathrm{ge}}(\boldsymbol{Q}) = M_{\mathrm{ge}}(\boldsymbol{Q}_0) + \sum_j \frac{\partial M_{\mathrm{ge}}}{\partial Q_j}(Q_j - Q_{j,0}) + \frac{1}{2}\sum_{j,k} \times \frac{\partial^2 M_{\mathrm{ge}}}{\partial Q_j \partial Q_k}(Q_j - Q_{j,0})(Q_k - Q_{k,0}) + \ldots \quad (78)$$

Truncation of the Taylor expansion (78) after the second term yields the Born–Oppenheimer–Franck–Condon–Herzberg–Teller (BO–FC–HT) approximation for the transition dipole moment. Applications of the BO–FC–HT treatment based on the semi-empirical QCFF/PI [269] method as well as calculations based the ab initio CIS [270,271], CASSCF [263,272] and TD-DFT [266] methods have been reported; the agreement with experimental spectra is usually moderate to good. A physical explanation of the transition dipole moment coordinate dependence is that displacements of nuclei result in a perturbation of the electron–nuclear interaction. Thus, a mixing of the excited state electronic wavefunction with other excited state electronic wavefunctions occurs which leads to a mixing of the corresponding transition moments [268,273] ("intensity borrowing" from dipole-allowed transitions).

Eq. (77) for the rR polarizability is the so-called Albrecht A-term expression for excitation within an allowed absorption band [274,275]. Non-Condon mechanisms of Raman scattering arising from the transition dipole moment coordinate dependence are usually classified through the HT expansion of an electronic wavefunction in a Taylor's series in terms of displacements of the nuclear coordinates from the ground state equilibrium geometry. This allows the breakdown of the Raman polarizability into several terms of distinct physical origin [274,275]:

$$(\alpha_{\rho\lambda})_{I\to F} = A + B + C \ldots \quad (79)$$

The B-term arises from the HT expansion of the excited state electronic wavefunctions in terms of the states evaluated at the ground state equilibrium geometry whereas the C-term originates from the corresponding expansion of the ground state electronic wavefunction. The A-term is expected to be the most important contributor to rR intensities of fundamentals, overtone, and combination bands. Non-Condon terms must be considered if the electronic excitation is to a weakly allowed or electric dipole forbidden transition or for scattering into non-totally symmetric vibrational final states. In this case the FC factors in the absorption and resonance Raman expressions are no longer pure vibrational overlap integrals of the type $\langle\nu_n|i\rangle$ and $\langle\nu_n|f\rangle$, but involve matrix elements with one or more vibrational coordinates. The relationship between rR intensities and excited state vibrational dynamics is clearest when A-term scattering is dominant (vide infra), and rR spectra that are dominated by totally symmetric vibrations are often interpreted assuming A-term activity alone. Although non-Condon contributions in absorption and rR cross-sections are not always negligible, we will not consider these effects in the following.

The direct calculation of absorption spectra and rR excitation profiles in the FC approximation requies the evaluation of multidimensional overlap integrals of vibrational wavefunctions (Eq. (74)), commonly known as FC integrals (factors). Different methods [276–284] have been proposed for the evaluation of these integrals in the cases where the ground and excited PESs are of a general harmonic form. In spite of the existence of elaborate numerical algorithms, only a few programs have been reported which allow the routine calculation of vibronic structure of absorption spectra and rR intensities. The most comprehensive implementations are found in the programs HOTFCHT [285] and FCfast [267] for computing the vibronic fine structure of electronic spectra at different temperatures. The intensities of different vibronic transitions of large organic molecules have been predicted with reasonable accuracy by means of these programs in several papers [266,267,285].

For harmonic PES's the nuclear motion may be represented by the following Hamiltonians, which are written in terms of dimensionless normal coordinates (DNC's):

$$\hat{H}_g = \sum_i^N \frac{\hbar\omega_{gi}}{2}(p_{gi}^2 + q_{gi}^2) \quad (80)$$

$$\hat{H}_e = \sum_i^N \frac{\hbar\omega_{ei}}{2}(p_{ei}^2 + q_{ei}^2) \quad (81)$$

where we label ground-state quantities by index g and excited-state quantities by index e; $\hat{H}_g$ and $\hat{H}_e$ are the ground and excited surface Hamiltonians; ω_{gi} and ω_{ei} are the corresponding harmonic frequencies for the ith normal mode. $\boldsymbol{p}$ and $\boldsymbol{q}$ denote the dimensionless momentum and coordinate vectors, whose elements correspond to the normal modes:

$$p_i = \left(\frac{1}{\hbar\omega_i}\right)^{1/2} P_i \quad (82)$$

$$q_i = \left(\frac{\omega_i}{\hbar}\right)^{1/2} Q_i \quad (83)$$

P_i and Q_i being the conjugate momentum and the normal coordinate, respectively, of the ith mode. In the general case $\boldsymbol{q}_{\mathrm{e}}$ and $\boldsymbol{q}_{\mathrm{g}}$ are related by the linear transformation:

$$\boldsymbol{q}_{\mathbf{e}} = \boldsymbol{S}\boldsymbol{q}_{\mathbf{g}} - \boldsymbol{\Delta} \quad (84)$$

$\boldsymbol{S}$ is Duschinsky rotation matrix which allows the ground-state and the excited-state normal modes to be different. $\boldsymbol{\Delta}$ is the dimensionless displacement between the equilibrium configurations of the two electronic states. The vibrational wavefunctions

of the ground- and excited-states have the following form:

$$\psi_{\mathrm{s}\mathbf{m}} = \prod_{i}^{N} \psi_{m_i}(q_{si}), \quad s = \mathrm{g},\ \mathrm{e} \tag{85}$$

where

$$\psi_{m_i}(q_{si}) = \pi^{-1/4}(m_i!2^{m_j})^{-1/2} \exp\left(-\frac{q_i^2}{2}\right) H_{m_i}(q_{si}) \tag{86}$$

is the m_ith eigenfunction of the ith mode and $H_{m_i}(q_{si})$ is the Hermite polynomial of the m_ith order. It follows from Eqs. (82)–(86), that the FC factors depend directly on the structural difference between the ground and excited electronic states. Thus, the lineshape of the electronic absorption spectrum and rR excitation profiles reflect the geometrical structure and vibrational force field in the excited-state. In order to calculate σ_A and $(\alpha_{\rho\lambda})_{I\to F}$ one needs to perform the summation over all multidimensional vibrational eigenstates of the excited-state surfaces. The computational cost of this procedure scales as $\sim N^L$, where L is the maximum number of vibrational excitation quanta. The latter number is usually chosen in a way that ensures that higher excitations give negligible contributions to the final intensities. From the scaling considerations it is immediately evident that such calculations become computationally prohibitive as the size of the molecule and the corresponding number of modes grows. In addition, Eqs. (76) and (77) do not lend themselves easily to qualitative interpretations due to the many nested summations and possible interference effects. Thus, it is difficult to determine which aspects of the excited-state PESs play a dominant role in the rR enhancement mechanisms of different vibronic bands within a given electronic transition. When working with large molecules, it appears preferable to begin at the simplest reasonable level of approximation, where the vibronic transitions and rR intensities depend only on a small number of parameters that can be related to certain topological characteristics of the excited-state PESs, and at the same time can be determined from the experimental data in a straightforward way.

5.1.1. The IMDHO model

The simple approach used for the evaluation of the multidimensional FC factors is to assume that the ground- and excited-states are harmonic, have the same normal modes compositions ($S_{ij} = \sqrt{\omega_{ei}/\omega_{gi}}\delta_{ij}$, i.e. no Duschinsky effect) and differ only in equilibrium positions and vibrational frequencies. This special case is the "independent mode, displaced harmonic oscillator" (IMDHO) model. In fact, in this model on usually even assumes identical vibrational frequencies in the ground- and excited-states and only allows for a shift in the minima of the excited state harmonic PESs relative to the harmonic ground state PES. Under these strongly simplifying approximations, a system of N vibrational modes can be treated as a collection of N independent pairs of harmonic oscillators. Each degree of freedom is completely described by a vibrational frequency ω_i and its origin shift Δ_i in dimensionless normal coordinates (*vide infra*). For this case Manneback [276] derived recursion relations for one-dimensional FC factors, from which it is readily deduced that the electronic absorption lineshape and rR intensities depend on $\mathbf{\Delta}$, and, in the case of excited-state frequency changes, on $\{R_i\}$, where $R_i = \omega_{gi}/\omega_{ei}$. The origin shift Δ_i along the ith mode makes the major contribution to the rR intensity I_i of the ith fundamental, though the overall shape of the rR excitation profile depends on the displacements along all normal modes. This behaviour is perhaps best understood from the time-dependent theory of absorption and rR intensities (vide infra). If, on the other hand, the origin shift is zero, then the Raman fundamental is forbidden by parity, but overtones may appear with non-negligible intensity if there is a frequency change on the excitation.

5.1.2. The Shorygin approach

The semiclassical theory of Shorygin [286,287], which combines the polarizability theory with the dispersion equation, permits a direct relation between rR intensities and excited-state PES gradients in the case of A-term activity. This theory has met at least with qualitative success although it departs from the correct theory by certain drastic approximations. Later, Krushinskii and Shorygin [288,289], presented a "quantum model" to modify the semiclassical theory. Assuming the potentials of the ground and excited states to be harmonic and identical in force constants, they obtained the following approximate expression for the A-term in the case of an isolated electronic transition:

$$A = (M_{\mathrm{ge}})^2 \left[\frac{(E_{\mathrm{ge}}^{\mathrm{v}})^2 + E_L^2}{(E_{\mathrm{ge}}^{\mathrm{v}})^2 - E_L^2}\right] 2k\Delta\langle i|q|f\rangle \tag{87}$$

where $E_{\mathrm{ge}}^{\mathrm{v}}$ is the vertical transition energy; k the force constant for given normal mode, Δ the dimensionless displacement of excited-state PES along this mode.

5.1.3. Savin's equation

The rR excitation profiles of different vibrational modes in the same molecule may have considerably different lineshapes. Therefore, the relative intensities of two Raman lines at any given excitation energy in the resonance region may not be directly related to the displacements along the corresponding modes. However, relative Raman intensities of fundamentals behave quite regularly in the preresonance region, for which a simple approximation has been derived [269,275,290–292]:

$$|(\alpha_{\rho\lambda})_{0\to 1}|^2 \left|\frac{\Delta_s\omega_s}{(E_0 - E_L + i\Gamma_p)(E_0 - E_L + \omega_s + i\Gamma_p)}\right|^2 \tag{88}$$

where Δ_{s} and ω_{s} are the dimensionless displacement and frequency of the vibrational mode the intensity of which is being measured. As the detuning energy $(E_0 - E_{\mathrm{L}})$ becomes large, Eq. (88) reduces to

$$|(\alpha_{\rho\lambda})_{0\to 1}|^2 \frac{\Delta_s^2\omega_s^2}{(E_0 - E_L)^4} \tag{89}$$

Eq. (89) is usually referred to as Savin's formula [269,275,290–292]. Its importance is that although the FC factors depend upon Δ alone, the preresonant Raman intensities have a strong dependence on the vibrational frequency. Savin's

formula is likely to present the simplest possible parameterization of rR data in the case of A-term activity and is widely used in analysis of experimental results for isolated electronic transitions [247,251,293].

5.1.4. Transform theory

Another approach which is used for the calculations of rR intensities is the so-called transform theory. This theory is based on the 'optical theorem', which connects the optical absorption with the imaginary part of the polarizability tensor components through the Kramers–Kroning relations between the real and the imaginary parts of the polarizability tensor components [294]. The relations may be used to deduce polarizability-dependent quantities, like rR intensities, from optical absorption spectra. The transform theory approaches to rR scattering were developed independently by Blazej and Peticolas [295] and by Tonks and Page [296,297]. For the IMDHO model it was shown that the shape of rR excitation profiles for fundamental, overtone, and combination bands depends only on the absorption bandshape and the mode frequency, whereas the absolute scaling of the excitation profiles depend on the corresponding excited-state displacements Δ [298]. For a single electronic transition the absolute value of Δ can be obtained from the absorption spectrum and absolute Raman cross-section for the mode of interest. Commonly, absolute cross-sections are not measured, and Δ can be obtained from the overtone to fundamental ratio, as the overtone and fundamental intensities depend on different powers of Δ. If overtone intensities are not available, relative values of Δ for different modes can still be obtained from their relative rR intensities at a single excitation wavelength. Modifications of the transform theory approach for the calculations of rR intensities have also been made in order to include excited-state frequency changes [299,300] and Duschinsky rotations [301]. The transform approach is more general than direct modeling techniques, as it is valid in the presence of arbitrary and unknown frequency changes, anharmonicities, or Duschinsky rotations in modes other than the ones of interest. However, from the methodological viewpoint the transform approach has the significant drawback that its formalism for the calculation of rR intensities has been developed for the case of a single excited electronic state. In practice, the excited-state distortions are calculated from rR intensities, or, vice-versa, rR intensities are determined from Δ by utilizing an absorption bandshape which is either the experimental one [254] or a crude approximation like a simple Gaussian band [255]. Thus, the method is difficult to apply if the rR spectrum is obtained for an excitation frequency at which several electronic states are in resonance with the incident light. Under such circumstances, one first needs to deconvolve the absorption spectrum into its constituent bands, which is difficult, if not impossible, without a direct modeling technique involving a joint fit of the absorption spectrum and the rR intensities. Furthermore, transform theory relies on the relationship between the absorption spectrum and the Raman polarizability, which is not preserved in any simple form if the measured absorption spectrum is not that of a single molecule. Therefore, the validity of utilization of experimental absorption spectrum, which is usually characterized by significant inhomogeneous broadening, in order to construct rR excitation profiles seems to be questionable.

5.1.5. Time dependent techniques

Since the sum-over-states formulation of the absorption cross-section and rR polarizability turns out to be very difficult to evaluate exactly for large molecules with many vibrational degrees of freedom, many workers have chosen to solve the problem in the time-domain. The most attractive feature of this approach is that it features a linear scaling of the computational effort with the number of vibrational modes. A successful application of this approach thus avoids the necessity to calculate the entire spectrum of eigenvalues and eigenvectors of a complex system, and, at the same time, clearly reveals the connection between the rR intensities and the excited-state nuclear dynamics, which is obscured in sum-over-states methods. Two time-domain approaches have been developed. The first one employs Green's function techniques [302,303]. The molecular lineshapes are expressed in terms of Fourier transforms of appropriate time-correlation functions which may be evaluated in closed form for a general harmonic molecule including equilibrium displacements, frequency changes and Duschinsky rotations [303]. This technique has also the advantage of considering finite-temperature effects, but it is mathematically more involved than the second, and more widely used, time-dependent approach, which is based on wave packet dynamics developed by Heller [304] and applied to rR scattering by Lee and Heller [304,305]. The wave packet formulation of the rR scattering provides a simple and intuitively appealing physical picture of this process. Initially, the corresponding expression for the rR polarizability was derived directly from time-dependent perturbation theory, but it is actually more easily obtained starting from the usual sum-over-states formula. The denominator in the expression for the rR polarizability (Eq. (77)) can be written as a half-Fourier transform [247,306]:

$$\begin{aligned}(\alpha_{\rho\lambda})_{I\to F} &= \sum_n M_{0n,\rho} M_{0n,\lambda} \sum_{\nu_n} \frac{\langle f|\nu_n\rangle\langle\nu_n|i\rangle}{(\varepsilon_{\nu n} - \varepsilon_{i0} + E_{0n} - E_L) - i\Gamma_n} \\ &= \sum_n M_{0n,\rho} M_{0n,\lambda} \int_0^\infty \sum_{\nu_n} \langle f|\nu_n\rangle\langle\nu_n|i\rangle \\ &\quad \times \mathrm{e}^{-i((\varepsilon_{\nu n} - \varepsilon_{i0} + E_{0n} - E_L) - i\Gamma_n)t}\mathrm{d}t \end{aligned} \tag{90}$$

where the integration time is chosen to have the unit, which is reciprocal to energy. Since:

$$\langle\nu_n|\mathrm{e}^{-i(\varepsilon_{\nu n}+E_{0n})t} = \langle\nu_n|\mathrm{e}^{-i\hat{H}_n t} \tag{91}$$

where $\hat{H}_n$ is the vibrational Hamiltonian for the nth, Eq. (90) can be rewritten as:

$$(\alpha_{\rho\lambda})_{I\to F} = \sum_n M_{0n,\rho} M_{0n,\lambda} \int_0^\infty \langle f|i_n(t)\rangle \mathrm{e}^{i(E_L+\varepsilon_{i0}+i\Gamma_n)t}\mathrm{d}t \tag{92}$$

where $e^{-i\hat{H}_n t}$ is the propagator considered to operate on the right-hand side; $i_n(t) = \mathrm{e}^{-i\hat{H}_n t}|i\rangle$ is the time-dependent nuclear wavefunction corresponding to the nth excited state.

Likewise, the transformation of the absorption cross-section to the time domain is done by replacing in Eq. (76) the energy denominator by a real part of a half-Fourier transform [248,307]:

$$\sigma(E_L) = \frac{4\pi}{3\hbar c} E_L \sum_n (M_{0n})^2 \mathrm{Re} \int_0^\infty \langle i|i_n(t)\rangle \mathrm{e}^{i(E_L+\varepsilon_{i0}+i\Gamma_n)t} \mathrm{d}t \tag{93}$$

Eq. (93) may be interpreted as a Fourier transform of the overlaps of wave packets moving on the excited PES's with the initial vibrational wavefunction at a time zero $|i\rangle$ [307,308]. Eq. (92) involves the same wave packets and their overlaps with the final vibrational state $|f\rangle$ [305].

The central part in the derivations of Heller and coworkers is the solution for a propagating wave packet $i_n(t)$. The initial vibrational state is a multivariate Gaussian (at $T = 0$ K). In this case (as follows for Ehrenfest's theorem) in harmonic potentials, Gaussian wave packets remain Gaussian, and undergo periodic motions. Furthermore, the expectation values of position and momenta obey the classical equations of motion, although the Gaussian wavepacket among other features, may spread or acquire phase factors. Thus, relatively few parameters serve to specify a complete quantum wavefunction $i_n(t)$ and its exact solution has been found in the general harmonic case including equilibrium displacements, frequency changes and Dushinsky rotations [306]. In this way the absorption cross-section and the rR polarizabilitiy (Eqs. (76) and (77) can be accurately evaluated in the case of general harmonic potentials by means of the equivalent integral expressions (Eqs. (92) and (93)).

In particular, for the case of the IMDHO model, the resulting overlap integrals in Eqs. (92) and (93) take on the relatively simple forms:

$$\langle f|i_n(t)\rangle = \prod_k \left\{ \frac{(-1)^{m_k}(\Delta_k^n)^{m_k}}{(2^{m_k} m_k!)^{1/2}} (1-\mathrm{e}^{-i\omega_k t})^{m_k} \right\} \times \mathrm{e}^{-\sum_j s_j^n (1-\mathrm{e}^{-i\omega_j t})} \mathrm{e}^{-i(E_{0n}+\varepsilon_{i0})t} \tag{94}$$

$$\langle i|i_n(t)\rangle = \mathrm{e}^{-\sum_j s_j^n (1-\mathrm{e}^{-i\omega_j t}) - i(\varepsilon_{i0}+E_{0n})t} \tag{95}$$

where Δ_k^n is the dimensionless origin shift of the nth excited-state PES along kth normal mode; $s_k^n = (\Delta_k^n)^2/2$; m_k is the excitation number of the kth mode in the final vibrational state $|f\rangle$.

Thus, the final expressions for absorption cross-section and rR polarizabilities in the IMDHO model have the following form:

$$\sigma(E_L) = \frac{4\pi}{3}\alpha(a_0)^2 E_L \sum_n (M_{0n})^2 \times \mathrm{Re} \int_0^\infty \mathrm{e}^{i(E_L-E_{0n})t - \Gamma_n t - \sum_j s_j^n (1-\mathrm{e}^{-i\omega_j t})} \mathrm{d}t \tag{96}$$

$$(\alpha_{\rho\lambda})_{I\to F} = \sum_n M_{0n,\rho} M_{0n,\lambda} \prod_k \left\{ \frac{(-1)^{m_k}(\Delta_k^n)^{m_k}}{(2^{m_k} m_k!)^{1/2}} \right\} \times \int_0^\infty \prod_k \{(1-\mathrm{e}^{-i\omega_k t})^{m_k}\} \times \mathrm{e}^{i(E_L-E_{0n})t - \Gamma_n t - \sum_j s_j^n (1-\mathrm{e}^{-i\omega_j t})} \mathrm{d}t \tag{97}$$

where α is the dimensionless fine-structure constant given as 1/137.03599; $a_0 = 0.529167$; and transition dipole moments M_{0n} are expressed in atomic units. The cross-section σ (in Å^2/molecule) in Eq. (92) is related to the molar extinction coefficient ε (in M^{-1} cm^{-1}) by:

$$\varepsilon = \frac{1}{\ln(10)} 10^{-19} N_\mathrm{A} \sigma \tag{98}$$

where N_A is Avogadro's number. It follows from Eq. (97) that the computation of rR excitation profiles scales as $N_f = \prod_k \{(\Delta_k)^{2m_k}/(2^{m_k} m_k!)\}$. That is, although rR bands corresponding to different vibrational excitation numbers in the final state have different profile bandshapes, the intensities of overtone and combination bands necessarily correlates with those of the fundamental bands, which fact must be used in the analysis of experimental data as well as in the assignment of rR bands [13].

5.1.6. "Short-time" dynamics in resonance Raman scattering

When only times shorter than the fastest excited-state vibrational period make an important contribution to the integral (92), rR scattering is said to be in the "short-time limit", and many aspects of Raman scattering are greatly simplified [309]. There are several possibilities for recurrences in $\langle f|i(t)\rangle$ following the initial activity near $t \sim 0$ to become unimportant: (1) The incident photon energy E_L may be off resonance with excited electronic states. In this case the integrand of Eq. (92) oscillates rapidly causing the integral to self-cancel for $t > \tau$, where $\Delta E\tau \approx 1$ and ΔE is the energy mismatch. (2) If the homogeneous linewidth Γ is very large, the $\mathrm{e}^{-\Gamma t}$ factor truncates the integral at short times. It is generally agreed that the homogeneous linewidth does not exceed 1000 cm^{-1} in most systems. Therefore, as pointed out in ref. [9], it is unlikely that a large Γ by itself can be responsible for short-time behaviour on resonance, although it may be a contributing factor in conjunction with other effects. (3) There may be many displaced modes of different frequencies. Effectively, this is equivalent to a large damping term without having to assume a very large Γ. Thus, the simultaneous return of wave-packet $i(t)$ to the FC region is unlikely until relatively long times. However, recurrences that occur at long times are quenched by the phenomenological damping factor. Finally, significant Duschinsky rotations may also result in a large effective damping.

In the short-time regime the information about the excited potential energy surface that is required in order to calculate rR intensities is localized in the vicinity of the FC region. Fortunately, this means that electronic structure calculations in the FC

region will be sufficient to determine rR intensities (vide infra). Within the short-time approximation and under the assumption of no changes in the force constants in the excited state, the rR intensities of fundamental and overtone bands for a single electronic excitation are given by the following expressions [309]:

$$|(\alpha_{\rho\lambda})^{k}_{0\to 1}(E_L)|^2 \sim \frac{(V_{Q,k})^2}{2\omega_{gk}\sigma^4}\varepsilon_1\left(\frac{E_L - E_{ver}}{\sigma}\right) \tag{99}$$

$$|(\alpha_{\rho\lambda})^{k}_{0\to 2}(E_L)|^2 \sim \frac{(V_{Q,k})^4}{2(\omega_{gk})^2\sigma^6}\varepsilon_2\left(\frac{E_L - E_{ver}}{\sigma}\right) \tag{100}$$

where

$$2\sigma^2 = \sum_k \left(\frac{(V_{Q,k})^2}{\omega_{gk}}\right) \tag{101}$$

and

$$\varepsilon_n(\omega) = \left|\int_0^\infty \mathrm{e}^{(i\omega t)-(t^2/2)} t^n \mathrm{d}t\right|^2 \tag{102}$$

$V_{Q,k} = \partial E/\partial Q_k|_{Q=0}$ is the excited-state potential energy gradient along the kth normal mode at the ground-state equilibrium geometry and E_{ver} is the vertical excitation energy. At the same level of approximation the absorption spectrum is given by the formula:

$$\sigma_A(E_L) = \frac{2\sqrt{2}\pi^{3/2}}{3\hbar c\sigma} M^2 E_L \exp\left(\frac{(E_L - E_{ver})^2}{2\sigma^2}\right) \tag{103}$$

It follows from Eqs. (99)–(103) that relative rR intensities of fundamental lines are directly proportional to the square of partial derivatives of the excited-state electronic energy with respect to ground-state normal modes at the ground-state equilibrium position. The derivation of Eqs. (99)–(103) was based on the assumption of the locally harmonic excited-state PESs. Thus, the results are generally not restricted to harmonic potentials. It can be shown that in the IMDHO model rR intensities of fundamental bands in Eq. (99) become proportional to $\Delta_k^2\omega_{gk}^2$. The same behaviour was also found in the preresonance region using other approaches [269,275,290–292] (see Savin's formula (89)). The application of the gradient formulae (99)–(103) for analysis of experimental data and first principle calculation of rR spectra has been used in many papers [249–251,254,255,310]. Usually this method provides reasonable accuracy. However, it has several limitations. Firstly, although the results are intuitively appealing, it is not sensible to use Eqs. (99)–(103) to construct rR profiles and absorption bandshapes over the whole spectral range since the conditions for the short-time dynamics might not be fulfilled on resonance. Secondly, the vibrational overlap for overtones and combination bands develops more slowly than the overlap for fundamentals. Thus, when rR scattering is in the short-time limit, the overtones and combination bands are expected to be weak relative to the fundamentals [309]. In all these cases, the application of full-time dynamics is more appropriate. Thirdly, when the absorption spectrum and rR excitation profiles of a molecule reveal vibronic structure, the application of Eqs. (99)–(103) is not sensible since $\varepsilon_1(\omega)$, $\varepsilon_2(\omega)$ and $\sigma_A(E_{\mathrm{L}})$ give rise to featureless curves.

5.2. Implementation of Heller's theory

Since the problem of computing rR intensities, profiles and absorption bandshapes has been reduced to a manageable level through the many approximations discussed above, it is only necessary to know the transition dipole moments in the FC region and the excited state displacements. This information can either come from fitting the unknowns to experimental data or they can be deduced from quantum chemical calculations (vide infra). We have developed a general computer program which is linked to the ORCA electronic structure package. The program takes the transition moments and excited state displacements for any number of vibrational modes and electronic transitions and evaluates Eqs. (96) and (97) in order to predict the desired spectra which can then be directly compared to experimental measurements. Below we describe a few key aspects of the program. Full details will be provided elsewhere [311].

It can be shown that the calculation of absorption cross-section and rR polarizabilitiy (Eqs. (92)–(93)) can be reduced to the evaluation of the following elementary integral:

$$O(\omega, \{\omega_j\}, \{s_j\}, \Gamma) = \int_0^\infty \mathrm{e}^{i\omega t - \Gamma t - \sum_j s_j(1-\mathrm{e}^{-i\omega_j t})}\mathrm{d}t \tag{104}$$

It is necessary to calculate this integral consistently, since too few time steps in the numerical integration may result in severe baseline oscillations. Usually the density of integration points should be increased upon increase of $1/\Gamma$ and s, and when far off resonance ($\omega \gg 0$). Therefore, it is suggested that the total number of integration points is increased until the same number of points will provide convergence of the integral (104) and non-negativeness of its real part is ensured for the whole range of ω under study. According to our experience, the latter requirement is strong enough to automatically satisfy the first one.

Due to the linear scaling on the number of active modes the time-dependent method is particularly advantageous for large molecules. Though, the prefactor in the linear dependence is relatively high, and for the case of small number of normal modes or not very large displacements $\left(\sum_i s_i^2 \leq 1 \div 2\right)$ the original sum-over-states method is still faster. In such cases it is possible to develop the analytical expression of the integral in Eq. (104) as a power series in the $\{s_i\}$:

$$O(\omega) = \sum_{k=0}^{\infty} I_k(\omega) \tag{105}$$

The individual terms in the series (105) are calculated through the following straightforward recursion relations:

$$I_k(\omega) = \frac{1}{\omega + i\Gamma}\sum_j s_j\omega_j I_{k-1}(\omega - \omega_j) \tag{106}$$

with

$$I_0(\omega) = \frac{i}{\omega + i\Gamma} \tag{107}$$

The importance of high-order terms in the series (105) grows upon going to higher energies ($\omega > 0$), and the number of terms

necessary to include in the calculation correlates with the maximum vibrational excitation number in the excited state, which is characterized by some noticeable vibronic intensity. The power series method shows an efficiency similar to the original sum-over-states formulation for absorption and Raman cross-sections. By approximating the integral $O(\omega)$ with the first term $I_0(\omega)$ in the series (Eq. (105)) one recovers Savin's formula (Eq. (89)) for pre-resonance Raman intensities.

5.3. Quantum chemical modeling of electronic absorption spectra and RR intensities

Quantum chemical calculations can provide useful structural information for the ground and excited states, thus enabling first principles calculation of absorption spectra and rR excitation profiles. As discussed for example by Myers and Mathies [9], neither the normal mode compositions, nor the signs of the displacements parameters can be determined from experimental data alone. However, both are readily obtained from quantum chemical calculations. In such a way excited-state displacements can be explicitly related to certain geometrical changes in the excited state, including bond-length and bond-angle changes.

Assuming a purely harmonic behavior of excited-state PES, it is possible to choose between three methods of calculation of the origin shift Δ, excited-state frequencies and the Duschinsky rotation matrix:

(I) Δ is obtained from geometry optimization of the ground- and excited states. First, the excited-state normal mode displacement Δ_Q is calculated by projecting the differences in the mass-weighted Cartesian coordinates onto the excited-state normal coordinates:

$$\Delta_{Q,j} = \sum_i L_{ij} D_i^{(m)} \tag{108}$$

or, in matrix form,

$$\boldsymbol{\Delta}_Q = \boldsymbol{L}^T \boldsymbol{D}^{(m)} \tag{109}$$

where $\boldsymbol{L}$ is the transformation matrix between mass-weighted Cartesian and normal coordinates; $\boldsymbol{D}^{(m)}$ contains the mass-weighted differences in the Cartesian coordinates. Then the dimensionless displacements can be found according to the following formula:

$$\Delta_i = \left(\frac{\omega_{ei}}{\hbar}\right)^{1/2} \Delta_{Q,i} \tag{110}$$

The Duschinsky rotation matrix $\boldsymbol{S}$ and harmonic frequencies of the ground- and excited states are evaluated in energy second derivative calculations. Such an approach is applicable for example for the CIS, RPA, CASSCF, and TD-DFT methods, for which analytical gradients are available [312,313]. An excellent example of how vibronic fine structure may be simulated with TD-DFT based methods is the paper by Neugebauer et al. [314] on the vibronic fine structure of the permanganate ion. Despite of the small size of the molecule (5 atoms) the authors reported a set of vibronic basis states of size 35,389,440. While such a large calculation is feasible with today's computer facilities, a full solution of the vibronic problem in the way indicated by this study will remained confined to the domain of small molecules. Excited-state geometry optimizations with subsequent (numerical) force-field calculations on small molecules have been reported in several papers [255,266,267,271,285,315–319].

(II) For the harmonic potentials the same task can be accomplished by simply calculating the excited-state energy gradient and second derivatives at the ground-state equilibrium geometry. Under the harmonic approximation a single Newton–Raphson step then immediately leads to the excited state minimum. This procedure has obvious advantages over the first method, since excited state geometry optimizations are far from trivial. In particular, geometry changes may induce changes in the ordering of the excited states or changes in the ordering of the orbitals involved in the transitions. It is even possible that no suitable minimum can be found for a particular excited-state. In all these cases, calculations using method I will fail or at least become very cumbersome.

(III) The parameters of excited PES's are evaluated through energy scan calculations. At present this is the only choice for the methods like MRCI calculations, and MRPT, for which analytical energy gradients are presently not available in the ORCA program.

There is some evidence that the neglect of Duschinsky rotations in quantum chemical calculations and analysis of experimental data may be justified. First of all, the reliability of excited-state force fields has not been systematically assessed which is primarily due to the lack of experimental data on the excited-state frequencies. Thus, a large calculated normal mode rotation upon excitation may be caused by an unbalanced theoretical treatment of the ground- and excited-states. A good example illustrating this point is given in ref. [271]. At the CIS/6-31G level of theory, the force fields of the ^1A_g and $^1B_{2u}$ states of the benzene molecule indicated that the b_{2u} mode submatrix showed a large degree of mixing if unscaled force fields were employed. This mixing was subsequently substantially reduced by a scaling procedure which was used to fit the experimental ground- and excited-state frequencies. Though the Duschinsky effect results in the modification of vibronic and rR intensities, it is difficult to distinguish it experimentally from the transition moment coordinate dependence, finite temperature, and anharmonic effects. The introduction of the Duschinky matrix as an additional set of parameters may lead to overparametrization of the experimental data, thus giving rise to spurious minima in the fitting procedure, though the overall quality of the fit may be considerably improved. In addition, in many cases, the accuracy of experimental rR data may not be high enough to allow the unambiguous identification of Duschinky rotations. Unlike the case of absorption spectroscopy the rR intensity calibration may introduce noticeable errors arising from self-absorption effects as well as the wavelength dependence of the detection system sensitivity, which are almost always ignored in experimental studies.

If the ground and excited-state surfaces normal modes are parallel, a simple relationship between the excited state energy gradients and the dimensionless displacements can be deduced for method (II). Since the expression for the excited-state potential energy in terms of the mass-weighted normal coordinates is of the form

$$E = E_0 + \frac{1}{2}\sum_k \omega_{ek}^2 (Q - \Delta_{Q,k})^2 \tag{111}$$

it follows that

$$V_{Q,k} = -\omega_{ek}^2 \Delta_{Q,k} \tag{112}$$

where $V_{Q,k} = \partial E/\partial Q_k|_{Q=0}$ is the excited-state potential energy gradient along the kth normal mode at the ground-state equilibrium geometry. It can be evaluated from the Cartesian energy gradient according to the formula

$$V_{Q,k} = \sum_i \frac{1}{\sqrt{m_i}} V_{X,i} L_{ik} \tag{113}$$

or, in matrix notation,

$$\boldsymbol{V}_Q = \boldsymbol{L}^T \boldsymbol{M}^{-1/2} \boldsymbol{V}_X \tag{114}$$

where $\boldsymbol{V}_X$ is the vector of Cartesian excited-state energy gradient; $\boldsymbol{M}$ is diagonal mass matrix.

If no frequency changes are assumed in the excited-state ($\omega_{ek} = \omega_{gk}$) then the displacements can be simply evaluated on the basis of energy-gradient calculations according to Eqs. (112)–(114). Otherwise, one should calculate $\{\omega_{ek}\}$ from the Cartesian excited-state energy second-derivative matrix:

$$W_{Q,kk} = \sum_{i,j} \frac{1}{\sqrt{m_i m_j}} W_{X,ij} L_{ik} L_{jk} \tag{115}$$

or, in matrix notation,

$$\boldsymbol{W}_Q = \boldsymbol{L}^T \boldsymbol{M}^{-1/2} \boldsymbol{W}_X \boldsymbol{M}^{-1/2} \boldsymbol{L} \tag{116}$$

where $\boldsymbol{W}_Q$ is the normal coordinate excited-state energy second-derivative matrix with the diagonal elements $W_{Q,kk} = \omega_{ek}^2$; $\boldsymbol{W}_X$ is the Cartesian excited-state energy second-derivative matrix.

The excited-state normal mode displacements and frequencies can be calculated through the fit of the excited-state potential energy of the form given in Eq. (111) to the energies which are evaluated for a set of molecules geometries that are displaced along the corresponding normal modes. There are two possibilities to perform such energy scan steps. In the first method, only the length of the displacement in the Cartesian coordinates along the kth normal mode ($d_{X,k}$) is initially specified. Then the corresponding vector of Cartesian displacements is calculated by the formula

$$\delta R_{X,ik} = \frac{d_{X,k}}{||\boldsymbol{T}_k||} T_{ik} \tag{117}$$

or, in vector form,

$$\boldsymbol{\delta R}_{X,k} = \frac{d_{X,k}}{\|\boldsymbol{T}_k\|} \boldsymbol{T}_k \tag{118}$$

where $\boldsymbol{\delta R}_{X,k}$ is the vector of Cartesian displacement along the kth normal mode; $\boldsymbol{T}_k$ is the kth mass-weighted normal mode unit vector expressed in Cartesian coordinates; $||\boldsymbol{T}_k||$ is its norm; $\boldsymbol{T}_k$ has the components $T_{ik} = (1/\sqrt{m_i})L_{ik}$. The length of the displacement along a mass weighted normal mode $d_{Q,k}$ which corresponds to a Cartesian displacement $d_{X,k}$ is calculated according to the formula

$$d_{Q,k} = \frac{d_{X,k}}{||\boldsymbol{T}_k||} \tag{119}$$

Alternatively, one can choose the step size according to an estimate of the expected change in the electronic energy ΔE_{exp} due to the displacement. It is reasonable to choose a ΔE_{exp} which is above the characteristic noise level of the given method of calculation. Then:

$$d_{Q,k} = \frac{\sqrt{2\Delta E_{\mathrm{exp}}}}{\omega_{gk}} \tag{120}$$

the corresponding displacement vector in Cartesian coordinates is given by expression

$$\delta \boldsymbol{R}_{X,k} = d_{Q,k} \boldsymbol{T}_k \tag{121}$$

If all calculations of $\Delta_{Q,k}$ in Eqs. (33)–(45) proceed in atomic units then the corresponding dimensionless displacements can be obtained from the simple formula

$$\Delta_k = \left(\frac{\omega_k^2}{m_{\mathrm{e}}}\right)^{0.25} \Delta_{Qk} \tag{122}$$

where all quantities are expressed in atomic units; m_{e} is the electron mass ($m_{\mathrm{e}} = 0.000548579903$ Da).

Owing to anharmonic effects, gradient and normal mode scan calculations will lead to values of $\{\Delta_k\}$ which generally differ from the 'true' values obtained by full geometry optimization. This means that the $\{\Delta_k\}$ do not precisely correspond to the shift of excited equilibrium geometry, but rather serve as some effective values to specify the local harmonic parameters of the excited PES's in the FC region. However, the local behaviour of the PESs determines the initial dynamics of propagating wavepackets which is of dominant importance for the absorption bandshape and rR intensities. Thus, quantum chemical methods like gradient and normal mode scan calculations, which are biased towards achieving accuracy in the FC region and not in the region of the potential minimum of the excited state, seem to be preferable over geometry optimization techniques for the calculations of the absorption bandshape and rR intensities.

Provided excited-state displacements $\boldsymbol{\Delta}$ were determined in the fitting of rR intensities together with the absorption bandshape, and normal mode compositions (i.e. the transformation matrix $\boldsymbol{L}$) as well as the signs of the displacements were calculated quantum chemically, then the difference in Cartesian coordinates between excited- and ground states $\boldsymbol{D}$ can be evaluated in the following way:

$$D_i = \sum_k \left(\frac{\hbar}{\omega_{ei}}\right)^{1/2} \frac{L_{ik}\Delta_k}{\sqrt{m_i}} \tag{123}$$

or, in the matrix form,

$$\boldsymbol{D} = \hbar^{1/2}\boldsymbol{\Omega}_{\mathrm{e}}^{-1/2}\boldsymbol{M}^{-1/2}\boldsymbol{L}\boldsymbol{\Delta} \tag{124}$$

where Ω_{e} is the diagonal matrix of excited-state frequencies.

While the present work was near completion a method which also directly models absorption spectra and rR intensities from quantum chemical calculations was presented [320]. This approach relies on Placzek-type polarizability theory valid for normal Raman and rR scattering [321–325]. RR excitation profiles were calculated from the derivatives of the frequency-dependent polarizabilities with respect to normal coordinates. The method is a short-time approximation to the KHD formalism. The calculation of the polarizability derivatives is an extension of a recent method to calculate the resonance and non-resonance polarizabilities by including the finite lifetime of the electronic excited-states into linear-response theory within TD-DFT [326]. The method successfully reproduced the rR spectra of uracil and pyrene [320].

5.4. An example: UV–vis, resonance Raman and quantum chemical study of transition metal bis-dithiolenes

The methodological approach presented above has been extensively tested in a combined UV–vis, rR, and quantum chemical study of a series of transition metal complexes involving the benzene-1,2-dithiol (L^{2-}) and Sellmann's 3,5-di-*tert*-butyl-benzene-1,2-dithiol(L^{Bu2-}) ligands [13]. Below we briefly explain the results obtained for the $[Ni^{II}(L)(L^{\bullet})]^{1-}$ system. This is a square planar complex with approximate D_{2h} symmetry. The electronic ground state is characterized by the electron configuration $(1a_u)^2(1b_{1u})^2(2b_{3g})^2\,(2b_{2g})^1(1b_{1g})^0$. The singly occupied the $2b_{2g}$ orbital is predominantly ligand based and consequently the system is best described as a delocalized ligand radical bound to a diamagnetic low-spin Ni(II) d^8 central metal [327]. As discussed in detail in ref. [327], this compound features an intense absorption band in the near IR region shown in Fig. 3. It can be decomposed into two bands which are assigned to the $1b_{1u} \rightarrow 2b_{2g}$ and $1a_u \rightarrow 2b_{2g}$ single electron excitations which are both best viewed as intervalence charge transfer (IVCT) transitions [327]. Detailed rR studies provided valuable insight into the nature of these transitions and have helped to identify important marker vibrations for the detection of ligand based radicals in similar complexes.

The ~77 K frozen-solution rR spectrum shown in Fig. 3 was obtained with laser excitation at 840 nm which falls into the region of the IVCT band. A rich set of vibrational peaks were observed between 150 and 1800 cm^{-1} which were assigned to vibrational fundamentals, overtones and combination bands. The detailed assignments followed from the comparison of calculated (BP86/TZVP) and observed vibrational fundamental frequencies which are presented in Table 12 (see ref. [13] for details). Since the FC mechanism is expected to dominate the rR enhancement, the most intense peaks were assigned to totally symmetric fundamentals. In the assignment of overtone and combination bands we have used the fact that under

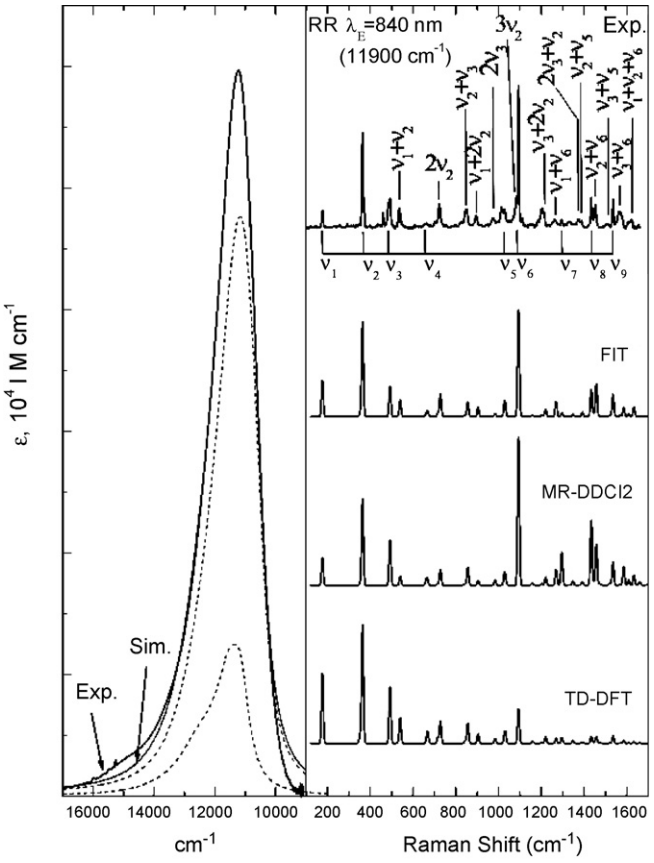

Fig. 3. Deconvoluted absorption spectrum of $[Ni^{II}(L)(L^{\bullet})]^{1-}$ in the range 9000–17,000 cm^{-1} (left); experimental and simulated rR spectra (right) corresponding to dimensionless normal coordinate displacements obtained from the fit, MR-DDCI2 and spin-unrestricted BP86 DFT calculations (Table 12). The two dotted lines represent the individual band shapes of the two different electronic transitions contributing to the observed absorption band. The solid line is their superposition and almost coincides with the experimental spectrum except for the hump ~15,000 cm^{-1} where another transition contributes to the spectrum which was not unambiguously identified or modeled.

the approximation of separable harmonic surfaces their intensities necessarily correlate with those of the fundamental bands ([9,306]; compare Eq. (97)). The observation of overtone and combination bands implies noticeable values of the associated excited state distortions. These values were evaluated through a nonlinear least-square fitting procedure based on the Heller analysis described above.

The two dominantly enhanced normal modes which are in resonance with the IVCT transition are the intense rR bands at ~360 and ~1100 cm^{-1}. They were assigned to Ni–S (ν_2) and C–C (ν_6) stretching vibrations, respectively. The fact that in addition to low-frequency Ni–S stretching modes there is significant enhancement of C–C stretching vibrations (1000–1600 cm^{-1}) already indicates significant ligand involvement in the electronic excitation.

In order to obtain more insight into these enhancement patterns, electronic structure calculations were used in order to estimate excited state dimensionless normal coordinate displacements (Δ_i^I where i labels normal modes and I electronic states). Having obtained reasonable estimates of the nonzero Δ_i^I,

Table 12
Calculated (BP86/TZVP) and experimental frequencies of the most important totally symmetric vibrations that appear in the rR spectra of $[Ni(L)_2]^{1-}$ compound, and corresponding dimensionless normal coordinate displacements for $1b_{1u} \rightarrow 2b_{2g}$ and $1a_u \rightarrow 2b_{2g}$ electronic transitions obtained from the fit, MR-DDCI2 and spin-unrestricted BP86 DFT methods

Vibration	Frequency		Δ					
	Calc.	Exp. RR	$1b_{1u} \rightarrow 2b_{2g}$			$1a_u \rightarrow 2b_{2g}$		
			TD-DFT	MR-DDCI2	Fit	TD-DFT	MR-DDCI2	Fit
Metal-ligand stretching (ν_1)	158.4	176	1.74	1.92	1.90	0.83	0.46	0.65
M—S stretching, C—deformation (ν_2)	343.7	364	1.03	1.47	1.36	0.50	0.72	0.99
Ring deformation, C—S stretching (ν_3)	477.2	492	0.51	0.73	0.52	0.36	0.45	0.67
Ring deformation, C—S stretching (ν_4)	663.4	662	0.03	0.19	0.09	0.12	0.04	0.22
C—C stretching, C—S stretching (ν_5)	1016.3	1028	0.08	0.16	0.16	0.0	0.05	0.07
C—C stretching, C—S stretching (ν_6)	1079.2	1093	0.18	0.57	0.44	0.26	0.37	0.46
C—C stretching (ν_7)	1324	1296	0.07	0.12	0.02	0.35	0.39	0.31
C—C stretching (ν_8)	1421.1	1433	0.08	0.31	0.20	0.31	0.35	0.32
C—C stretching (ν_9)	1522.3	1535	0.09	0.20	0.19	0.22	0.17	0.19

theoretical rR spectra can be deduced by combining these displacements with transition energies, transition moments as well as the phenomenological linewidth parameter Γ obtained from fitting the absorption bandshape. Since the theoretical displacements turned out to be reasonably accurate they needed little refinement in the subsequent fitting of the rR intensities. Note that it is sufficient to fit a single rR spectrum together with the absorption bandshape in order to obtain the displacements of all modes which are in resonance with the electronic transition studied [247]. In addition to detailed calculations, we will outline below a simple qualitative method that in many cases can explain the observed enhancement patterns without the need to perform elaborate quantum chemical calculations. All that is needed are the shapes of the normal modes involved and an electronic difference density from some kind of excited state calculation that we take to be TD-DFT together with the BP86 functional in the present case.

Unfortunately, the analysis of the experimental data is complicated by the fact that the laser excitation (840 nm) is such that the observed rR spectra (Fig. 3) falls in resonance with both of the electronic transitions described above which must consequently be accounted for in the fitting procedure. The calculated and fitted dimensionless normal coordinate displacements are compared in Table 12. The agreement between theory and experiment is striking despite the considerable number of simplifying assumptions made. In particular, the multireference ab initio based MR-DDCI2 results are more accurate than the more easily obtained TD-DFT values which are, however, also fairly reasonable. Interestingly, in spite of the large values found for Δ_1, mode ν_1 has a rather small rR intensity. This is explained by the significant frequency dependence of the rR intensities and more narrow excitation profiles for low-frequency modes as compared to high-frequency ones. The fit of the absorption spectrum between 9000 and 17,000 cm^{-1} clearly indicates that the peculiar bandshape of the intense near-IR IVCT transition results from the superposition of two electronic band systems. Together with the significant vibronic broadening the effective bandwidth is almost 2.5 times higher than the homogeneous linewidth.

In our opinion, these results are very encouraging and it is to be expected that techniques like the one used in this study will see much more widespread in the near future. Below, the computational results are qualitatively interpreted.

5.4.1. Enhancement mechanism for $1b_{1u} \rightarrow 2b_{2g}$ transitions

For this type of transition the donor $1b_{1u}$ MO is the bonding combination of the HOMO ($2b_2$) of two L^{2-} ligands [327], while the acceptor $2b_{2g}$ level is the antibonding combination. The b_{2g} ligand fragment MO can undergo a symmetry allowed back-bonding interaction with the Ni–d_{xz} orbital which was analyzed in detail previously [327]. Accordingly, the difference density plot for an $1b_{1u} \rightarrow 2b_{2g}$ transition (Fig. 4) indicates a loss of bonding for the M–S, C_3–C_4, C_1–C_2, C_1–C_6 and C_5–C_6 bonds, thus leading to their lengthening in the electronically excited state. At the same time the C–S bonds are expected to contract. Consequently, in addition to the expected Ni–S bond elongation the geometry changes associated with the $1b_{1u} \rightarrow 2b_{2g}$ excitation have a significant component that corresponds to quinoidal distortion (elongation of C_1–C_2, C_1–C_6 and C_5–C_6 bonds) of the aromatic ring. The totally symmetric normal modes with the largest projections onto this elongation and contraction pattern are expected to show the dominant enhancement in the rR spectra. These criteria are met by the ν_1 ($\sim$170 cm^{-1}), ν_2 ($\sim$350 cm^{-1}) and ν_6 ($\sim$1100 cm^{-1}) modes (Fig. 4). The latter mode features in-phase stretching of C_1–C_2, C_1–C_6 and C_5–C_6 bonds and thus has the largest projection onto the quinoidal component of the excited state distortion among the other C–C stretching vibrations.

5.4.2. Enhancement mechanism for $1a_u \rightarrow 2b_{2g}$ transitions

For the $1a_u \rightarrow 2b_{2g}$ IVCT transition the main difference is that the donor $1a_u$ MO is a non-bonding combination of the $2a_2$ MO of two L^{2-} fragment orbitals [327]. This implies less elongation of the M–S bonds upon excitation as compared to the $1b_{1u} \rightarrow 2b_{2g}$ case. This explains why the calculated excited state displacements Δ_1 and Δ_2 associated with the NiS stretching modes have smaller values (Table 12). The difference density

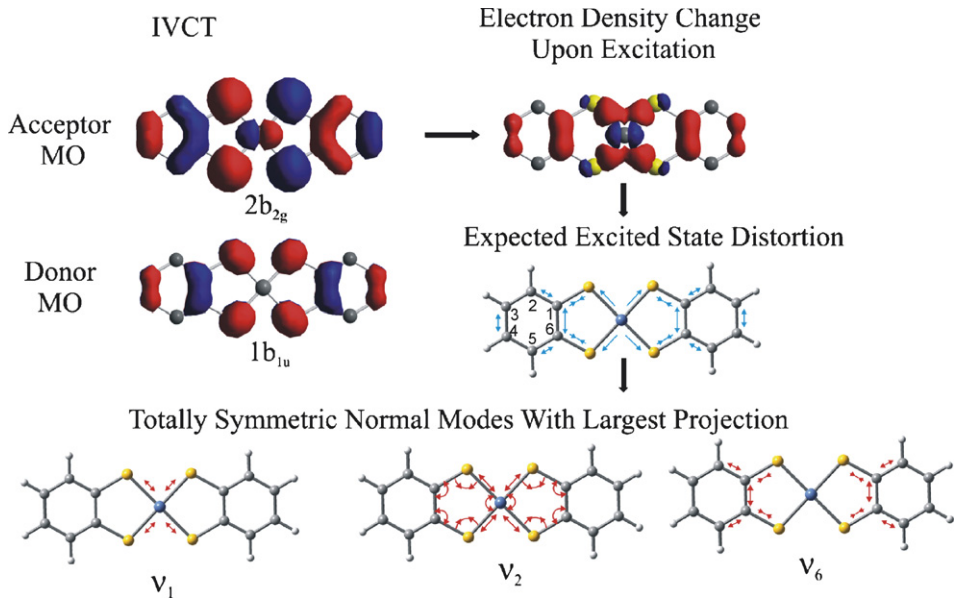

Fig. 4. Normal modes with the largest excited state displacements for the IVCT $1b_{1u} \rightarrow 2b_{2g}$ transition of $[Ni^{II}(L)(L^{\bullet})]^{1-}$ and their relation to the nature of excitation. Donor and acceptor MOs were obtained from spin-unrestricted BP86 DFT calculations. The corresponding electronic difference density is plotted for the isodensity value of 0.0008 a.u. (red and blue colors indicate a decrease and increase of the electronic density in the excited state, respectively). Bond length changes upon excitation are represented by outward arrows (bond elongation) and inward arrows (bond contraction). In the normal mode representation the length of arrows and arch-lines roughly designate the relative amplitude of bond stretching and bending, respectively. Internal coordinates vibrating in antiphase are denoted by inward and outward arrows.

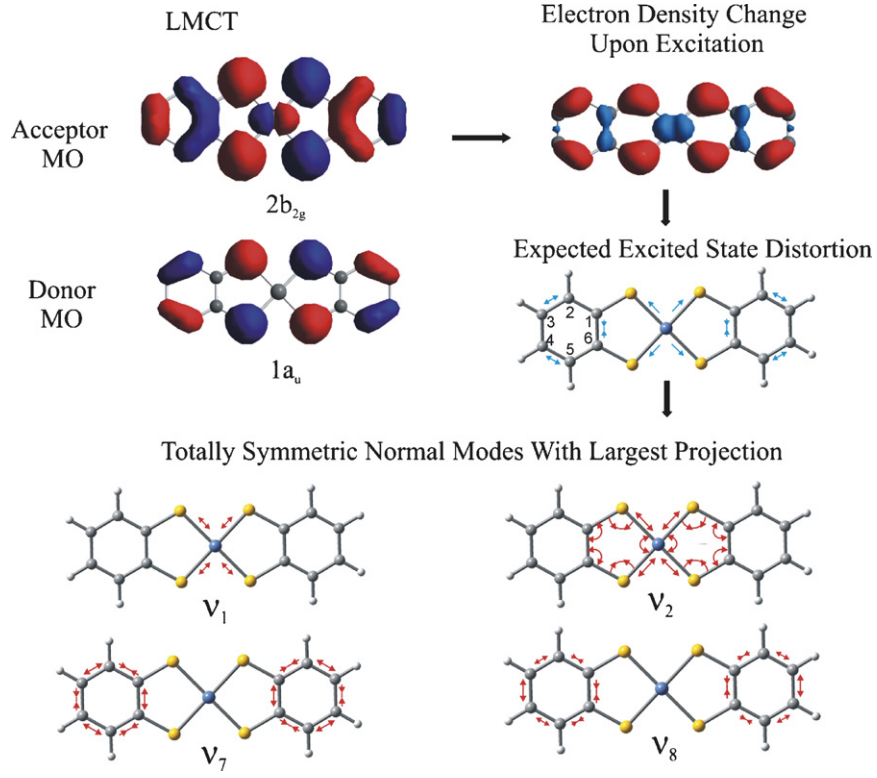

Fig. 5. Normal modes with the largest excited state displacements for the IVCT $1a_u \rightarrow 2b_{2g}$ transition of $[Ni^{II}(L)(L^{\bullet})]^{1-}$ and their relation to the nature of excitation. Donor and acceptor MOs obtained from spin-unrestricted BP86 DFT calculations. The corresponding electronic difference density is plotted for the isodensity value of 0.0008 a.u. (red and blue colors indicate a decrease and increase of the electronic density in the excited state, respectively). Bond length changes upon excitation are schematically represented by outward arrows (bond elongation) and inward arrows (bond contraction). In the normal mode representation the length of arrows and arch-lines roughly designate the relative amplitude of bond stretching and bending, respectively. Internal coordinates vibrating in antiphase are denoted by inward and outward arrows.

plot for the $1a_u \rightarrow 2b_{2g}$ transition (Fig. 5) indicates the loss of bonding for the C_2–C_3 and C_4–C_5 bonds and gain of bonding for the C_1–C_6 bond. This leads to the lengthening of the former and contraction of the latter bonds in the excited state. Similar to the case of a $1b_{1u} \rightarrow 2b_{2g}$ transition such a distortion pattern has a significant component along the ν_6 mode. In addition, there are significant projections of the excited state distortion onto the ν_7 and ν_8 modes which both feature in-phase stretching of the C_2–C_3 and C_4–C_5 bonds. The net effect is that according to the calculations and the fit to the experimental data, the excited state displacements along ν_6, ν_7 and ν_8 are almost equal upon $1a_u \rightarrow 2b_{2g}$ excitation (Table 11).

6. Concluding remarks

In this review, we have described in some detail ab initio approaches to several aspects of transition metal optical spectroscopy with emphasis on the methods used and developed in our laboratory. It was shown that the SORCI method on top of state-averaged CASSCF calculations represents an accurate method for the prediction of transition metal multiplets, even in conjunction with moderate basis sets. The method at its present stage of development can be applied to somewhat larger molecules with 30–50 atoms and ~500–700 basis functions. The popular TD-DFT method is distinctly less successful in the prediction of transition metal multiplets due to the various failures of its present realizations and the restrictions imposed by a single reference determinant in the Kohn–Sham framework. In our opinion, multiconfigurational ab initio methods which take care of static and at least differential dynamic correlation provide a natural framework for the calculation of such effects. The SORCI method is just one of the possible realizations of such a method. While it has been reasonably successful in the recent past, it definitely requires further implementational and conceptual improvements. Many of the remaining problems could be elegantly solved by reformulating the method in an internally contracted framework and replacing the a posteriori Davidson correction for size consistency with a more rigorous treatment of unlinked cluster effects, possibly along the lines of Staemmler's MCCEPA method [131]. Work in this direction is in progress in our laboratory.

In the second part of the review, the calculation of one- and two-electron SOC effects from first principles has been discussed. The recent implementation of the full spin-orbit mean-field (SOMF) operator provides a very accurate and efficient effective one-electron SOC treatment which closely reproduces the SOC constants of free atoms and ions, and by inference and experience, also gives a very good approximation to the full Breit-Pauli SOC operator in molecules. The SOMF approach is distinctly more accurate than popular effective potential SOC operator used in many DFT programs which may introduce errors of up to ~30% in calculated observables. We have described the incorporation of the SOMF operator into the multiconfigurational CASSCF and MRCI/SORCI modules of the ORCA program in some detail and it was shown that this combination of techniques yields accurate results. This implementation forms the basis for the calculation of various SOC dependent optical and magnetic properties of transition metal ions in complexes which are currently being explored. An obvious improvement is the formulation of the SOMF operator in the framework of the ZORA and DKH methods which will allow the successful application of the methodology to all-electron calculations on heavy elements, where kinematic relativistic effects become important.

In the third part of this review recent attempts were described to predict absorption bandshapes and resonance Raman intensities from first principles calculations. In particular, we have focused our attention on the exploration of local harmonic parameters of excited state potential energy surfaces at the ground state equilibrium geometry in combination with Heller's time dependent theory of absorption and resonance Raman theory. The latter provides a conceptually and computationally attractive framework. It fully avoids the laborious calculation of multidimensional Franck–Condon factors which quickly becomes a bottleneck in bandshape calculations on larger molecules. The combination with analytic or numeric partial gradient techniques, which only sample the shape the of the excited state PES in the Franck–Condon region, is particularly attractive due to two reasons: first, such techniques have been developed to high efficiency by the quantum chemical community over the past several decades and, in particular, are readily implemented for TD-DFT methods which are often accurate enough for at least a qualitative discussion of experimental results. However, we have shown above that even strongly simplified multireference ab initio methods can yield better agreement with experiment, at least for the cases studied so far. Secondly, the restriction to the Franck–Condon region is a big advantage over methods which require a more global sampling of excited states PESs since the latter is difficult to achieve in a stable and efficient way. The occurrence of curve crossings, conical intersections and avoided crossings makes geometry optimization on excited surfaces very challenging and unlikely to succeed for higher lying excited states of a given symmetry. Yet, the restriction to the Franck–Condon region is a sensible approximation for larger molecules since due to multimode interference effects, their absorption and resonance Raman spectra are usually dominated by short-time dynamics effects.

In conclusion, we believe that some progress in the treatment of transition metal optical spectra has been documented in this review. In our opinion, the prospects of theoretical transition metal optical spectroscopy are bright and we look forward to apply the methods described herein and their refinements in close conjunction with experimental investigations in the near future. This progress will be necessary in order to make contributions not only to inorganic spectroscopy itself but also to fields like inorganic photochemistry, which is of increasing importance in both, the industrial and the academic framework.

Acknowledgements

We are indebted to Dr. Michael Atanasov (University of Heidelberg) for careful reading and important comments on the manuscript. We also gratefully acknowledge the financial support of this work by the Max-Planck Gesellschaft, the pri-

ority program 1137 of the German Science Foundation, the Sonderforschungsbereich 663 at the university of Düsseldorf, the German-Israeli Foundation and the Fonds der Chemischen Industrie. Excellent technical assistance with the computer facilities used in this work by Mr. Rolf Trinoga is also gratefully acknowledged.

References

[1] J.S. Griffith, The Theory of Transition Metal Ions, Camebridge University press, Camebridge, 1964.
[2] L.E. Orgel, An Introduction to Transition Metal Chemistry, Ligand Field Theory, John Wiley and Sons, New York, 1966.
[3] E.I. Solomon, Comments Inorg. Chem. 3 (1984) 227.
[4] E.I. Solomon, A.B.P. Lever, in: E.I. Solomon, A.B.P. Lever (Eds.), Inorganic Electronic Structure and Spectroscopy, vol. 1, Wiley, New York, 1999, p. 1.
[5] E.I. Solomon, M.A. Hanson, in: E.I. Solomon, A.B.P. Lever (Eds.), Inorganic Electronic Structure and Spectroscopy, Wiley, New York, 1999, p. 1ff.
[6] M.A. Hitchman, M.A. Riley, in: E.I. Solomon, A.B.P. Lever (Eds.), Inorganic Electronic Structure and Spectroscopy, John Wiley and Sons, New York, 1999, p. 213.
[7] P.J. Stephens, J. Chem. Phys. 52 (1970) 3489.
[8] F. Neese, E.I. Solomon, Inorg. Chem. 38 (1999) 1847.
[9] A.B. Myers, R.A. Mathies, in: T.G. Spiro (Ed.), Biological Applications of Raman Spectroscopy, Wiley, New York, 1987, p. 1.
[10] J.I. Zink, K.S.K. Shin, Adv. Photochem. 16 (1991) 119.
[11] R.J.H. Clark, in: C.D. Flint (Ed.), Vibronic Processes in Inorganic Chemistry, Kluwer Academic Publishers, Amsterdam, 1989, p. 301.
[12] A. Vogler, H. Kunkley, Comments Inorg. Chem. 9 (1990) 201.
[13] T. Petrenko, K. Ray, K. Wieghardt, F. Neese, J. Am. Chem. Soc. 128 (2006) 4422.
[14] D. Herebian, K. Wieghardt, F. Neese, J. Am. Chem. Soc. 125 (2003) 10997.
[15] C.J. Ballhausen, Introduction to Ligand Field Theory, McGraw-Hill, New York, 1962.
[16] C.J. Ballhausen, H.B. Gray, Molecular Orbital Theory, Benjamin, New York, 1964.
[17] C.K. Jørgensen, Adv. Chem. Phys. 5 (1963) 33.
[18] C.K. Jørgensen, Struct. Bond. 1 (1966) 3.
[19] C.K. Jørgensen, Struct. Bond. 6 (1969) 94.
[20] C.E. Schäffer, C.K. Jørgensen, Mol. Phys. 9 (1965) 401.
[21] H.H. Schmidtke, Theor. Chim. Acta 20 (1971) 92.
[22] L.G. Vanquickenborne, A. Ceulemans, Coord. Chem. Rev. 48 (1983) 157.
[23] Y. Sugano, S. Tanabe, H. Kimura, Multiplets of Transition Metal Ions in Crystals, Academic Press, New York, 1970.
[24] F. Neese, E.I. Solomon, in: J.S. Miller, M. Drillon (Eds.), Magnetoscience—From Molecules to Materials, vol. IV, Wiley VCH, Weinheim, 2003, p. 345.
[25] W.J. Hehre, L. Radom, P.V.R. Schleyer, J.A. Pople, Ab Initio Molecular Orbital Theory, John Wiley and Sons, New York, 1986.
[26] J. Ridley, M.C. Zerner, Theor. Chim. Acta 32 (1973) 111.
[27] M.C. Zerner, G.H. Loew, R.F. Kirchner, U.T. Mueller-Westerhoff, J. Am. Chem. Soc. 102 (1980) 589.
[28] M.C. Zerner, in: K.B. Lipkowitz, D.B. Boyd (Eds.), Reviews in Computational Chemistry, vol. 2, VCH, Heidelberg, 1990, p. 315.
[29] W.P. Anderson, W.D. Edwards, M.C. Zerner, Inorg. Chem. 25 (1986) 272.
[30] M.C. Zerner, in: D.R. Salahub, N. Russo (Eds.), Metal-Ligand Interactions: From Atoms, to Clusters, to Surfaces, Kluwer Academic publishers, Amsterdam, 1992, p. 101.
[31] M.C. Zerner, in: N. Russo, D.R. Salahub (Eds.), Metal Ligand Interactions, Kluwer Academic, Amsterdam, 1996, p. 493.
[32] S.N. Greene, N.G.J. Richards, Inorg. Chem. 45 (2006) 17.
[33] V.K.K. Praneeth, C. Näther, G. Peter, N. Lehnert, Inorg. Chem. 45 (2006) 2795.
[34] M. Mader-Cosper, F. Neese, A.V. Astashkin, M.A. Carducci, A.M. Raitsimring, J.H. Enemark, Inorg. Chem. 44 (2005) 1290.
[35] M. Ottonelli, G.M.M. Izzo, F. Rizzo, G. Musso, G. Dellepiane, R. Tubino, J. Phys. Chem. B 109 (2005) 19249.
[36] T.A. O'Brien, J. Phys. Chem. A 108 (2004) 5016.
[37] A. DelMedico, E.S. Dodsworth, A.B.P. Lever, W.J. Pietro, Inorg. Chem. 43 (2004) 2654.
[38] T.A. Jackson, A. Karapetian, A.-F. Miller, T.C. Brunold, J. Am. Chem. Soc. 126 (2004) 12477.
[39] S.N. Greene, N.G. Richards, Inorg. Chem. 43 (2004) 7030.
[40] T. Paine, E. Bothe, E. Bill, T. Weyhermüller, L. Slep, F. Neese, P. Chaudhuri, Inorg. Chem. 43 (2004) 7324.
[41] A.P. Meacham, K.L. Druce, Z.R. Bell, M.D. Ward, J.B. Keister, A.B.P. Lever, Inorg. Chem. 42 (2003) 7887.
[42] H. Masui, A.L. Freda, M.C. Zerner, A.B.P. Lever, Inorg. Chem. 39 (2000) 141.
[43] F. Neese, J.M. Zaleski, K.E. Loeb, E.I. Solomon, J. Am. Chem. Soc. 122 (2000) 11703.
[44] R. Metcalfe, A.B.P. Lever, Inorg. Chem. 36 (1997) 4762.
[45] W. Koch, M.C. Holthausen, A Chemist's guide to Density Functional Theory, Wiley-VCH, Weinheim, 2000.
[46] H. Chermette, Coord. Chem. Rev. 178–180 (1998) 699.
[47] T. Lovell, F. Himo, W.-G. Han, L. Noodleman, Coord. Chem. Rev. 238–239 (2003) 211.
[48] I. Ciofini, C.A. Daul, Coord. Chem. Rev. 238–239 (2003) 187.
[49] J. Autschbach, T. Ziegler, Coord. Chem. Rev. 238–239 (2003) 83.
[50] F.M. Bickelhaupt, E.J. Baerends, in: K.B. Lipkowitz, D.B. Boyd (Eds.), Rev. Comp. Chem., Wiley-VCH, New York, 2000, p. 1.
[51] M. Diedenhofen, T. Wagener, G. Frenking, in: T.R. Cundari (Ed.), Computational Organometallic Chemistry, Marcel Dekker, New York, 2001, p. 69.
[52] E.K.U. Gross, W. Kohn, Adv. Quantum Chem. 21 (1990) 255.
[53] M.E. Casida, in: D.P. Chong (Ed.), Recent Advances in Density Functional Methods, World Scientific, Singapore, 1995, p. 155.
[54] R. Bauernschmitt, R. Ahlrichs, Chem. Phys. Lett. 256 (1996) 454.
[55] R. Bauernschmitt, M. Häser, O. Treutler, R. Ahlrichs, Chem. Phys. Lett. 264 (1997) 573.
[56] J.F. Dobson, in: J.F. Dobson, et al. (Eds.), Electronic Density Functional Theory: Recent Progress and New Directions, Plenum Press, New York, 1998.
[57] F. Furche, J. Chem. Phys. 114 (2001) 5982.
[58] S. Grimme, M. Parac, Chem. Phys. Chem. 3 (2003) 292.
[59] A. Dreuw, M. Head-Gordon, Chem. Rev. 105 (2005) 4009.
[60] K. Andersson, P.A. Malmquvist, B.O. Roos, A.J. Sadlej, K. Wolinski, J. Phys. Chem. 94 (1990) 5483.
[61] K. Andersson, P.A. Malmquvist, B.O. Roos, J. Chem. Phys. 96 (1992) 1218.
[62] K. Andersson, Theor. Chim. Acta 91 (1995) 31.
[63] K. Andersson, B.O. Roos, in: D. Yarkony (Ed.), Modern Electronic Structure Theory, World Scientific, Singapore, 1995, p. 55.
[64] K. Pierloot, in: T.R. Cundari (Ed.), Computational Organometallic Chemistry, Marcel Dekker, New York, 2001, p. 123.
[65] B.O. Roos, K. Andersson, M.P. Fülscher, P.A. Malmquist, L. Serrano-Andres, K. Pierloot, M. Merchan, in: I. Prigogine, S.A. Rice (Eds.), Advances in Chemical Physics, vol. XCIII, John Wiley & Sons, New York, 1996, p. 219.
[66] B.O. Roos, K. Andersson, M.P. Fülscher, L. Serrano-Andres, K. Pierloot, M. Merchan, V. Molina, J. Mol. Struct. (Theochem.) 388 (1996) 257.
[67] F. Neese, ORCA—an ab initio, density functional and semi-empirical program package, Max-Planck institute for bioinorganic chemistry, Mülheim an der Ruhr, Germany, 2005.
[68] F. Neese, J. Chem. Phys. 119 (2003) 9428.
[69] F. Neese, J. Inorg. Biochem. 100 (2006) 716.
[70] F. Neese, J. Am. Chem. Soc. (2006), in press.
[71] M. Wanko, M. Hoffmann, P. Strodel, W. Thiel, F. Neese, T. Frauenheim, M. Elstner, J. Phys. Chem. B 109 (2005) 3606.
[72] J. Schöneboom, F. Neese, W. Thiel, J. Am. Chem. Soc. 127 (2005) 5840.

[73] K. Ray, T. Weyhermüller, F. Neese, K. Wieghardt, Inorg. Chem. 44 (2005) 5345.
[74] A. Fouqeau, M.E. Casida, L.M. Lawson, A. Hauser, F. Neese, J. Chem. Phys. 122 (2005), 044110/1.
[75] S. Blanchard, F. Neese, E. Bothe, E. Bill, T. Weyhermüller, K. Wieghardt, Inorg. Chem. 44 (2005) 3636.
[76] F. Neese, Magn. Reson. Chem. 42 (2004) S187.
[77] A. Fouqueau, S. Mer, M.E. Casida, L.M.L. Daku, A. Hauser, T. Mieva, F. Neese, J. Chem. Phys. 120 (2004) 9473.
[78] E. Bill, E. Bothe, P. Chaudhuri, K. Chlopek, D. Herebian, S. Kokatam, K. Ray, T. Weyhermüller, F. Neese, K. Wieghardt, Chem. Eur. J. 11 (2004) 204.
[79] B. Huron, J.P. Malrieu, P. Rancurel, J. Chem. Phys. 58 (1973) 5745.
[80] S. Evangelisti, J.P. Daudey, J.P. Malrieu, Chem. Phys. 75 (1983) 91.
[81] R.J. Buenker, S.D. Peyerimhoff, Theor. Chim. Acta 35 (1974) 33.
[82] R.J. Buenker, S.D. Peyerimhoff, Theor. Chim. Acta 39 (1975) 217.
[83] M. Hanrath, B. Engels, Chem. Phys. 225 (1997) 197.
[84] J. Miralles, O. Castell, R. Caballol, J.P. Malrieu, Chem. Phys. Lett. 172 (1993) 33.
[85] V.M. Garcia, O. Castell, R. Caballol, J.P. Malrieu, Chem. Phys. Lett. 238 (1995) 222.
[86] A. Szabo, N.S. Ostlund, Modern Theoretical Chemistry, MacMillan Pub. Inc., New York, 1982.
[87] Basis sets were obtained from the Extensible Computational Chemistry Environment Basis Set Database, Version 02/25/04, as developed and distributed by the Molecular Science Computing Facility, Environmental and Molecular Sciences Laboratory which is part of the Pacific Northwest Laboratory, P.O. Box 999, Richland, Washington 99352, USA, and funded by the U.S. Department of Energy. The Pacific Northwest Laboratory is a multi-program laboratory operated by Battelle Memorial Institute for the U.S. Department of Energy under contract DE-AC06-76RLO 1830. Contact Karen Schuchardt for further information.
[88] F. Jensen, Introduction to Computational Chemistry, Wiley, New York, 1999.
[89] P.E.M. Siegbahn, M.R.A. Blomberg, M. Svenson, Chem. Phys. Lett. 223 (1994) 35.
[90] T.D. Crawford, H.F. Schaefer III, in: K.B. Lipkowitz, D.B. Boyd (Eds.), Reviews in Computational Chemistry, vol. 14, Wiley-VCH, New York, 2000, p. 33.
[91] H.J. Werner, in: K.P. Lawley (Ed.), Ab Initio Methods in Quantum Chemistry II, John Wiley and Sons, New York, 1987, p. 1.
[92] U. Meier, V. Staemmler, Theor. Chim. Acta 76 (1989) 95.
[93] R. Sheppard, in: K.P. Lawley (Ed.), Ab initio Methods in Quantum Chemistry II, John Wiley and Sons, New York, 1987, p. 63.
[94] B.O. Roos, in: K.P. Lawley (Ed.), Ab initio Methods in Quantum Chemistry II, John Wiley and Sons, New York, 1987, p. 399.
[95] B.O. Roos, in: B.O. Roos (Ed.), Lecture Notes in Quantum Chemistry, Springer, Berlin, 1992, p. 177.
[96] H.J. Werner, P.J. Knowles, MOLPRO, Cardiff (UK) and Stuttgart, Germany, 2005.
[97] K. Andersson, M. Barysz, A. Bernhardson, M.R.A. Blomberg, D.L. Cooper, M.P. Fülscher, C. de Graaf, B.A. Hess, G. Karlström, R. Lindh, P.A. Malmqvist, T. Nakajima, P. Neogrady, J. Olsen, B.O. Roos, B. Schimmelpfennig, M. Schütz, L. Seijo, L. Serrano-Andres, P.E.M. Siegbahn, J. Stalring, T. Thosteinson, V. Veryazov, P.-O. Widmark, MOLCAS, Lund, Sweden, 2002.
[98] H.J. Werner, F.R. Manby, P.J. Knowles, J. Chem. Phys. 118 (2003) 8149.
[99] G. Hetzer, P. Pulay, H.J. Werner, Chem. Phys. Lett. 290 (1998) 143.
[100] A. El Azhary, G. Rauhut, P. Pulay, H.J. Werner, J. Chem. Phys. 108 (1998) 5185.
[101] G. Rauhut, P. Pulay, H.J. Werner, J. Comp. Chem. 19 (1998) 1241.
[102] F. Weigend, M. Häser, H. Patzelt, R. Ahlrichs, Chem. Phys. Lett. 294 (1998) 143.
[103] F. Weigend, A. Köhn, C. Hättig, J. Chem. Phys. 116 (2002) 3175.
[104] P. Pulay, S. Saebo, K. Wolinski, Chem. Phys. Lett. 344 (2001) 543.
[105] C. Angeli, R. Cimiraglia, S. Evangelisti, T. Leininger, J.P. Malrieu, J. Chem. Phys. 114 (2001) 10252.
[106] C. Angeli, R. Cimiraglia, J.P. Malrieu, J. Chem. Phys. 117 (2002) 9138.
[107] E.R. Davidson, A.A. Jarzecki, in: K. Hirao (Ed.), Recent Advances in Multireference Methods, World Scientific, Singapore, 1999, p. 31.
[108] R. Cimiraglia, Int. J. Quantum Chem. 60 (1996) 167.
[109] R. Cimiraglia, M. Persico, J. Comp. Chem. 8 (1987) 39.
[110] S. Grimme, M. Waletzke, Phys. Chem. Chem. Phys. 2 (2000) 2075.
[111] K. Hirao, Chem. Phys. Lett. 190 (1992) 374.
[112] P.M. Kozlowski, E.R. Davidson, J. Chem. Phys. 100 (1994) 3672.
[113] J.P. Malrieu, J.L. Heully, A. Zaitsevskii, Theor. Chim. Acta 90 (1995) 167.
[114] R.B. Murphy, R.P. Messmer, Chem. Phys. Lett. 183 (1991) 443.
[115] H. Nakano, J. Chem. Phys 99 (1993) 7983.
[116] H. Nakano, J. Nakatani, K. Hirao, J. Chem. Phys. 114 (2001) 1133.
[117] H. Nakano, R. Uchiyama, K. Hirao, J. Comp. Chem. 23 (2002) 1166.
[118] Y. Nakao, Y.-K. Choe, K. Nakayama, K. Hirao, Mol. Phys. 100 (2002) 729.
[119] K. Wolinski, P. Pulay, J. Chem. Phys. 90 (1989) 3647.
[120] H.A. Witek, Y.-K. Choe, J.P. Finley, K. Hirao, J. Comp. Chem. 23 (2002) 957.
[121] G. Ghigo, B.O. Roos, P.A. Malmqvist, Chem. Phys. Lett. 396 (2004) 142.
[122] W. Meyer, in: H.F. Schaefer III (Ed.), Methods of Electronic Structure Theory, Plenum Press, New York, 1977, p. 413.
[123] K. Andersson, Multiconfigurational Perturbation Theory, Ph.D. Thesis, University of Lund, Lund, Sweden, 1992.
[124] R. Ahlrichs, in: G.H.F. Diercksen, S. Wilson (Eds.), Methods in Computational Molecular Physics, D. Reidel, Dordrecht, 1983, p. 209.
[125] H. Lischka, R. Shepard, R. Pitzer, I. Shavitt, M. Dallos, T. Müller, P.G. Szalay, M. Seth, G.S. Kedziora, S. Yabushita, Z. Zhang, Phys. Chem. Chem. Phys. 3 (2001) 664.
[126] V.R. Saunders, J.H. van Lenthe, Mol. Phys. 48 (1983) 923.
[127] W. Meyer, R. Ahlrichs, C.E. Dykstra, in: C.E. Dykstra (Ed.), Advanced Theories and Computational Approaches to the Electronic Structure of Molecules, NATO Advanced Science Inst. Ser. C, New York, 1984, p. 19.
[128] G. Hirsch, P.J. Bruna, S.D. Peyerimhoff, R.J. Buenker, Chem. Phys. Lett. 52 (1977) 442.
[129] R.J. Gdanitz, R. Ahlrichs, Chem. Phys. Lett. 143 (1988) 413.
[130] P.G. Szalay, R.J. Bartlett, Chem. Phys. Lett. 214 (1993) 481.
[131] R. Fink, V. Staemmler, Theor. Chim. Acta 87 (1993) 129.
[132] L. Visscher, E. van Lenthe, Chem. Phys. Lett. 306 (1999) 357.
[133] P. Strange, Relativistic Quantum Mechanics, Cambridge University Press, Cambridge, 1998.
[134] H.J.A. Jensen, T. Saue, L. Visscher, V. Bakken, E. Eliav, T. Enevoldsen, T. Fleig, O. Fossgaard, T. Helgaker, J. Laerdahl, C.V. Larsen, P. Norman, J. Olsen, M. Pernpointner, J.K. Pedersen, K. Ruud, P. Salek, J.N.P. van Stralen, J. Thyssen, O. Visser, W.T. Dirac, a relativistic ab initio electronic structure program, release dirac04.0. (http://dirac.chem.sdu.dk), 2004.
[135] E. van Lenthe, J.G. Snijders, E.J. Baerends, J. Chem. Phys. 105 (1996) 6505.
[136] B.A. Hess, Phys. Rev. A 32 (1985) 756.
[137] B.A. Hess, Phys. Rev. A 333 (1986) 3742.
[138] G. Jansen, B.A. Hess, Phys. Rev. A 39 (1989) 6016.
[139] C. van Wüllen, J. Chem. Phys. 109 (1998) 392.
[140] M. Filatov, Chem. Phys. Lett. 365 (2002) 222.
[141] W. Klopper, E. van Lenthe, A.C. Hennum, J. Chem. Phys. 113 (2000) 9957.
[142] E. Van Lenthe: The ZORA Equation, Ph.D. thesis, Vrije Universiteit Amsterdam, Amsterdam, 1996.
[143] A. Wolf, M. Reiher, B.A. Hess, J. Chem. Phys. 117 (2002) 9215.
[144] F. Neese, A. Wolf, M. Reiher, T. Fleig, B.A. Hess J. Chem. Phys. 122 (2005), 204107/1.
[145] K.G. Dyall, E. van Lenthe, J. Chem. Phys. 111 (1999) 1366.
[146] E.U. Condon, G.H. Shortley, The Theory of Atomic Spectra, Cambridge University Press, Cambridge, 1964.
[147] D.S. McClure, J. Chem. Phys. 20 (1952) 682.
[148] S. Koseki, M.W. Schmidt, M.S. Gordon, J. Phys. Chem. 96 (1992) 10768.
[149] S. Koseki, M.S. Gordon, M.W. Schmidt, N. Matsunaga, J. Phys. Chem. 99 (1995) 12764.

[150] S. Koseki, M.W. Schmidt, M.S. Gordon, J. Phys. Chem. A 102 (1998) 10430.
[151] W. Pauli, Z. Phys. 43 (1927) 601.
[152] G. Breit, Phys. Rev. 34 (1929) 553.
[153] G. Breit, Phys. Rev. 36 (1930) 363.
[154] G. Breit, Phys. Rev. 39 (1932) 616.
[155] H. Bethe, E. Salpeter, Quantum Mechanics of One- and Two-Electron Atoms, Springer, Berlin, 1957.
[156] D.G. Fedorov, M.S. Gordon, J. Chem. Phys. 112 (2000) 5611.
[157] L. Veseth, J. Phys. B: At. Mol. Phys. 14 (1981) 795.
[158] T.R. Furlani, H.F. King, J. Chem. Phys. 82 (1985) 5577.
[159] M. Sjovoll, O. Gropen, J. Olsen, Theor. Chem. Acc. 97 (1997) 301.
[160] A. Berning, M. Schweizer, H.J. Werner, P.J. Knowles, P. Palmieri, Mol. Phys. 98 (2000) 1823.
[161] C.M. Marian, U. Wahlgren, Chem. Phys. Lett. 251 (1996) 357.
[162] D.R. Yarkony, Int. Rev. Phys. Chem. 11 (1992) 195.
[163] B.A. Hess, C.M. Marian, U. Wahlgren, O. Gropen, Chem. Phys. Lett. 251 (1996) 365.
[164] F. Neese, J. Chem. Phys. 122 (2005) 034107.
[165] O.L. Malkina, B. Schimmelpfennig, M. Kaupp, B.A. Hess, P. Chandra, U. Wahlgren, V.G. Malkin, Chem. Phys. Lett. 296 (1998) 93.
[166] K. Ruud, B. Schimmelpfennig, H. Agren, Chem. Phys. Lett. 310 (1999) 215.
[167] L. Gagliardi, B. Schimmelpfennig, L. Maron, U. Wahlgren, A. Willetts, Chem. Phys. Lett. 344 (2001) 207.
[168] P.A. Malmqvist, B.O. Roos, B. Schimmelpfennig, Chem. Phys. Lett. 357 (2002) 230.
[169] M. Kleinschmidt, J. Tatchen, C.M. Marian, J. Comp. Chem. 23 (2002) 824.
[170] A.V. Arbuznikov, J. Vaara, M. Kaupp, J. Chem. Phys. 120 (2004) 2127.
[171] O.L. Malkina, J. Vaara, B. Schimmelpfennig, M. Munzarova, V.G. Malkin, M. Kaupp, J. Am. Chem. Soc. 122 (2000) 9206.
[172] Z. Rinkevicius, L. Telyatnyk, P. Salek, O. Vahtras, H. Agren, J. Chem. Phys. 119 (2003) 10489.
[173] B. Schimmelpfennig, AMFI—An Atomic Mean Field Integral Program, University of Stockholm, Stockholm, Sweden, 1996.
[174] S. Patchkovskii, G. Schreckenbach, in: M. Kaupp, M. Bühl, V.G. Malkin (Eds.), Calculation of NMR and EPR Parameters, Wiley-VCH, Weinheim, 2004, p. 505.
[175] G. Schreckenbach, T. Ziegler, J. Phys. Chem. A 101 (1997) 3388.
[176] M. Atanasov, C. Daul, C. Rauzy, Struct. Bond. 106 (2004) 97.
[177] M. Atanasov, C. Daul, Chimia 59 (2005) 504–510.
[178] C. Anthon, J. Bendix, C.E. Schaffer, Inorg. Chem. 42 (2003) 4088.
[179] C. Anthon, J. Bendix, C.E. Schaffer, Inorg. Chem. 43 (2004) 7882.
[180] A.J.H. Wachters, J. Chem. Phys. 52 (1970) 1033.
[181] C.W. Bauschlicher Jr., S.R. Langhoff, H. Partridge, L.A. Barnes, J. Chem. Phys. 91 (1989) 2399.
[182] A. Schäfer, C. Huber, R. Ahlrichs, J. Chem. Phys. 100 (1994) 5829.
[183] R. Ahlrichs and co-workers, Universität Karlsruhe, Karlsruhe, 2006, ftp.chemie.uni-karlsruhe.de/pub/basen.
[184] J.L. Whitten, J. Chem. Phys. 58 (1973) 4496.
[185] O. Vahtras, J. Almlöf, M.W. Feyereisen, Chem. Phys. Lett. 213 (1993) 514.
[186] K. Eichkorn, F. Weigend, O. Treutler, R. Ahlrichs, Theor. Chem. Acc. 97 (1997) 119.
[187] K. Eichkorn, O. Treutler, H. Öhm, M. Häser, R. Ahlrichs, Chem. Phys. Lett. 240 (1995) 283.
[188] B.I. Dunlap, J.W.D. Connolly, J.R. Sabin, J. Chem. Phys. 71 (1979) 3396.
[189] R.A. Marcus, Chem. Rev. 88 (1988) 1475.
[190] J.K. Beattie, S.P. Best, B.W. Skelton, A.H. White, J. Chem. Soc. Dalton Trans. (1981) 2105.
[191] F.A. Cotton, L.M. Daniels, C.A. Murillo, J.F. Quesada, Inorg. Chem. 32 (1993) 4861.
[192] N. I. o. S. a. Technology in, 2005.
[193] S. Grimme, M. Parac, M. Waltezke, Chem. Phys. Lett. 334 (2001) 99.
[194] A. Ghosh, P.R. Taylor, Curr. Opin. Chem. Biol. 7 (2003) 113.
[195] K.K. Stavrev, M.C. Zerner, Int. J. Quantum Chem. 65 (1997) 877.
[196] M.C. Zerner, Int. J. Quant. Chem. XXXV (1989) 567.
[197] E.I. Solomon, C.J. Ballhausen, J. Mol. Phys. 29 (1975) 279.
[198] M.J. Harding, S.F. Mason, D.J. Robbins, A.J. Thomson, J. Chem. Soc. A 19 (1971) 3058.
[199] M.J. Harding, S.F. Mason, D.J. Robbins, A.J. Thomson, J. Chem. Soc. A 19 (1971) 3047.
[200] B.A. Hess, R.J. Buenker, P. Chandra, Int. J. Quantum Chem. 29 (1986) 737.
[201] B.A. Hess, C.M. Marian, S.D. Peyerimhoff, in: D. Yarkony (Ed.), Modern Electronic Structure Theory, World Scientific Publishing Company, Singapore, 1995.
[202] B.A. Hess, C.M. Marian, in: P. Jensen, P.R. Bunker (Eds.), Computational Molecular Spectroscopy, John Wiley & sons, New York, 2000, p. 169ff.
[203] A. Wolf, M. Reiher, B.A. Hess, J. Chem. Phys. 120 (2004) 8624.
[204] J. Tomasi, B. Mennucci, R. Cammi, Chem. Rev. 105 (2005) 2999.
[205] A. Klamt, G. Schüürmann, J. Chem. Soc. Perkin Trans. (1993) 799.
[206] F. Wennmohs, M. Diedenhofen, A. Klamt, F. Neese, Manuscript in preparation, 2006.
[207] S. Sinnecker, A. Rajendran, A. Klamt, M. Diedenhofen, F. Neese, J. Phys. Chem. A 110 (2006) 2235.
[208] A.D. Becke, Phys. Rev. A 38 (1988) 3098.
[209] A.D. Becke, J. Chem. Phys. 98 (1993) 5648.
[210] C. Lee, W. Yang, R.G. Parr, Phys. Rev. B 37 (1988) 785.
[211] F. Wang, T. Ziegler, J. Chem. Phys. 122 (2005) 074109.
[212] S. Grimme, M. Parac, Chem. Phys. Chem. 4 (2003) 292.
[213] D. Sundholm, Chem. Phys. Lett. 317 (2000) 317.
[214] D.J. Tozer, R.A. Amos, N.C. Handy, B.O. Roos, L. Serrano-Andres, J. Chem. Phys. 97 (1999) 859.
[215] C.K. Jørgensen, Acta Chem. Scand. 9 (1955) 1362.
[216] O.G. Holmes, D.S. McClure, J. Chem. Phys. 26 (1957) 1686.
[217] B.N. Figgis, M.A. Hitchman, Ligand Field Theory and its Applications, Wiley-VCH, New York, 2000.
[218] C. Dobe, C. Noble, G. Carver, P.L.W. Tregenna-Piggott, G.J. McIntyre, A.-L. Barra, A. Neels, S. Janssen, F. Juranyi, J. Am. Chem. Soc. 126 (2004) 16639.
[219] P.L.W. Tregenna-Piggott, H. Weihe, A.-L. Barra, Inorg. Chem. 42 (2003) 8504.
[220] P.W.L. Tregenna-Piggott, M.C.M. O'Brien, H. Weihe, H. Güdel, J. Chem. Phys. 109 (1998) 2967.
[221] P.W.L. Tregenna-Piggott, C.J. Noble, J.R. Pilbrow, J. Chem. Phys. 113 (2000) 3289.
[222] J. Landry-Hum, G. Bussiere, C. Daniel, C. Reber, Inorg. Chem. 40 (2001) 2595.
[223] E.I. Solomon, T.C. Brunold, M.I. Davis, J.N. Kemsley, S.K. Lee, N. Lehnert, F. Neese, A.J. Skulan, Y.S. Yang, J. Zhou, Chem. Rev. 100 (2000) 235.
[224] S. Iuchi, A. Morita, S. Kato, J. Chem. Phys. 121 (2004) 8446.
[225] M.A. Hitchman, Comments Inorg. Chem. 15 (1994) 197.
[226] K. Tanaka, H. Johansen, Int. J. Quantum Chem. 64 (1997) 453.
[227] M.E. Rose, Elementary Theory of Angular Momentum, John Willey & Sons, New York, 1967.
[228] D.G. Fedorov, S. Koseki, M.W. Schmidt, M.S. Gordon, Int. Rev. Phys. Chem. 22 (2003) 551.
[229] C.M. Marian, in: K.B. Lipkowitz, D.B. Boyd (Eds.), Reviews in Computational Chemistry, Wiley-VCH, New York, 2001.
[230] F. Neese, E.I. Solomon, in: J.S. Miller, M. Drillon (Eds.), Magnetoscience—From Molecules to Matirials, Wiley, NewYork, 2002.
[231] M.E. Rose, Elementary Theory of Angular Momentum, John Willey & Sons, New York, 1967.
[232] F. Neese, E.I. Solomon, Inorg. Chem. 37 (1998) 6568.
[233] R. McWeeny, Methods of Molecular Quantum Mechanics, Academic Press Limited, London, 1992.
[234] M. Böckmann, M. Klessinger, M.C. Zerner, J. Phys. Chem. 100 (1996) 10570.
[235] D.G. Fedorov, J.P. Finley, Phys. Rev. A 6404 (2001).
[236] T. Helgaker, P. Joergensen, J. Olsen, Molecular Electronic Structure Theory, John Wiley and Sons, New York, 2000.

[237] W. Duch, J. Karwowski, Comp. Phys. Rep. 2 (1985) 93.
[238] M.A. Robb, U. Niazi, Comp. Phys. Rep. 1 (1984) 129.
[239] R. Pauncz, Spin Eigenfunctions. Construction and Use, Plenum Press, New York, 1979.
[240] R. Pauncz, The Symmetric Group in Quantum Chemistry, CRC Press, Boca Raton, 1995.
[241] S.F. Boys, C.M. Reeves, I. Shavitt, Nature 178 (1956) 1207.
[242] I.L. Cooper, R. McWeeny, J. Chem. Phys. 42 (1966) 226.
[243] B.T. Sutcliffe, J. Chem. Phys. 42 (1966) 235.
[244] C.M. Reeves, Comm. ACM 9 (1966) 276.
[245] R. Manne, M.C. Zerner, Int. J. Quantum Chem. Symp. 19 (1986) 165.
[246] A. Golebiewski, E. Broclawik, Int. J. Quantum Chem. 27 (1985) 613.
[247] A.B. Myers, R.A. Mathies, D.J. Tannor, E.J. Heller, J. Chem. Phys. 77 (1982) 3857.
[248] D.J. Tannor, J.I. Sundberg, E.J. Heller, J. Phys. Chem. 86 (1982) 1822.
[249] J.L. Wootton, J.I. Zink, J. Phys. Chem. 99 (1995) 7251.
[250] A.B. Myers, Chem. Rev. 96 (1996) 911.
[251] L.M. Markham, B.S. Hudson, J. Phys. Chem. 100 (1996) 2731.
[252] S.E. Bailey, J.I. Zink, F.N. Nelsen, J. Am. Chem. Soc. (2003) 5939.
[253] W.L. Peticolas, T.I. Rush, J. Comput. Chem. 16 (1995) 1261.
[254] P.G. Szalay, G. Fogarasi, Chem. Phys. Lett. 270 (1997) 406.
[255] J. Neugebauer, B.A. Hess, J. Chem. Phys. 120 (2004) 11564.
[256] D.A. Long, The Raman Effect: A Unified Treatment of the Theory of Raman Scattering by Molecules, John Wiley & Sons Ltd., 2002.
[257] H.A. Kramers, W. Heisenberg, Z. Phys. 31 (1925) 681.
[258] A.M. Dirac, Proc. R. Soc. 114 (1927) 710.
[259] J. Franck, Trans. Faraday Soc. 21 (1925) 536.
[260] E.U. Condon, Phys. Rev. 28 (1925) 1182.
[261] E.U. Condon, Phys. Rev. 32 (1928) 858.
[262] F. Negri, M.Z. Zgierski, J. Chem. Phys. 99 (1993) 4318.
[263] F. Negri, M.Z. Zgierski, J. Chem. Phys. 102 (1995) 5165.
[264] A.M. Mebel, M. Hayashi, K.K. Liang, S.H. Lin, J. Phys. Chem. 103 (1999) 10674.
[265] J.-L. Chang, Y.-T. Cheng, J. Chem. Phys. 116 (2002) 7518.
[266] M. Dierksen, S. Grimme, J. Chem. Phys. 120 (2004) 3544.
[267] M. Dierksen, S. Grimme, J. Phys. Chem. 108 (2004) 10225.
[268] G. Herzberg, E. Teller, Z. Phys. Chem. Abt. B 21 (1933) 410.
[269] A. Warshel, P. Dauber, J. Chem. Phys. 66 (1977) 5477.
[270] F. Zerbetto, M.Z. Zgierski, J. Chem. Phys. 98 (1993) 4822.
[271] G. Orlandi, P. Palmieri, R. Tarroni, F. Zerbetto, M.Z. Zgierski, J. Chem. Phys. 100 (1994) 2458.
[272] W.J. Buma, F. Zerbetto, J. Chem. Phys. 103 (1995) 10492.
[273] P.W. Atkins, R.S. Friedman, Molecular Quantum Mechanics, Oxford University Press, New York, 1997.
[274] A.C. Albrecht, J. Chem. Phys. 34 (1961) 1476.
[275] J. Tang, A.C. Albrecht, in: H.A. Szymanski (Ed.), Raman Spectroscopy, Theory and Practice, Plenum Press, New York-London, 1970, p. 33.
[276] C. Manneback, Physica 17 (1951) 1001.
[277] T.E. Sharp, H.M. Rosenstock, J. Chem. Phys. 41 (1964) 3453.
[278] E.V. Doktorov, I.A. Malkin, V.I. Man'ko, J. Mol. Spectrosc. 56 (1975) 1.
[279] E.V. Doktorov, I.A. Malkin, V.I. Man'ko, J. Mol. Spectrosc. 64 (1977) 302.
[280] T.R. Faulkner, F.S. Richardson, J. Chem. Phys. 70 (1979) 1201.
[281] H. Kupka, P.H. Cribb, J. Chem. Phys. 85 (1986) 1303.
[282] K. Chen, C. Pei, Chem. Phys. Lett. 165 (1990) 523.
[283] V.I. Baranov, D.Y. Zelentsov, J. Mol. Struct. 272 (1992) 283.
[284] H. Kikuchi, M. Kubo, N. Watanabe, H. Suzuki, J. Chem. Phys. 119 (2003) 729.
[285] R. Berger, C. Fischer, M. Klessinger, J. Phys. Chem. A 102 (1998) 7157.
[286] P.P. Shorygin, Docl. Akad. Nauk. SSSR 87 (1952) 201.
[287] P.P. Shorygin, Docl. Akad. Nauk. SSSR Ser. Fiz 17 (1953) 581.
[288] L.L. Krushinskii, P.P. Shorygin, Opt. i Spectroskopiya 11 (1961) 24.
[289] L.L. Krushinskii, P.P. Shorygin, Opt. i Spectroskopiya 11 (1961) 151.
[290] F.A. Savin, Opt. i Spectroskopiya 19 (1965) 555.
[291] F.A. Savin, Opt. i Spectroskopiya 19 (1965) 743.
[292] F.A. Savin, Opt. i Spectroskopiya 20 (1966) 989.
[293] D.C. Blazei, W.L. Peticolas, Proc. Natl. Acad. Sci. U.S.A. 74 (1977) 2639.
[294] S. Hassing, O.S. Mortensen, J. Chem. Phys. 73 (1980) 1078.
[295] D.C. Blazei, W.L. Peticolas, J. Chem. Phys. 72 (1980) 3134.
[296] D.L. Tonks, G.B. Page, Chem. Phys. Lett. 66 (1979) 449.
[297] D.L. Tonks, G.B. Page, J. Chem. Phys. 75 (1981) 5694.
[298] P.M. Champion, A.C. Albrecht, Chem. Phys. Lett. 82 (1981) 410.
[299] D.L. Tonks, G.B. Page, J. Chem. Phys. 76 (1982) 5820.
[300] J.R. Cable, A.C. Albrecht, Chem. Phys. Lett. 84 (1986) 1969.
[301] C.K. Chan, G.B. Page, D.L. Tonks, O. Brafman, B. Khodadoost, C.T. Walker, J. Chem. Phys. 82 (1985) 4813.
[302] S. Mukamel, S. Abe, Y.J. Yan, R. Islampour, J. Phys. Chem. 89 (1985) 201.
[303] Y.J. Yan, S. Mukamel, J. Chem. Phys. 85 (1986) 5908.
[304] E.J. Heller, J. Chem. Phys. 62 (1975) 1544.
[305] S.-Y. Lee, E.J. Heller, J. Chem. Phys. 71 (1979) 4777.
[306] D.J. Tannor, E.J. Heller, J. Chem. Phys. 77 (1982) 202.
[307] K.C. Kulander, E.J. Heller, J. Chem. Phys. 69 (1978) 2439.
[308] E.J. Heller, J. Chem. Phys. 68 (1978) 2066.
[309] E.J. Heller, R.L. Sundberg, D.J. Tannor, J. Phys. Chem. 86 (1982) 1822.
[310] J. Neugebauer, E.J. Baerendes, E.V. Efremov, F. Ariese, C. Gooijer, J. Phys. Chem. A 109 (2005) 2100.
[311] T. Petrenko, F. Neese, in preparation.
[312] F. Furche, R. Ahlrichs, J. Chem. Phys. 117 (2002) 7433.
[313] J. VandeVondele, J. Hutter, J. Chem. Phys. 118 (2003) 4365.
[314] J. Neugebauer, E.J. Baerendes, M. Nooijen, J. Phys. Chem. A 109 (2005) 1168.
[315] H. Torii, M. Tasumi, J. Chem. Phys. 101 (1994) 4496.
[316] P. Hildebrandt, K. Nemeth, C. Kneip, F. Mark, Biophys. J. 74 (1998) A133.
[317] C. Kneip, P. Hildebrandt, K. Nemeth, F. Mark, K. Schaffner, Chem. Phys. Lett. 311 (1999) 479.
[318] M.A. Mroginski, K. Nemeth, I. Magdo, M. Muller, U. Robben, C. Della Vedova, P. Hildebrandt, F. Mark, J. Phys. Chem. B 104 (2000) 10885.
[319] I. Magdo, K. Nemeth, F. Mark, P. Hildebrandt, K. Schaffner, J. Phys. Chem. A 103 (1999) 289.
[320] L. Jensen, L.L. Zhao, J. Autschbach, G.C. Schatz, J. Chem. Phys. 123 (2005) 174110.
[321] S.-Y. Lee, J. Chem. Phys. 78 (1983) 723.
[322] S.-Y. Lee, J. Chem. Phys. 76 (1982) 3064.
[323] J.M. Schulman, R. Detrano, J.I. Musher, Phys. Rev. A 5 (1972) 1125.
[324] J.M. Schulman, R. Detrano, Phys. Rev. A 10 (1974) 1192.
[325] W.S. Schulman, J.M. Lee, J. Chem. Phys. 74 (1981) 4930.
[326] L. Jensen, J. Autschbach, G.C. Schatz, J. Chem. Phys. 122 (2005) 224115.
[327] K. Ray, T. Weyhermüller, F. Neese, K. Wieghardt, Inorg. Chem. 44 (2005) 5345.